Effects of dissolved organic matter on the phototransformation of aromatic amines in surface waters

THÈSE Nᵒ 7304 (2016)

PAR

Frank Jonathan LERESCHE

(EPFL)

ÉCOLE POLYTECHNIQUE
FÉDÉRALE DE LAUSANNE

Suisse
2016

Remerciements

J'aimerais tout d'abord adresser mes remerciements les plus chaleureux à Silvio Canonica pour le soutien et les conseils qu'il m'a apportés tout au long de ce projet. Il a été une grande source de motivation par l'intérêt qu'il a pris dans ce projet, que ce soit au fil des longues discussions que nous avons eues, ou simplement le matin lorsqu'il venait dans mon bureau pour s'enquérir des résultats des expériences de la veille. J'aimerais également adresser des remerciements chaleureux à Urs von Gunten, qui m'a accueilli dans son groupe, pour la supervision efficace et pour le soin qu'il prend des doctorants dont il a la charge. J'aimerais encore remercier les techniciens qui s'assurent du bon maintien des laboratoires et qui prodiguent volontiers conseils et assistance : Elisabeth Salhi, Ursula Schönenberger, Hans-Ulrich Laubscher, Caroline Stengel et Thomas Rüttimann. Je voudrais aussi remercier l'équipe de uni-hockey: Fabian Soltermann, toujours prêt à discuter du dernier concert ou de la prochaine séance de cinéma à aller voir à Zurich, Matthias Rudolf von Rohr, Tony Merle et Marc Bourgin. Mes remerciements aussi à Sungeun Lim et Xiaodan Zhao avec qui j'ai eu le plaisir de partager de longues discussions qui m'ont fait découvrir certains aspects de la culture coréenne et chinoise.

Mes remerciements encore à tous les autres membres anciens ou présent du groupe d'Urs, collègues et amis qui contribuent à l'atmosphère de travail à la fois détendue et efficace : Amisha Shah, Sabrina Bahnmüller, Kangmin Chon, Justine Criquet, Linda Oennby, Daniel Stalter, Sebastian Stoll, Peter Tentscher, Zhengqian Liu, Yael Schindler, Paul Borer, Hana Mestankova, Philippe Stolz, Léa Freydier, Adrian Pulgarin, Boris Droz, Nadine Czekalski, Emy Cretegny, Minju Lee, Jannis Wenk, Tobias Widler, Michèle Heeb, Saskia Zimmermann, Ana Sanchez-Polo, Stephanie Spahr, Florian Breider et Shaogang Liu. Je souhaite remercier les membres suivants de l'EAWAG, du département des Ressources aquatiques et de l'eau potable, de l'administration, du service informatique ou d'autres départements : Stefano Basso, Anna-Caterina Senn, Claire Wedema, Daniel Pellanda, Elisabeth Janssen, Anja Bretzler, Jagannath Briwakarma, Behnam Doulatyari et Rani Bakkour.

Je voudrais aussi remercier Petr Klán pour le chaleureux accueil qu'il m'a réservé au laboratoire de photochimie organique à Brno et à Dominik Heger, Lucie Ludvíková, Luboš Jílek et Jakob Wirz pour les conseils, discussions, et pour l'assistance technique qu'ils m'ont promulguée. Mes remerciements encore autres membres du groupe : Eduardo Palao, Tomáš Slanina, Pablo Corrochano, Anton Stasyuk, Lenka Filipová, Jamaludin Al Anshori, Otman Abida, Lubica Krausková, Ján Krausko, Vít Ladányi et Gabriela Bičanová pour leur accueil qui a contribué m'a laissé, lors de de mes séjours en République Tchèque, des souvenirs mémorables.

Je profite de l'occasion pour remercier mes parents, Jacques et Gudrun, mes frères, Samuel, Nils et Wolfgang, et toute ma famille étendue ainsi que tous mes amis qui avec beaucoup de compréhension et d'amitié m'ont supporté et soutenu, non seulement pendant cette thèse mais tout au long de ma vie. Pour conclure, mes remerciements au Fonds national de la recherche scientifique pour le financement de ce projet.

Zurich, le 25 août 2016

Résumé

La matière organique dissoute (MOD) est un mélange complexe de milliers de molécules organiques, omniprésentes dans les eaux de surface. Son influence sur la photodégradation des contaminants est un sujet complexe. Historiquement, la MOD a principalement été considérée pour ses aspects positifs (provoquant la dégradation des contaminants), mais récemment il a été découvert que pour certains composés, la MOD peut également avoir des effets négatifs (inhibition de la dégradation des contaminants) dans les eaux de surfaces. Ces propriétés duales de la MOD, à savoir les propriétés photosensibilisantes et inhibitrices de la MOD sont le sujet qui est présenté dans cette thèse. L'objectif visé par cette thèse est une meilleure compréhension de la photoréactivité de la MOD aux contaminants des eaux de surface.

Pour étudier les effets duaux de la MOD, une étude préliminaire a été réalisée afin de trouver un composé modèle, sujet à la fois aux effets photosensibilisants et inhibiteurs de la MOD. Neuf molécules pharmaceutiques ou modèles, appartenant à la classe des amines aromatiques, ont été sélectionnées et leur photodégradation étudiée sous un simulateur solaire dans des eaux comprenant plusieurs types de MOD. Cette étude a mené à la sélection du N,N-dimethyl-4-cyanoaniline (DMABN) comme composé modèle. Sa phototransformation indirecte a été caractérisée et survient principalement avec des états triplets de la MOD. La phototransformation indirecte a aussi été étudiée dans différentes eaux et mélanges d'eaux, et des équations modélisant les effets photosensibilisants et inhibiteurs de la MOD ont étés développées. Un mécanisme de réaction a été proposé pour DMABN où, après l'oxydation initiale de DMABN par des états triplets de la MOD qui amène à la formation du radical cation de DMABN (DMABN$^{\bullet+}$), suit une déprotonation dudit radical cation, pour amener ensuite par déméthylation à la formation de N-methyl-4-cyanoaniline et de formaldéhyde. L'absence d'effets isotopiques sur l'effet inhibiteur du phénol (utilisé comme substitut à la MOD), dans la phototransformation indirecte de DMABN indique que l'inhibition a lieu par transfert d'électron.

Des investigations utilisant la photolyse par flash laser (PFL) ont été menées pour détecter des intermédiaires à courte durée de vie et mesurer leurs constantes élémentaires de réaction. Les constantes de réaction entre DMABN et une série de cétones aromatiques dans leur état triplet (utilisées comme substitut aux états triplet de la MOD) ont été mesurées et suivaient la relation développées par Rehm et Weller dans le cadre de la théorie de Marcus sur le transfert d'électrons. DMABN$^{\bullet+}$ a été observé à l'échelle de la microseconde comme le produit primaire résultant de la réaction entre DMABN et les états triplets des photosensibilisateurs. Les constantes de réaction entre DMABN$^{\bullet+}$ et une série de phénols ont pu être décrites par une relation quantitative structure à activité en utilisant les descripteurs σ^+ de Hammett, et, avec une série de DOM, ont étés observées être proportionnelles à la capacité de donner des électrons des MOD utilisés. L'effet cinétique isotopique a confirmé que la réaction procède par transfert d'électrons. Un antibiotique, la sulfadiazine, a également été étudié par PFL. Qualitativement les observations ont été similaires à celles observées pour DMABN avec l'exception que le radical cation de la sulfadiazine a été observé être sujet à spéciation avec un radical neutre non-réactif.

Mots-clés

Phototransformation, état triplet, matière organique dissoute, antioxydant, photolyse par flash laser, destin environnemental, contaminant.

Abstract

Dissolved Organic Matter (DOM) is a complex mixture of thousands of organic molecules ubiquitously present in surface waters. Its influence on the photodegradation of organic contaminants is a complicated topic. For decades DOM had been mostly assumed to have a positive effect (i.e., promoting the degradation of contaminants), but more recently it was discovered that for some compounds, DOM can also have negative effects (i.e., inhibiting the photodegradation of contaminants) in surface waters. These dual properties of DOM are the subject of the investigations of this thesis, in which DOM is considered for both its photosensitizing and inhibitory properties. The goal of this thesis is to achieve a better understanding of the photoreactivity of DOM towards contaminants in surface waters.

To investigate the dual effect of DOM, an initial screening study was done to look for an optimal probe compound, subject to both photosensitizing and inhibitory effects. Nine candidate pharmaceuticals or model compounds, almost exclusively aromatic amines, were selected and their photodegradation evaluated under simulated sunlight in various water matrices. This study lead to the selection of N,N-dimethyl-4-cyanoaniline (DMABN) as a probe compound. The indirect photodegradation of DMABN was characterized and shown to proceed mostly through excited triplet states of DOM. The indirect photodegradation kinetics of DMABN was also studied in various waters and mixtures of waters, and model equations describing the effect of the photosensitizing and inhibitory properties of DOM on photodegradation rates constants were developed. An indirect phototransformation pathway for DMABN was proposed, in which following initial oxidation of DMABN by triplet DOM, deprotonation of the formed radical cation of DMABN (DMABN$^{\bullet+}$) occurred. Subsequently, demethylation of DMABN took place, forming N-methyl-4-cyanoaniline and formaldehyde. The absence of deuterium kinetic isotope effect on the inhibitory effect of phenol, used as a surrogate for DOM, on the indirect phototransformation of DMABN indicated that the inhibition proceeds by electron transfer.

To study the inhibitory effect of DOM, laser flash photolysis (LFP) investigations to detect short-lived reaction intermediates and measure their reaction rate constants were performed. The rate constant for DMABN-induced quenching of a series of triplet-aromatic ketones, used as proxies for excited triplet DOM were found to follow well-known relationships in the frame of Marcus theory of electron transfer. DMABN$^{\bullet+}$ was observed on a microsecond time scale as the primary species resulting from the reaction between the excited triplet photosensitizers and DMABN. The decay kinetics of this radical cation was studied in the presence and absence of phenols or DOM. DMABN$^{\bullet+}$ was found, as expected, to be quenched by both phenols and DOM, confirming the postulated model for the inhibitory effect. Electron-rich phenols reacted faster than phenol with DMABN$^{\bullet+}$, while the rate constants for quenching by DOM were proportional to the electron donating capacity of the DOM. Finally, a similar study as for DMABN was performed with sulfadiazine, a well-known antibiotic, as target compound. Results were qualitatively similar to those for DMABN but their interpretation was more complex probably due to deprotonation of the intermediate radical product.

Keywords

Photodegradation, Triplet State, Dissolved Organic Matter, Antioxidant, Laser Flash Photolysis, Environmental Fate, Contaminant

Contents

List of frequently used abbreviations

DOC	Dissolved organic carbon
DOM	Dissolved organic matter
PLFA	Pony Lake fulvic acid
SRFA	Suwannee River fulvic acid
SRHA	Suwannee River humic acid
ISC	Intersystem crossing
PhOH	Phenol
UV	Ultraviolet
UV-Vis	Ultraviolet-visible
$^3DOM^*$	Triplet state of dissolved organic matter
$^1O_2$	Singlet oxygen
FFA	Furfuryl alcohol
$^{\bullet}OH$	Hydroxyl radical
$CO_3^{\bullet-}$	Carbonate radical
DMABN	4-Dimethylaminobenzonitrile or *N,N*-dimethyl-4-cyanonaniline
MABN	4-Methylaminobenzonitrile or *N*-methyl-4-cyanoaniline
RB	Rose Bengal
SD	Sulfadiazine
LFP	Laser flash photolysis

Chapter 1   Introduction

From the development of the first cities on the shore of the Tigris or Euphrates, rivers have been used as a source of food, directly in the case of fishes and seafood but also as water for irrigation, drinking water and also as sewers and as a practical system to get rid of wastes that are produced in every city. With the development of modern sanitization techniques and the development of cities, invention of phosphate based detergents and ammonium nitrate fertilizers, the natural purification strength of the receiving rivers tended to be overwhelmed, leading to occasional eutrophication or algae blooms. The method of getting rid of wastes by discharging them into rivers was not anymore a good one as they will reappear downstream in the drinking water of the neighbour's community.

To remediate to these problems, wastewater treatment plants were implemented to remove the main macropollutants (Lausanne in 1964, Geneva and Bern 1967, Lucerne 1974), phosphorus removal steps were implemented (from 1973 in Switzerland), and legislatives measures (e.g. phosphate based laundry detergents were banned in 1986 in Switzerland) were implemented leading to a global improvement of the qualities of receiving lakes and rivers waters. With the improvement of analytical techniques, the detection of compounds present, at very low concentration (μM and below, so-called micropollutants) became possible and lead to the detection in the river waters or in the drinking water of compounds that have either escaped the wastewater treatment or arrived directly into the rivers by surface runoffs from fields or groundwater infiltration.

Figure 1, The sky reflects itself in the water of Lake Greifensee.

The fate of contaminants that escape wastewater treatment or arrive directly from field to surface rivers depends on their physico-chemical properties. Low-molecular weight molecules without strong interaction with water will tend to volatilize in the atmosphere. Apolar compounds are prone to sedimentation in the organic carbon rich riverbed, microorganisms can transform easily degradable organic molecules and solar light can promote the photodegradation of contaminants through direct absorption of light by the contaminant itself or through production of reactive species from the water matrix that will degrade contaminant (see Fig. 1 as an example of a natural system in which the photodegradation of contaminants can take place). In this thesis, we will report

investigations on the phototransformation of contaminants, and the influence of the dissolved organic matter on the phototransformation.

1.1 Phototransformation of contaminants in surface water

The first law of photochemistry also called Grotthuss-Draper law states that in order for a photochemical reaction to take place, a photon needs to be absorbed. The observations at the base of this law were done independently by T. Grotthuss and J. W. Draper at the beginning of the nineteenth century. [1, 2] This law reflects the need to consider light in its corpuscular state (and not wavelike) for photochemistry, and that the wavelength of the light needs to be considered because absorbance of substances is strongly wavelength-dependent.

The major photoactive species in surface waters (rivers, ponds, lakes and seas) besides the contaminants themselves are the dissolved organic matter (DOM), nitrite and nitrate anions (see Fig. 2). The electronic absorption of these compounds takes place predominantly in the ultraviolet (UV) and violet spectral region, therefore the short-wavelength part of the spectrum of terrestrial sunlight is usually the most active towards photodegradation of contaminants. Only when a compound absorbs significantly light above 400nm will the visible part of the solar spectrum be relevant.
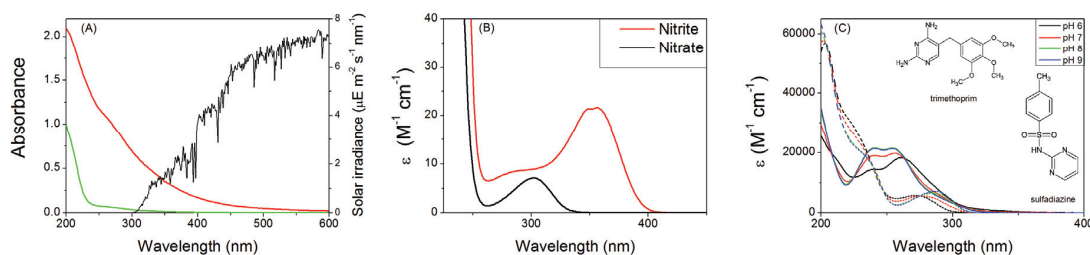

Figure 2. (A) UV-Vis absorbance spectra of Lake Greifensee (green) and Etang de la Gruère (red) water, solar spectral photon irradiance at Air Mass 1.5 (global tilt, calculated using ASTM G173-03 standard & SMART v2.92 data, black). (B) Spectral molar absorption coefficient of sodium nitrite (red) and sodium nitrate (black) in water. (C) Spectral molar absorption coefficient of sulfadiazine (plain lines) and trimethoprim (dashed lines) for varying pH values in phosphate buffered water.

According to the aforementioned ways of light absorption, in aquatic photochemistry two main types of processes are direct and indirect photodegradation. While direct photodegradation implies light absorption by the contaminant, for indirect photodegradation one or more of the aforementioned constituents of the water matrix (DOM, nitrate, nitrite) absorbs light and produces reactive species that react with the target compound, promoting its photodegradation.

1.1.1 Direct photodegradation

In surface waters, the direct photodegradation of a contaminant (CT) to give a photodegradation product (CT') can occur after absorption of a photon by CT (see eq. 1.1):

$$CT + h\nu \rightarrow CT' \tag{1.1}$$

A significant overlap between the UV-vis absorption spectrum of the contaminant and the solar spectrum is necessary to have a relevant direct photolysis. Due to the competition of various non-reactive, photophysical relaxation mechanisms (e.g. fluorescence, see fig. 3), the quantum yield of the direct photolysis is very variable among diverse compounds [3-7]. In surface water DOM filters the UV part of the sunlight preferentially (see fig.2), limiting often the direct photodegradation to the first centimeters of the top-layer of the water.
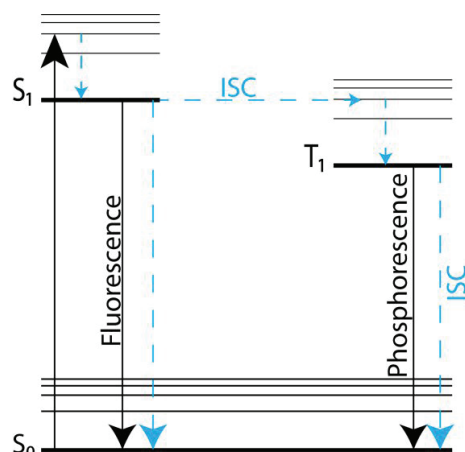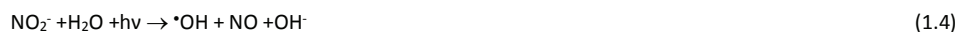
Figure 3: Jablonski diagram. Plain black arrows represent transition with absorption or emission of a photon, blue dashed arrows represent radiationless transition, e.g. internal conversion or intersystem crossing, ISC). S_0 represent the ground state of the molecule, S_1 represents the first electronic excited state of the molecule, T_1 represents the first excited triplet state.

1.1.2 Indirect photodegradation

Several reactive species are involved in the indirect photodegradation of contaminants, e.g.: triplet state of dissolved organic matter ($^3DOM^*$), singlet oxygen ($^1O_2$), hydroxyl radical ($^\bullet OH$), carbonate radical ($CO_3^{\bullet-}$). All these reactive species are mostly produced through irradiation of DOM, nitrite and nitrate (see eqs. 1.2 to 1.5 and 1.10).

$$DOM + h\nu \rightarrow {}^1DOM^* \rightarrow {}^3DOM^* \tag{1.2}$$

$$NO_3^- + H_2O + h\nu \rightarrow {}^\bullet OH + NO_2 + OH^- \tag{1.3}$$

$$NO_2^- + H_2O + h\nu \rightarrow {}^\bullet OH + NO + OH^- \tag{1.4}$$

$$DOM + h\nu \rightarrow DOM' + {}^\bullet OH \tag{1.5}$$

Hydroxyl radical

The hydroxyl radical is a non-selective oxidant that reacts with many substances at nearly diffusion-controlled rates. [8] In surface waters it is mostly produced through photolysis of nitrate, nitrite and DOM (eq. 1.3-1.5). [9-13] A major depletion pathway for the hydroxyl radical is its reaction with DOM (second-order rate constant of $\approx 3.1 \bullet 10^4$ l mg_C^{-1} s^{-1} for eq. 1.6) leading to low ($< 10^{-15}$M) steady-state concentration of the hydroxyl radical in surface waters.[14-16]

$$DOM + {}^\bullet OH \rightarrow DOM' \tag{1.6}$$

Another sink for hydroxyl radical is its reaction with the carbonate or bicarbonate anions present in surface waters, leading to the production of the carbonate radical (eqs. 1.7 and 1.8). The relevance of this reaction is limited to water with high carbonate concentration and a relatively high pH, due to the speciation of carbonate (pK_a of 10.33 for the second deprotonation of carbonic acid) and a higher reactivity of hydroxyl radical towards carbonate than bicarbonate (second-order rate constant of $4.2 \bullet 10^8$ M^{-1} s^{-1} for reaction 1.7 vs $1.5 \bullet 10^7$ M^{-1} s^{-1} for reaction 1.8). [17, 18]

$$CO_3^{2-} + {}^\bullet OH \rightarrow {}^\bullet CO_3^- + OH^- \tag{1.7}$$

$$HCO_3^- + {}^\bullet OH \rightarrow {}^\bullet CO_3^- + H_2O \tag{1.8}$$

Carbonate radical

The carbonate radical is formed in surface waters through the aforementioned reactions of the hydroxyl radical (eqs. 1.7 and 1.8) and possibly through oxidation of the carbonate and bicarbonate anions by $^3DOM^*$ (eq. 1.9). [19] The oxidation potential of the carbonate radical is 1.59 V [20, 21] at pH 7, which makes it an efficient oxidant of electron-rich compounds such as anilines or phenols. [22-

[24] Similarly as for the hydroxyl radical, a major depletion pathway for the carbonate radical in surface waters is its reaction with DOM (second-order rate constant of 40-280 L mg_C^{-1} s^{-1}). [19, 23]

$$CO_3^{2-} + {}^3DOM^* \rightarrow {}^\bullet CO_3^- + DOM^{\bullet-} \tag{1.9}$$

Excited triplet DOM

Most of the light entering a water body is absorbed by the chromophoric part of dissolved organic matter. Upon absorption of a photon an electron is transferred from the highest occupied molecular orbital (HOMO) of a DOM chromophore to the lowest unoccupied molecular orbital (LUMO) or to a higher unoccupied orbital, generating a singlet state of DOM. One of the relaxation mechanisms of this excited state is intersystem crossing (ISC) to the triplet state generating ${}^3DOM^*$ (see fig. 3). The quantum yield for ${}^3DOM^*$ formation is usually estimated in the 1-8% range indicating that the ISC is in competition with other relaxation mechanisms. [25-27] It is believed that an important fraction of photoactive chromophores of DOM are aromatic ketones due to the observations that:

- the photoreactivity of DOM was decreased greatly after sodium borohydride reduction, a treatment that transforms aromatic ketones and aldehydes to alcohols [27].

- the photoreactivity of aromatic ketones used as triplet photosensitizers is similar as DOM photoreactivity towards phenols. [28]

The mean excited triplet energy of ${}^3DOM^*$ is estimated to be $\approx$250 kJ/mol, [29] and the main deactivation mechanism of ${}^3DOM^*$ is their reaction with ground state triplet oxygen either by physical quenching (eq. 1.11) or to give singlet oxygen (eq. 1.10). [30]

$$^3DOM^* + O_2 \rightarrow DOM + {}^1O_2 \tag{1.10}$$

$$^3DOM^* + O_2 \rightarrow DOM + O_2 \tag{1.11}$$

${}^3DOM^*$ can react by several pathways with contaminants. Anilines are known to react with triplet states of aromatic ketones as proxy for ${}^3DOM^*$ by electron transfer, phenols by electron transfer or by hydrogen transfer, and alkenes are prone to reaction by energy transfer leading to isomerization. [26, 29, 31, 32]

Singlet Oxygen

Singlet oxygen (${}^1O_2$) is produced upon reaction of oxygen with ${}^3DOM^*$ in surface waters (see eq. 1.10) and has a relatively low energy of the transition from ${}^1O_2$ to ground state triplet oxygen (94 kJ mol^{-1}). [33] The main decay pathway of ${}^1O_2$ is physical quenching by water, which limits its lifetime to $\approx$4μs in any surface water. [33] ${}^1O_2$ is a selective oxidant which is particularly reactive towards compounds containing activated C-C double bonds, making the reactivity of ${}^1O_2$ towards contaminants rather variable with constants of reaction that can vary over several orders of magnitude. [34-37]

Other reactive species

Several other reactive species such as the superoxide radical anion ($O_2^{\bullet-}$), hydrogen peroxide, low-level hydroxylating species or halide radicals ($X_2^{\bullet-}$), are known or suspected to play a role in the photodegradation of contaminants in surface waters. Further studies are necessary to characterize their exact properties and relevance in the photodegradation of contaminants. [38-42]

Deconvolution of the photodegradation rate

The steady-state concentration of reactive species under sunlight is in the atto to pico molar concentration range (see Table 1). The influence of the reactive species involved in the photodegradation of a contaminant can be estimated typically by using quenchers or probe compounds (e.g. furfuryl alcohol and sodium azide for ${}^1O_2$, trimethylphenol for ${}^3DOM^*$, isopropanol or methanol for ${}^\bullet OH$). Typically, direct photolysis tends to be the dominant photodegradation pathway for compounds that absorb significantly the available light. For the indirect photodegradation, compounds that have significant reactivity towards ${}^3DOM^*$ or ${}^1O_2$ will react mostly through reaction with these species, ${}^\bullet OH$ is generally a significant oxidant only for compounds with low ${}^3DOM^*$ or ${}^1O_2$ reactivity due to the usually low concentration of ${}^\bullet OH$ present in surface water (see Fig. 4).

Table 1, Typical concentration of reactive species in fresh surface water under sunlight. [a] from [29, 43, 44], [b] from [29, 45], [c] from [46]

$[^1O_2]_{ss}$	$[^3DOM*]_{ss}$	$[^{\bullet}OH]_{ss}$
$1 \bullet 10^{-14}$ - $1 \bullet 10^{-12}$ M [a]	$1 \bullet 10^{-14}$ - $1 \bullet 10^{-12}$ M [b]	$1 \bullet 10^{-18}$ - $1 \bullet 10^{-15}$ M [c]

An illustrative example of the influence of several of the aforementioned reactive species in the photodegradation of six contaminants in constructed wetlands is presented in Figure 4. The direct photodegradation is the dominant transformation pathway for *N*-nitrosodimethylamine (NDMA), while for the other presented compounds both direct and indirect photodegradation are important. The pH has an effect on both the speciation of the target molecules and on the concentration of the reactive species (e.g. the carbonate radical and hydroxyl radical concentrations are higher and lower, respectively, at pH 10 than 8).
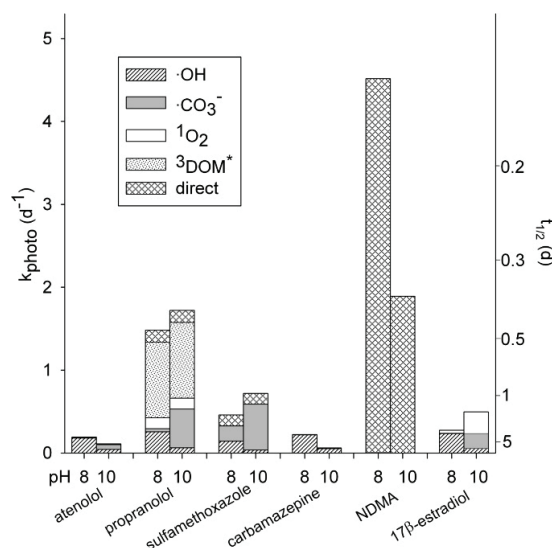

Figure 4. Predicted contribution at pH 8 and 10 of the direct photolysis, carbonate radical, hydroxyl radical, singlet oxygen and triplet state of the dissolved organic matter in the photodegradation rate constants of six compounds (four pharmaceutical, one hormone, and n-nitrosodimethylamine) under natural sunlight (June21, 40°N latitude) in constructed wetland water([DOC] = 8mgC/L, [NO$_3^-$] = 20mg$_N$/L, [HCO$_3^-$] + [CO$_3^{2-}$] = 60mg$_C$/L) . Reprinted with permission from [47], Copyright (2013), American Chemical Society.

1.2   Properties of dissolved organic matter

DOM is a mixture of thousands of compounds that originate mostly from degradation of plants, animals or aquatic microorganisms. In a sense it can be considered as a waste product, but it can still be used by bacteria as a source of energy. [48, 49] The DOM composition in a given place or water will shift over time reflecting the variety of processes that influence the DOM pool: the increased photosynthesis, photobleaching and various other photo-processes during summer, the precipitation or temperature patterns, the possible winter ice coverage and storm events. [50-52] The average DOM structure is a crossed-linked network with a carbon based skeleton that reflects its provenance (see Fig.5).

The use of DOM extracts is an interesting choice for the disentanglement of the influence of the DOM from the influence of the water matrix. The extracts also allow easy inter-laboratories comparison of results and to freely adjust the DOM concentration without being limited by the total DOM concentration as for natural waters.

Subcategories of DOM are usually considered to allow discussion on its properties. The first distinction is usually based on the provenance of the DOM, the two extremes being DOM generated in the water body, called autochthonous DOM, which is microbial or algal derived, and DOM generated outside of the water body, called allochthonous DOM, that is usually derived from the degradation of higher plants.

A second key distinction is made according to the extraction procedure of the DOM. The soluble fraction following an adsorption-fractionation of the DOM at low pH (under pH 2) is called fulvic acid (FA) while the precipitated DOM is called humic acid (HA). The DOM extraction from natural waters is now often done using reverse-osmosis techniques followed by electro-dialysis, which has a high DOM recovery avoiding so a selective extraction of DOM.[53-55]
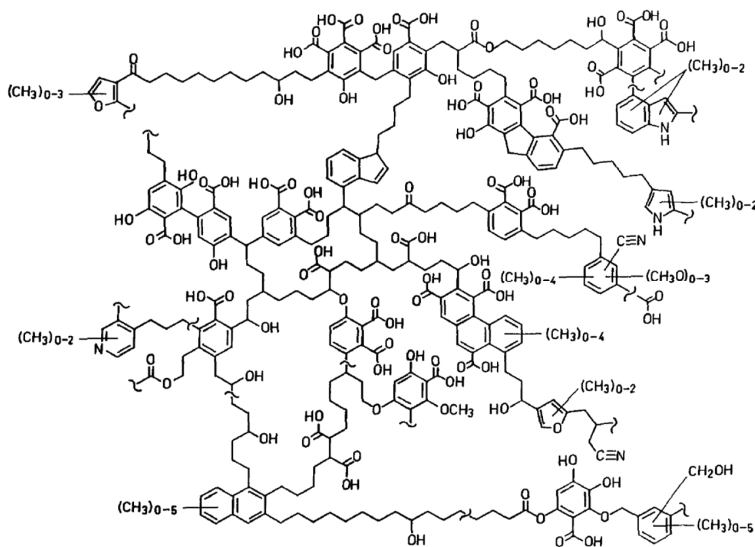

Fig. 1. Schematic, biomacromolecular HA structure developed from the tentatively proposed chemical network of humic substances [1,8] on the basis of analytical pyrolysis; spectroscopic, chemical, oxidative/reductive degradation, and colloid-chemical and electron microscope results

Figure 5. Tentative structure of soil Humic Acid. [56], reprinted with permission of Springer, ©Springer-Vorlag, 1993.

1.2.1 Light absorption characteristics and photoreactivity of DOM

The UV-Vis spectra of DOM present a characteristic exponential-like decrease in absorption coefficient upon increase of wavelength (see fig. 2). If most of the absorption spectra can be reasonably explained in term of superposition of the spectra of the different chromophores of DOM, it was hypothesized that the low-energetic ($\lambda{>}400$ nm) absorption results from intermolecular charge-transfer interactions involving the chromophores of DOM. [57-59]

The low-molecular weight fractions of the DOM tend to be more photoactive than the high ones as indicated by a decrease in $^3DOM^*$ and $^1O_2$ concentration with an increase of the molecular size. Such a trend was also shown to be analogous to the one observed for the fluorescence quantum yield of DOM. [60] The quantum yields of production of reactive species from photoirradiated DOM also tends to decrease with an increase in excitation wavelength.[25, 61]

## 1.2.2 Redox properties of DOM

The redox-active moieties of DOM are mostly believed to consist of quinone functional groups, but other species such as thiols or complexed metals may also play a minor redox role depending on the composition of the DOM. [62-69] The electron-donating capacity (EDC) of DOM involves mostly phenolic moieties of DOM, which agrees with the good correlation between the EDC value and the titrated phenol contend of several types of DOM, [62] and from the fact that EDC of DOM increases with pH. This pH-dependence may be explained by the deprotonation of phenolic moieties, which renders them more susceptible to donate an electron. [66, 70]

1.3 Inhibitory effect of dissolved organic matter

Until recently the effects of dissolved organic matter on the photodegradation of contaminants were considered only positively, i.e. increasing the photodegradation. Latterly it was discovered that DOM can not only promote the photodegradation of contaminants but concomitantly also inhibit it. The first observation of this inhibitory effect was made on a series of aquatic contaminants, includ-

ing pharmaceuticals and herbicides, using an aromatic ketone to mimic the photoreactivity of DOM in terms of ^{3}DOM*, and employing SRFA as DOM with prominent inhibitory action and negligible photosensitizing effect (due to the relatively low concentration it was applied). It was observed that the presence of SRFA decreased the photodegradation rate of part of the studied contaminants. This inhibitory effect was rationalized in terms of an electron transfer from electron donating moieties of SRFA to a radical cation intermediate, formed upon triplet-sensitized oxidation of the target compound. This resulted in the re-formation of the parent compound, whose depletion rate was thus decreased. It was also seen that the inhibitory effect was well described by the kinetic equations corresponding to scheme 1. [71]

A later study showed that the inhibitory effect of DOM was more important for DOM of terrestrial origin than for DOM of aquatic origin, and extended the kinetic model (see scheme 1) to allow for a non-inhibited transformation pathway concomitantly to the inhibited one. It was observed that the extended model provided better fits to the experimental results.[72]
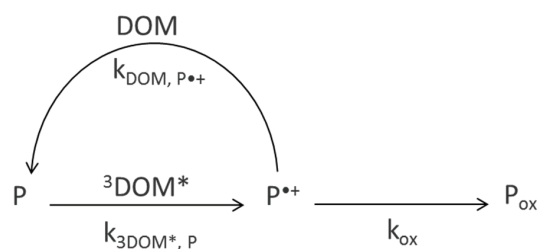
Scheme 1. Kinetic scheme showing the degradation of a contaminant P through ^{3}DOM* photosensitization and the inhibitory effect of DOM on the photodegradation. Adapted with permission from [72]. Copyright (2011) American Chemical Society.

A further study showed that the inhibitory effect of DOM could be mimicked by phenols used as model antioxidants and that the photodegradation of such phenols was increased by the presence of the target compounds, indicating that the phenols were acting as sacrificial electron donors. [73] A method for detecting compounds subject to the inhibitory effect was developed, consisting in studying the photodegradation of a target compound in the absence and in the presence of a small quantity (e.g. 10 µM) of phenol or another antioxidant. [73, 74] The direct phototransformation of tryptophan was seen to be subject to the inhibitory effect. [75] As the first step of tryptophan direct photodegradation is a photoionization, similar compounds such as phenols or anilines that are also known to be subject to photoionization should be expected to have a direct photodegradation also subject to the inhibitory effect. [76-79]

The effects of several oxidative treatments (ozonation or exposure to chlorine dioxide or chlorine) on the photochemical properties of DOM indicate that the inhibitory effect is correlated with the EDC of the DOM and that the overall rate of photodegradation of a target compound subject to the inhibitory effect can be increased or decreased upon DOM oxidation depending on the relative decrease in photosensitizing and inhibiting moieties. [80, 81] The phenolic content of a DOM was found to be correlated to the EDC of the DOM, supporting the hypothesis that the phenolic moieties are responsible, partially or totally, for the inhibitory effect. The observed inhibitory effect of model phenols concurs with this observation. [62, 73]

1.4   Thesis outline

The project of this thesis, funded through a grant from the Swiss National Science Foundation (project No. 200021-140815), had the following main goals:

1) To further investigate the mechanisms of the inhibitory effects of DOM on indirect phototransformation of organic contaminants. Up to know, based on thermodynamic considerations, the inhibition mechanism was assumed to be an electron transfer process; verification of this hypothesis is an aim of this thesis

2) To evaluate the effect of DOM acting as an inhibitor and at the same time as photosensitizer in the photodegradation of contaminants.

3) To evaluate the effects of DOM characteristics such as composition or concentration on the photodegradation of contaminants.This would allow for a better understanding and prediction of the fate of contaminants in the environment.

These three goals were pursued in the different parts of this thesis, which are listed and described below.

Chapter 1

Chapter one provides a general introduction to the topic of the fate of contaminants in surface water and describes the influence of the photo-produced reactive species and of the water matrix on the phototransformation of contaminants in the aquatic environment.

Chapter 2

Chapter two aims at first to select an optimal compound for further investigations on the inhibitory effect. With the selected model compound *N,N*-dimethyl-4-cyanoaniline (DMABN), detailed investigations on the effect of DOM characteristics, concentration, and DOM mixtures on the overall photodegradation of this model compounds were performed. The deconvolution of the influence of the different reactive species involved in the photodegradation of DMABN under realistic environmental condition was done to fully characterize the above-mentioned DOM effects. The reaction pathway for the photodegradation of DMABN with ^{3}DOM*, investigated using steady-state photoirradiation and analysis of stable reaction products, appeared to proceed by demethylation of the aniline group to yield *N*-methyl-4-cyanoaniline and formaldehyde with a selectivity of ≈80%. Finally the obtained information was used to simulate the photodegradation of DMABN in binary mixtures of DOM taking into account both the photosensitizing and the inhibitory effects of both DOM components.

Chapter 3

Chapter three describes a nanosecond laser flash photolysis (LFP) study of the transient species generated upon direct irradiation of the model compound DMABN (selected as in Chapter 2), and in a second part of photo-excited sensitizers chosen to mimic triplet photosensitization of DMABN by DOM. Upon direct laser irradiation of DMABN the triplet state of DMABN, the radical cation of DMABN (DMABN$^{\bullet+}$) and the hydrated electron are produced. The production and the lifetime of those species was studied under diverse conditions (aerated, oxygenated, degassed, N$_2$O aerated) and as a function of pH to investigate the influence of oxygen and the hydrated electron on the lifetime of DMABN$^{\bullet+}$.

The rate constants for the quenching of the excited triplet state of several photosensitizers (^{3}Sens*) by DMABN were measured and found to follow a Rehm-Weller relationship, which relates the bimolecular quenching rate constant to the free enthalpy of the one-electron transfer reaction from DMABN to ^{3}Sens*. DMABN$^{\bullet+}$ production was also observed upon reaction of DMABN with ^{3}Sens*, confirming the electron transfer hypothesis.

Chapter 4

In chapter four, further LFP experiments are presented, using the triplet-sensitized system for the formation of DMABN$^{\bullet+}$ developed in chapter three. The reactivity of DMABN$^{\bullet+}$ towards electron transfer from several phenols was studied and shown to follow a Hammett-like relationship, well described by the phenols σ^+ descriptors. These experiments confirmed so the proposed inhibition mechanism: that after the first photosensitized electron transfer step between ^{3}DOM* and DMABN, the formed radical cation (DMABN$^{\bullet+}$) can be reduced by an electron transfer reaction from the phenols to give back the parent compound (DMABN). Similarly as the experiments with phenols, the effects of various types of DOM as inhibitors were investigated and the amplitude of the inhibition was seen to be correlated to the EDC of the DOMs.

In the second part of this chapter, a study of the triplet-sensitized LFP of sulfadiazine (SD) is presented. The photodegradation mechanism of SD was seen to be similar to the one of DMABN, also subject to the inhibitory of phenols and DOM. The main observed difference was a speciation of the produced radical cation of sulfadiazine (SD$^{\bullet+}$).

Chapter 5

Chapter five presents the general conclusions that can be drawn from this thesis and an outlook of this work.

1.5   References for the chapter 1

1. Turner, L. A., The excited systems formed by the absorption of light. *J. Phys. Chem.* **1928,** *32*, (4), 507-515.
2. Albini, A., Some remarks on the first law of photochemistry. *Photoch. Photobiol. Sci.* **2016,** *15*, (3), 319-324.
3. Lu, Z.; Challis, J. K.; Wong, C. S., Quantum Yields for Direct Photolysis of Neonicotinoid Insecticides in Water: Implications for Exposure to Nontarget Aquatic Organisms. *Environ. Sci. Technol. Let.* **2015,** *2*, (7), 188-192.
4. Kelly, M. M.; Arnold, W. A., Direct and indirect photolysis of the phytoestrogens genistein and daidzein. *Environ. Sci. Technol.* **2012,** *46*. 5396-5403.
5. Ryan, C. C.; Tan, D. T.; Arnold, W. A., Direct and indirect photolysis of sulfamethoxazole and trimethoprim in wastewater treatment plant effluent. *Water Res.* **2011,** *45*, (3), 1280-1286.
6. Boreen, A. L.; Arnold, W. A.; McNeill, K., Photochemical fate of sulfa drugs in the aquatic environment: sulfa drugs containing five-membered heterocyclic groups. *Environ. Sci. Technol.* **2004,** *38*, (14), 3933-3940.
7. Wammer, K. H.; Korte, A. R.; Lundeen, R. A.; Sundberg, J. E.; McNeill, K.; Arnold, W. A., Direct photochemistry of three fluoroquinolone antibacterials: Norfloxacin, ofloxacin, and enrofloxacin. *Water Res.* **2013,** *47*, (1), 439-448.
8. Buxton, G. V.; Greenstock, C. L.; Helman, W. P.; Ross, A. B., Critical-Review of Rate Constants for Reactions of Hydrated Electrons, Hydrogen-Atoms and Hydroxyl Radicals (OH/O) in Aqueous-Solution. *J. Phys. Chem. Ref. Data* **1988,** *17*, (2), 513-886.
9. Mack, J.; Bolton, J. R., Photochemistry of nitrite and nitrate in aqueous solution: a review. *Photoch. Photobiol. A* **1999,** *128*, (1-3), 1-13.
10. Sun, L. N.; Qian, J. G.; Blough, N. V.; Mopper, K., Insights into the Photoproduction Sites of Hydroxyl Radicals by Dissolved Organic Matter in Natural Waters. *Environ. Sci. Technol. Let.* **2015,** *2*, (12), 352-356.
11. Zafiriou, O. C., Sources and Reactions of OH and Daughter Radicals in Seawater. *Geophys. Res.* **1974,** *79*, (30), 4491-4497.
12. Vione, D.; Minella, M.; Minero, C.; Maurino, V.; Picco, P.; Marchetto, A.; Tartari, G., Photodegradation of nitrite in lake waters: role of dissolved organic matter. *Environ. Chem.* **2009,** *6*, (5), 407-415.
13. Goldstein, S.; Rabani, J., Mechanism of nitrite formation by nitrate photolysis in aqueous solutions: The role of peroxynitrite, nitrogen dioxide, and hydroxyl radical. *J. Am. Chem. Soc.* **2007,** *129*, (34), 10597-10601.
14. Haag, W. R.; Hoigne, J., Photo-Sensitized Oxidation in Natural-Water Via .Oh Radicals. *Chemosphere* **1985,** *14*, (11-12), 1659-1671.
15. Zepp, R. G.; Hoigne, J.; Bader, H., Nitrate-Induced Photooxidation of Trace Organic-Chemicals in Water. *Environ. Sci. Technol.* **1987,** *21*, (5), 443-450.
16. Westerhoff, P.; Aiken, G.; Amy, G.; Debroux, J., Relationships between the structure of natural organic matter and its reactivity towards molecular ozone and hydroxyl radicals. *Water Res.* **1999,** *33*, (10), 2265-2276.
17. Haynes, W. M., *CRC handbook of chemistry and physics*. CRC press, 2014.
18. Weeks, J. L.; Rabani, J., Pulse Radiolysis of Deaerated Aqueous Carbonate Solutions .I. Transient Optical Spectrum and Mechanism .2. Pk for OH Radicals. *J. Phys. Chem. Us* **1966,** *70*, (7), 2100-2106.
19. Canonica, S.; Kohn, T.; Mac, M.; Real, F. J.; Wirz, J.; von Gunten, U., Photosensitizer method to determine rate constants for the reaction of carbonate radical with organic compounds. *Environ. Sci. Technol.* **2005,** *39*, (23), 9182-9188.
20. Armstrong, D. A.; Waltz, W. L.; Rauk, A., Carbonate radical anion - Thermochemistry. *Can. J. Chem.* **2006,** *84*, (12), 1614-1619.
21. Huie, R. E.; Clifton, C. L.; Neta, P., Electron-Transfer Reaction-Rates and Equilibria of the Carbonate and Sulfate Radical-Anions. *Radiat. Phys. Chem.* **1991,** *38*, (5), 477-481.
22. Burns, J. M.; Cooper, W. J.; Ferry, J. L.; King, D. W.; DiMento, B. P.; McNeill, K.; Miller, C. J.; Miller, W. L.; Peake, B. M.; Rusak, S. A.; Rose, A. L.; Waite, T. D., Methods for reactive oxygen species (ROS) detection in aqueous environments. *Aq. Sci.* **2012,** *74*, (4), 683-734.
23. Larson, R. A.; Zepp, R. G., Reactivity of the Carbonate Radical with Aniline Derivatives. *Environ. Toxicol. Chem.* **1988,** *7*, (4), 265-274.
24. Neta, P.; Huie, R. E.; Ross, A. B., Rate Constants for Reactions of Inorganic Radicals in Aqueous-Solution. *J.Phys. Chem. Ref. Data* **1988,** *17*, (3), 1027-1284.
25. Marchisio, A.; Minella, M.; Maurino, V.; Minero, C.; Vione, D., Photogeneration of reactive transient species upon irradiation of natural water samples: Formation quantum yields in different spectral intervals, and implications for the photochemistry of surface waters. *Water Res.* **2015,** *73*, 145-156.
26. Grebel, J. E.; Pignatello, J. J.; Mitch, W. A., Sorbic acid as a quantitative probe for the formation, scavenging and steady-state concentrations of the triplet-excited state of organic compounds. *Water Res.* **2011,** *45*, (19), 6535-44.
27. Golanoski, K. S.; Fang, S.; Del Vecchio, R.; Blough, N. V., Investigating the mechanism of phenol photooxidation by humic substances. *Environ. Sci. Technol.* **2012,** *46*, (7), 3912-3920.
28. Canonica, S.; Hellrung, B.; Wirz, J., Oxidation of phenols by triplet aromatic ketones in aqueous solution. *J. Phys. Chem. A* **2000,** *104*, (6), 1226-1232.
29. Zepp, R. G.; Schlotzhauer, P. F.; Sink, R. M., Photosensitized Transformations Involving Electronic-Energy Transfer in Natural-Waters - Role of Humic Substances. *Environ. Sci. Technol.* **1985,** *19*, (1), 74-81.
30. Schweitzer, C.; Schmidt, R., Physical mechanisms of generation and deactivation of singlet oxygen. *Chem. Rev.* **2003,** *103*, (5), 1685-1757.

31. Canonica, S.; Jans, U.; Stemmler, K.; Hoigne, J., Transformation kinetics of phenols in water: photosensitization by dissolved natural organic material and aromatic ketones. *Environ. Sci. Technol.* **1995,** *29*, (7), 1822-1831.

32. Erickson, P. R.; Walpen, N.; Guerard, J. J.; Eustis, S. N.; Arey, J. S.; McNeill, K., Controlling factors in the rates of oxidation of anilines and phenols by triplet methylene blue in aqueous solution. *J. Phys. Chem. A* **2015,** *119*, (13), 3233-3243.

33. Wilkinson, F.; Helman, W. P.; Ross, A. B., Rate Constants for the Decay and Reactions of the Lowest Electronically Excited Singlet-State of Molecular-Oxygen in Solution - an Expanded and Revised Compilation. *J. Phys. Chem. Ref. Data* **1995,** *24*, (2), 663-1021.

34. Boreen, A. L.; Edhlund, B. L.; Cotner, J. B.; McNeill, K., Indirect photodegradation of dissolved free amino acids: The contribution of singlet oxygen and the differential reactivity of DOM from various sources. *Environ. Sci. Technol.* **2008,** *42*, (15), 5492-5498.

35. Latch, D. E.; Stender, B. L.; Packer, J. L.; Arnold, W. A.; McNeill, K., Photochemical fate of pharmaceuticals in the environment: cimetidine and ranitidine. *Environ. Sci. Technol.* **2003,** *37*, (15), 3342-3350.

36. al Housari, F.; Vione, D.; Chiron, S.; Barbati, S., Reactive photoinduced species in estuarine waters. Characterization of hydroxyl radical, singlet oxygen and dissolved organic matter triplet state in natural oxidation processes. *Photoch. Photobiol. Sci.* **2010,** *9*, (1), 78-86.

37. Scully, F. E.; Hoigne, J., Rate Constants for Reactions of Singlet Oxygen with Phenols and Other Compounds in Water. *Chemosphere* **1987,** *16*, (4), 681-694.

38. Pochon, A.; Vaughan, P. P.; Gan, D. Q.; Vath, P.; Blough, N. V.; Falvey, D. E., Photochemical oxidation of water by 2-methyl-1,4-benzoquinone: Evidence against the formation of free hydroxyl radical. *J. Phys. Chem. A* **2002,** *106*, (12), 2889-2894.

39. Zhang, Y.; Del Vecchio, R.; Blough, N. V., Investigating the mechanism of hydrogen peroxide photoproduction by humic substances. *Environ. Sci. Technol.* **2012,** *46*, (21), 11836-11843.

40. Zhang, Y.; Simon, K. A.; Andrew, A. A.; Del Vecchio, R.; Blough, N. V., Enhanced Photoproduction of Hydrogen Peroxide by Humic Substances in the Presence of Phenol Electron Donors. *Environ. Sci. Technol.* **2014.** *46*, (21) 11836-11843.

41. Grebel, J. E.; Pignatello, J. J.; Mitch, W. A., Effect of Halide Ions and Carbonates on Organic Contaminant Degradation by Hydroxyl Radical-Based Advanced Oxidation Processes in Saline Waters. *Environ. Sci. Technol.* **2010,** *44*, (17), 6822-6828.

42. Jammoul, A.; Dumas, S.; D'Anna, B.; George, C., Photoinduced oxidation of sea salt halides by aromatic ketones: a source of halogenated radicals. *Atmos. Chem. Phys.* **2009,** *9*, (13), 4229-4237.

43. Haag, W. R.; Hoigne, J., Singlet Oxygen in Surface Waters .3. Photochemical Formation and Steady-State Concentrations in Various Types of Waters. *Environ. Sci. Technol.* **1986,** *20*, (4), 341-348.

44. Peterson, B. M.; McNally, A. M.; Cory, R. M.; Thoemke, J. D.; Cotner, J. B.; McNeill, K., Spatial and temporal distribution of singlet oxygen in Lake Superior. *Environ. Sci. Technol.* **2012,** *46*, (13), 7222-7229.

45. McNeill, K.; Canonica, S., Triplet state dissolved organic matter in aquatic photochemistry: Reaction mechanisms, substrate scope, and photophysical properties. *Environ. Sci. Process. Impacts* **2016**.

46. Faust, B. C., Aquatic photochemical reactions in atmospheric surface and marine waters, influences on oxidant formation and pollutant degradation. In *The Handbook of Environmental chemistry*, Boule, P., Ed. Springer-Verlag: Berlin, 1999; Vol. 2 (part L), pp 101-122.

47. Jasper, J. T.; Sedlak, D. L., Phototransformation of wastewater-derived trace organic contaminants in open-water unit process treatment wetlands. *Environ. Sci. Technol.* **2013,** *47*, (19), 10781-10790.

48. Leenheer, J. A.; Croue, J. P., Characterizing aquatic dissolved organic matter. *Environ. Sci. Technol.* **2003,** *37*, (1), 18A-26A.

49. Yamada, E.; Ohara, S.; Uehara, T.; Hirota, T.; Hatori, N.; Fuse, Y.; Aoki, S., Biodegradation of Dissolved Organic Matter (DOM) Released from Phytoplankton in Lake Biwa. *Anal. Sci.* **2012,** *28*, (7), 675-681.

50. Chen, M.; He, W.; Choi, I.; Hur, J., Tracking the monthly changes of dissolved organic matter composition in a newly constructed reservoir and its tributaries during the initial impounding period. *Environ. Sci. Pollut. Res. Int.* **2016,** *23*, (2), 1274-1283.

51. Wagner, S.; Riedel, T.; Niggemann, J.; Vahatalo, A. V.; Dittmar, T.; Jaffe, R., Linking the Molecular Signature of Heteroatomic Dissolved Organic Matter to Watershed Characteristics in World Rivers. *Environ. Sci. Technol.* **2015,** *49*, (23), 13798-13806.

52. Wilson, H. F.; Saiers, J. E.; Raymond, P. A.; Sobczak, W. V., Hydrologic Drivers and Seasonality of Dissolved Organic Carbon Concentration, Nitrogen Content, Bioavailability, and Export in a Forested New England Stream. *Ecosystems* **2013,** *16*, (4), 604-616.

53. Thurman, E. M.; Malcolm, R. L., Preparative Isolation of Aquatic Humic Substances. *Environ. Sci. Technol.* **1981,** *15*, (4), 463-466.

54. Serkiz, S. M.; Perdue, E. M., Isolation of Dissolved Organic-Matter from the Suwannee River Using Reverse-Osmosis. *Water Res.* **1990,** *24*, (7), 911-916.

55. Sun, L.; Perdue, E. M.; Mccarthy, J. F., Using Reverse-Osmosis to Obtain Organic-Matter from Surface and Ground Waters. *Water Res.* **1995,** *29*, (6), 1471-1477.

56. Schulten, H. R.; Schnitzer, M., A State-of-the-Art Structural Concept for Humic Substances. *Naturwissenschaften* **1993,** *80*, (1), 29-30.

57. Del Vecchio, R.; Blough, N. V., On the origin of the optical properties of humic substances. *Environ. Sci. Technol.* **2004,** *38*, (14), 3885-3891.

58. Sharpless, C. M.; Blough, N. V., The importance of charge-transfer interactions in determining chromophoric dissolved organic matter (CDOM) optical and photochemical properties. *Environ. Sci. Process. Impacts* **2014,** *16*, (4), 654-671.

59. Ma, J. H.; Del Vecchio, R.; Golanoski, K. S.; Boyle, E. S.; Blough, N. V., Optical Properties of Humic Substances and CDOM: Effects of Borohydride Reduction. *Environ. Sci. Technol.* **2010,** *44*, (14), 5395-5402.

60. Boyle, E. S.; Guerriero, N.; Thiallet, A.; Del Vecchio, R.; Blough, N. V., Optical properties of humic substances and CDOM: relation to structure. *Environ. Sci. Technol.* **2009,** *43*, (7), 2262-2268.

61. Mostafa, S.; Korak, J. A.; Shimabuku, K.; Glover, C. M.; Rosario-Ortiz, F. L., Relation between Optical Properties and Formation of Reactive Intermediates from Different Size Fractions of Organic Matter. *Advances in the Physicochemical Characterization of Dissolved Organic Matter: Impact on Natural and Engineered Systems* **2014,** *1160*, 159-179.

62. Aeschbacher, M.; Graf, C.; Schwarzenbach, R. P.; Sander, M., Antioxidant properties of humic substances. *Environ. Sci. Technol.* **2012,** *46*, (9), 4916-4925.

63. Nurmi, J. T.; Tratnyek, P. G., Electrochemistry of Natural Organic Matter. *Aq. Red. Chem.* **2011,** *1071*, 129-151.

64. Ratasuk, N.; Nanny, M. A., Characterization and quantification of reversible redox sites in humic substances. *Environ. Sci. Technol.* **2007,** *41*, (22), 7844-7850.

65. Scott, D. T.; McKnight, D. M.; Blunt-Harris, E. L.; Kolesar, S. E.; Lovley, D. R., Quinone moieties act as electron acceptors in the reduction of humic substances by humics-reducing microorganisms. *Environ. Sci. Technol.* **1998,** *32*, (19), 2984-2989.

66. Struyk, Z.; Sposito, G., Redox properties of standard humic acids. *Geoderma* **2001,** *102*, (3-4), 329-346.

67. Szulczewski, M. D.; Helmke, P. A.; Bleam, W. F., XANES spectroscopy studies of Cr(VI) reduction by thiols in organosulfur compounds and humic substances. *Environ. Sci. Technol.* **2001,** *35*, (6), 1134-1141.

68. Aeschbacher, M.; Vergari, D.; Schwarzenbach, R. P.; Sander, M., Electrochemical Analysis of Proton and Electron Transfer Equilibria of the Reducible Moieties in Humic Acids. *Environ. Sci. Technol.* **2011,** *45*, (19), 8385-8394.

69. Macalady, D. L.; Walton-Day, K., Redox Chemistry and Natural Organic Matter (NOM): Geochemists' Dream, Analytical Chemists' Nightmare. *Aq. Red. Chem.* **2011,** *1071*, 85-111.

70. Foti, M. C., Antioxidant properties of phenols. *The Journal of pharmacy and pharmacology* **2007,** *59*, (12), 1673-1685.

71. Canonica, S.; Laubscher, H. U., Inhibitory effect of dissolved organic matter on triplet-induced oxidation of aquatic contaminants. *Photoch. Photobiol. Sci.* **2008,** *7*, (5), 547-551.

72. Wenk, J.; von Gunten, U.; Canonica, S., Effect of dissolved organic matter on the transformation of contaminants induced by excited triplet states and the hydroxyl radical. *Environ. Sci. Technol.* **2011,** *45*, (4), 1334-1340.

73. Wenk, J.; Canonica, S., Phenolic antioxidants inhibit the triplet-induced transformation of anilines and sulfonamide antibiotics in aqueous solution. *Environ. Sci. Technol.* **2012,** *46*, (10), 5455-5462.

74. Bahnmuller, S.; von Gunten, U.; Canonica, S., Sunlight-induced transformation of sulfadiazine and sulfamethoxazole in surface waters and wastewater effluents. *Water Res.* **2014,** *57*, 183-192.

75. Janssen, E. M.; Erickson, P. R.; McNeill, K., Dual roles of dissolved organic matter as sensitizer and quencher in the photooxidation of tryptophan. *Environ. Sci. Technol.* **2014,** *48*, (9), 4916-4924.

76. Feitelso.J; Hayon, E.; Treinin, A., Photoionization of Phenols in Water - Effects of Light-Intensity, Oxygen, Ph, and Temperature. *J. Am. Chem. Soc.* **1973,** *95*, (4), 1025-1029.

77. Grabner, G.; Kohler, G.; Zechner, J.; Getoff, N., Pathways for Formation of Hydrated Electrons from Excited Phenol and Related Compounds. *Photoch. Photobiol.* **1977,** *26*, (5), 449-458.

78. Saito, F.; Tobita, S.; Shizuka, H., Photoionization of aniline in aqueous solution and its photolysis in cyclohexane. *J. Chem. Soc.Faraday Trans.***1996,** *92*, (21), 4177-4185.

79. Saito, F.; Tobita, S.; Shizuka, H., Photoionization mechanism of aniline derivatives in aqueous solution studied by laser flash photolysis. *Photoch. Photobiol. A* **1997,** *106*, (1-3), 119-126.

80. Wenk, J.; Aeschbacher, M.; Salhi, E.; Canonica, S.; von Gunten, U.; Sander, M., Chemical oxidation of dissolved organic matter by chlorine dioxide, chlorine, and ozone: effects on its optical and antioxidant properties. *Environ. Sci. Technol.* **2013,** *47*, (19), 11147-11156.

81. Wenk, J.; Aeschbacher, M.; Sander, M.; von Gunten, U.; Canonica, S., Photosensitizing and Inhibitory Effects of Ozonated Dissolved Organic Matter on Triplet-Induced Contaminant Transformation. *Environ. Sci. Technol.* **2015,** *49*, (14), 8541-8549.

Chapter 2

Probing the photosensitizing and inhibitory effects of dissolved

organic matter by using *N,N*-dimethyl-4-cyanoaniline (DMABN)

Frank Leresche, Urs von Gunten, Silvio Canonica

Abstract

Dissolved organic matter (DOM) can act as a photosensitizer and an inhibitor in the phototransformation of several nitrogen-containing organic contaminants in surface waters. The present study was performed to select a probe molecule that is suitable to measure these antagonistic properties of DOM. Out of nine studied nitrogen-containing aromatic compounds, 4-cyanoaniline, N,N-dimethyl-4-cyanoaniline (DMABN), sotalol (a β-blocker) and sulfadiazine (a sulfonamide antibiotic) exhibited a marked photosensitized transformation that could be substantially inhibited by addition of phenol as a model antioxidant. The photosensitized transformation of DMABN, the selected probe compound, was characterized in detail under UV-A and visible irradiation ($\lambda > 320$ nm) to avoid direct phototransformation. Low reactivity of DMABN with singlet oxygen was found (second-order rate constant $<2\times10^7$ $M^{-1}s^{-1}$). Typically at least 85% of the reactivity of DMABN could be inhibited by DOM or the model antioxidant phenol. The photosensitized transformation of DMABN mainly proceeded (>72%) through demethylation yielding N-methyl-4-cyanoaniline and formaldehyde as primary products. In solutions of standard DOM extracts and their mixtures the phototransformation rate constant of DMABN was shown to vary non-linearly with DOM concentration. Model equations describing the dependence of such rate constants on DOM and model antioxidant concentrations were successfully used to fit experimental data.

2.1 Introduction

Contaminants with electron-rich moieties in their molecular structure are susceptible to light-induced oxidation reactions in the aquatic environment. Experimental evidence accumulated during the last two decades points at excited triplet states of the dissolved organic matter (DOM) as key photooxidants responsible for these reactions. The contaminants that have been shown so far to react with excited triplet DOM (^{3}DOM*) and presumably undergo oxidative transformation comprise many compounds with phenolic or aniline moieties. They include phenols with simple electron-donating substituents,[1] bisphenol A,[2] phenolic phytoestrogens,[3, 4] ring- or *N*-substituted anilines,[5, 6] sulfonamide antibiotics,[6-8] aminopyrimidine antibiotics,[9, 10] phenylurea herbicides,[11] and further pesticides.[12] Model photosensitizers were used to mimick DOM chromophores that can generate oxidizing ^{3}DOM* upon photoexcitation, and laser flash photolysis studies with such photosensitizers were performed to further clarify the nature of the reaction between oxidizing ^{3}DOM* and various substrates in aqueous solution.[13-15] Second-order rate constants for the quenching of the excited triplet state of selected aromatic ketones by a series of substituted phenols were rationalized in terms of a one-electron transfer.[13] An analogous conclusion was drawn for the quenching of excited triplet methylene blue by substituted anilines.[15] However, the latter triplet state appeared to react through a proton-coupled electron transfer with substituted phenols.[15]

The radicals formed after the initial oxidation step, such as aniline radical cations, are relatively strong one-electron oxidants (standard reduction potentials of ≈1.0±0.2 V vs. NHE for a series of *para*-substituted aniline radical cations[16]). Nevertheless they may lose a proton, which leads to a significant loss in oxidative strength. The radical cations or their deprotonated counterparts can further react to yield stable transformation products, as can be deduced from the observed depletion of parent compound in photoirradiated samples (see the aforementioned examples of contaminants). It has been postulated that oxidation intermediates of the substrate, but primarily the radical cations, may react with electron-rich moieties in the DOM, leading to reformation of the substrate.[6] This hypothesis was put forward to explain the decrease in depletion rate constants observed for several aromatic contaminants and model compounds, particularly those containing aromatic amino groups, in steady-state irradiation experiments.[6, 17] This effect has been referred to as "inhibition of triplet-induced oxidation (or transformation)" and shown to also occur in model systems in which DOM had been replaced by phenols, either unsubstituted or bearing electron-donating substituents.[18] Recently, for partially oxidized humic substances a good correlation was found between the electron donating capacity (EDC) and the inhibitory effect on triplet-induced oxidation,[19] which corroborates the idea that antioxidant moieties of the DOM, in particular phenolic components, are responsible for the inhibition of triplet-induced oxidation.

The concept of inhibition of transformation as described above has been used to date to understand and describe the rates of direct and indirect phototransformations in surface waters-like conditions.[20, 21] The present study was conceived to further develop the application of this concept to DOM-induced indirect phototransformations in surface waters. We primarily aimed at selecting a model compound that may be employed as a probe to assess the inhibition of triplet-induced oxidation in natural waters. In the first part of the study, several organic compounds were photoirradiated in aqueous solutions containing DOM, with or without the addition of phenol as an antioxidant, to evaluate their suitability as model compounds. One of these compounds, namely *N,N*-dimethyl-4-cyanoaniline (abbreviated as DMABN from the alternative name 4-dimethylaminobenzonitrile) was selected and further investigated to characterize its direct and indirect phototransformation pathways. These investigations included the assessment of the role of singlet oxygen in the indirect phototransformation, the identification of the main reaction products as well as the measurements of the phototransformation rate constants of DMABN in aqueous solutions of DOM mixtures and surface water mixtures.

2.2 Materials and methods

2.2.1 Chemicals and Solutions

All chemicals were commercially available and used as received. A complete list of chemicals is given in the Supporting Information (SI), Text S2.1. All solutions were made in ultrapure water (resistivity 18.2 MΩ cm) obtained from a Barnstead Nanopure® purification system. Stock solutions of target compounds (≈500 μM) were kept in the dark at 4 °C. Suwannee River fulvic acid (SRFA, catalogue number 1S101F) and Pony Lake fulvic acid (PLFA, 1R109F) were purchased from the International Humic Substances Society (IHSS, St. Paul, Minnesota). Stock solutions of the fulvic acids were prepared at a concentration of ≈50 mg$_C$ L^{-1}. The concentration of the first stock solutions of PLFA and SRFA was quantified by total organic carbon (TOC) analysis, while the concentration of

subsequent stock solutions was determined spectrophotometrically using the first two stock solutions as references. Full characteristics of the fulvic acids are given in the SI, Table S2.1 and Figure S2.1.

2.2.2 Natural Waters

Natural water samples were taken on November 18th, 2014 from the outlet of Lake Greifensee (GW) (47.3727 N, 8.6557 E), a small eutrophic lake in northern Switzerland described in detail elsewhere,[22] and on November 14th, 2014 near the outlet of Etang de la Gruère (EG) (47.2376 N, 7.0494 E), a small pond surrounded by timbers and boggy wetland (surface area ~30'000 m^2). Waters were filtered on pre-washed 0.45 µm pore size cellulose nitrate filters and stored in the dark at 4 °C. GW had a rather low DOM concentration (3.3 mg$_C$ L^{-1}) and pH 8.3, while EG was high in DOM concentration (22.8 mg$_C$ L^{-1}) with a pH of 7.7 (see SI, Table S2.2 and Figure S2.2 for more physicochemical parameters).

2.2.3 Irradiation Experiments

Irradiations were performed using either a solar simulator (Heraeus model Suntest CPS$^+$) or a merry-go-round photoreactor (DEMA model 125, Hans Mangels, Bornheim-Roisdorf, Germany) equipped with a medium-pressure mercury lamp and a borosilicate glass cooling jacket. A detailed description of the irradiation equipment is available elsewhere.[1, 23, 24] The merry-go-round photoreactor (see sketch in the SI, Figure S2.3) was operated using two different setups. For irradiations of solutions containing DOM as a photosensitizer, a Heraeus Noblelight medium-pressure Hg lamp, model TQ 718, operated at 500 W, and a 0.15 M sodium nitrate filter solution were used, whereby irradiation wavelengths <320 nm were cut-off. Experiments with rose Bengal (RB) as a photosensitizer were done using a Heraeus Noblelight medium pressure Hg lamp, model TQ 150, operated at 150 W and a filter solution containing 0.25 M sodium nitrate and 0.05 M sodium nitrite, whereby irradiation wavelengths <370 nm were cut-off. In addition, for the latter experiments the cooling jacket was wrapped with two stainless steel wire cloths to reduce irradiance by a factor of ≈6. The spectral distributions of the light sources in the wavelength range of 250–450 nm (see SI, Figure S2.4) were measured using a calibrated spectroradiometer system model ILT950-UV (International Light Technologies, Peabody, MA, U.S.A.). The photon fluence rate, measured by chemical actinometry using an aqueous solution of *p*-nitroanisole (10 µM) and pyridine (600 µM) according to a well-established procedure[25] (see SI, Text S2.2 and Table S2.3), was determined to be 165 (±15%) µE m^{-2} s^{-1} for the solar simulator in the 290–400 nm range. This value is representative for conditions found at the surface of a natural water at midday of a clear-sky day between summer and autumn at 40° N latitude.[20]

Aqueous samples containing 5 µM of a single target compound, variable concentrations of DOM and, except for natural waters, 5 mM phosphate buffer (final solution pH 8.0) were irradiated at 25±1 °C in glass-stoppered quartz tubes (internal diameter 15 mm, external diameter 18 mm). The presence and concentration of additional components, such as phenol and individual photosensitizers or scavengers, is specified when discussing the results of the corresponding experiments. In the experiments using a mixture of GW and EG waters, the pH of GW was adjusted to the pH of EG using small amounts of hydrochloric acid (0.03M). Aliquot samples of 400 µL were taken at regular time intervals during the irradiation experiments.

2.2.4 Analytical Instrumentation

Total organic carbon analyses of solutions and water samples were done using a Shimadzu TOC-L CSH total organic carbon (TOC) analyzer. The concentration of target compounds (including furfuryl alcohol), phenol and the reaction product N-methyl-4-cyanoaniline were determined using high-performance liquid chromatography (HPLC). A complete description of the HPLC system and methods is given in the SI, Text S2.3 and Table S2.4. Electronic absorption spectra were recorded using an Agilent Cary 100 UV-Vis spectrophotometer. A Metrohm model 632 pH meter equipped with a Thermo scientific pH electrode (model Orion 8115SC) and a Metrohm model 712 conductometer were employed to measure pH and conductivity, respectively. Formaldehyde was quantified using the Hantzsch colorimetric titration method [26, 27] following the experimental details given in the SI, Text S2.4.

2.2.5 Determination of Rate Constants

Pseudo-first-order phototransformation rate constants, k_{TC}^{obs} (s^{-1}), for a given target compound (TC) were obtained by linear regression of its natural logarithmic relative residual concentration over irradiation time *t*, according to the following relationship:

$$\ln\left(\frac{[TC]_t}{[TC]_0}\right) = -k_{TC}^{obs} t \cdot \tag{2.1}$$

For merry-go-round irradiation experiments these rate constants were corrected for light screening caused by DOM, as described in the SI, Text S2.5. In the case of experiments performed in the presence of high phenol concentration, excited triplet quenching by phenol was included in the correction as described in the SI, Text S2.6. Rate constants for experiments conducted using RB as a photosensitizer were calculated according to the special procedure described in the SI, Text S2.7, which takes partial degradation of RB during irradiation into account. All corrected rate constants are termed as $k_{TC}^{obs,c}$. All data fits to non-linear model equations were performed using the software Origin, version 8.0 (Origin Lab) by applying the Levenberg-Marquardt minimization algorithm.

2.3   Results and Discussion

2.3.1   Screening Study on Selected Compounds Using Simulated Sunlight.

Selection of Compounds. Nine compounds (for chemical structures see SI, Figure S2.6) were selected to perform the first, exploratory part of the study. The compounds were chosen among possible candidates satisfying the following conditions: (1) Triplet-induced oxidation was known or expected to play a substantial role in their transformation under sunlight in surface waters; (2) Inhibition of triplet-induced oxidation by DOM or model antioxidants was known or expected. The first criterion applies to many actual organic contaminants and model compounds that are prone to oxidation (e.g., phenol and aniline derivatives, see *Introduction* section for a more detailed list) and for which the direct phototransformation is of minor relevance. The second criterion mainly applies to aromatic amines. Five of the selected compounds were substituted anilines: 4-Cyanoaniline, 4-*N,N*-dimethylcyanoaniline (both model compounds) and 4-aminobenzoic acid (a sunscreen agent), and in addition the two sulfonamide antibiotics sulfadiazine and sulfadimethoxine. Two aminopyrimidine derivatives used as antibiotics, namely trimethoprim and ormethoprim were also selected as representatives of heteroaromatic amines. Finally, the two β-blockers propranolol (a 2-naphthol derivative) and sotalol (a sulfonamide derivative) were selected to check if naphthol and sulfonamide functionalities also undergo inhibition of triplet-induced oxidation by DOM.

Phototransformation Experiments. The phototransformation kinetics of each selected compound dissolved in buffered ultrapure water, in slightly diluted natural water (GW 90%/ultrapure water 10% (vol/vol)), and in PLFA or SRFA solutions (5 mgC L^{-1}, pH8) was studied under simulated sunlight. For each compound, four additional samples of the same composition as aforementioned but amended with phenol (10 μM final concentration) were also investigated to assess a possible inhibition of transformation caused by this model antioxidant. Pseudo-first-order phototransformation rate constants for all compounds and solution compositions are represented in Figure 2.1. Rate constants for phototransformation in ultrapure water solution, which was assumed to represent direct phototransformation, were lower than overall phototransformation rate constants in the presence of DOM for many of the studied compounds. The electronic absorption spectra of the compounds (see SI, Figure S2.6) significantly overlap with the emission spectrum of the solar simulator (see SI, Figure S2.4). Values of the direct phototransformation quantum yields, determined as described elsewhere,[20] are displayed in Figure 2.1 and collected together with the phototransformation rate constants in Table S2.6 of the SI. They are generally on the order of 10^{-3} mol einstein^{-1} except for sotalol, which has by far the highest value of about 0.2 mol einstein^{-1}. This explains why, although the absorption spectrum of sotalol has a very small overlap with the spectrum of the solar simulator, its direct phototransformation rate constant was rather high.

The presence of DOM affected in most cases the phototransformation rate constants in comparison to buffered pure water solutions, except for 4-aminobenzoic acid, for which no significant effect was observed. However, the effect depended strongly on the type of DOM. In PLFA solutions and lake water (GW), a substantial increase in phototransformation rate constants with respect to ultrapure water was often observed. For SRFA such an increase was less prominent, and in some cases (sotalol, DMABN) even a decrease of the rate constant was observed.
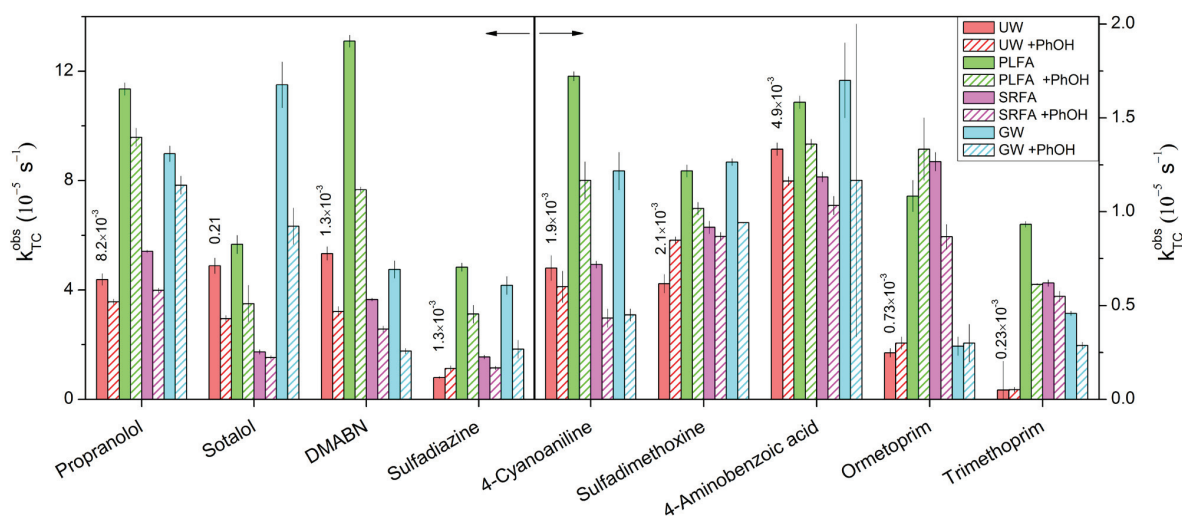
Figure 2.1. Phototransformation rate constants of the investigated compounds under simulated sunlight ($\lambda > 290$ nm). Bar colors designation (from left to right): Red for ultrapure water (UW, the quantum yield for direct phototransformation is given above the bar), green for Pony Lake fulvic acid (PLFA, 5.0 mg$_C$ L^{-1}), magenta for Suwannee River fulvic acid (SRFA, 5.0 mg$_C$ L^{-1}), and blue for 90% (vol) lake Greifensee water (GW, 3.0 mg$_C$ L^{-1}). Fully colored and hatched bars represent data from experiments conducted in the absence and presence of 10 µM phenol (PhOH), respectively. Error bars represent standard errors obtained from linear regression. Note the scale magnification on the right y-axis of the diagram for the compounds with lower photoreactivity.

Addition of phenol caused a marked reduction in phototransformation rate constants in PLFA and GW solution for the following compounds: sotalol, DMABN, sulfadiazine, 4-cyanoaniline and trimethoprim. In SRFA solution, addition of phenol caused a less important reduction in the photodegradation rate constants of these four compounds. A clear reduction of direct phototransformation rate constants (UW results) was observed only for sotalol and DMABN. A compound-specific discussion of the results from Figure 2.1 is given in the following.

Propranolol. This readily photoreactive β-blocker undergoes both direct [28, 29] and indirect phototransformation,[30] the latter probably due to ^{3}DOM*.[30] The rather small reduction of photoreactivity observed upon phenol addition makes it a weak indicator of the inhibitory effect. Moreover, the positive charge present on the protonated amino group at circumneutral pH (pK$_a$ = 9.5 [31]) favors the association of propranolol with DOM due to electrostatic attraction, and this could complicate its use as a model compound.

Sotalol. The photoreactivity pattern of sotalol is peculiar, because almost no photosensitization by PLFA could be observed, while SRFA strongly reduced the phototransformation rate constant with respect to UW. In contrast, an important enhancement of the rate constant was observed for GW, but the reason of this effect is unclear. This complex behavior hinders the use of sotalol as a model compound. The strong reduction of the phototransformation rate constants observed upon phenol addition indicates a possible role of DOM as an inhibitor, which should be considered in future studies on the phototransformation of sotalol.

DMABN. This compound exhibits the highest phototransformation rate constants among the investigated compounds in UW and PLFA solutions. The addition of phenol causes an important inhibitory effect, which is more pronounced in PLFA and GW solution than in SRFA solution. This behavior is similar to the one already observed for sulfadiazine and for sulfamethoxazole (for the latter compound regarding irradiation performed under UV-A) and extensively discussed in terms of the differential photosensitizing and inhibitory properties of the various DOMs.[20] Thus, DMABN appears to be a favorable model compound.

Sulfadiazine. The present results on this sulfonamide antibiotic are in agreement with data from previous studies,[6, 18, 20] which show the potential of this compound as a probe for the photosensitizing and inhibitory effects of DOM.

4-Cyanoaniline. The photoreactivity pattern of 4-cyanoaniline, including the effect of phenol addition, is similar to DMABN, its N,N-dimethylated derivative, but the absolute phototransformation rate constants are smaller by a factor of ≈4. Because of a less efficient phototransformation, it is less adequate than DMABN as a model compound.

Sulfadimethoxine. The phototransformation of sulfadimethoxine is enhanced at variable extents by the presence of DOM, in agreement with a previous study.[8] However, addition of phenol leads to a small reduction in phototransformation in the presence

of DOM, while a small increase is observed for UW solution. This small and ambiguous effect of phenol as well as the relatively slow phototransformation hinder the use of sulfadimethoxine as a convenient model compound.

4-Aminobenzoic acid. The direct phototransformation of this aniline appears to be the dominant mechanism. The absence of significant inhibition upon phenol addition makes this compound inadequate for the sake of the present study.

Ormetoprim. Indirect phototransformation appeared to be dominant in PLFA and SRFA solutions, but no inhibition effect upon phenol addition could be observed for this antibiotic, Due to the high structural similarity to trimethoprim, we refer to the following discussion regarding the possible phototransformation mechanisms.

Trimethoprim. The photoreactivity of trimethoprim, which is very low in UW, is highly enhanced by DOM, and the inhibitory effect of phenol is important. However, the rate constants are quite low. Previous experiments performed using the model photosensitizers 4-carboxybenzophenone (CBBP) and 2-acetonaphthone (2AN) [6, 17] showed that trimethoprim was highly reactive with triplet CBBP, which has a high one-electron reduction potential (1.83 V vs. NHE, calculated from data given elsewhere [32]) but reacted very slowly in the presence of 2AN, for which the reduction potential was calculated to be much lower (1.34 V vs. NHE). The low photoreactivity of trimethoprim, which is the main drawback against its use as a model compound, may thus be rationalized considering that ^{3}DOM* has an intermediate reduction potential compared to the excited triplet states of the model ketones.

Final Selection. Based on the aforementioned considerations we selected DMABN as the best-suited probe compound to be employed to explore the dual role of DOM as a photosensitizer and inhibitor of triplet-induced phototransformations. The main advantages of DMABN with respect to the other studied compounds are related to (a) a fast phototransformation and (b) an important inhibitory effect of phenol on the phototransformation. All potential probe compounds except trimethoprim (which was considered to be unsuited as a probe compound) exhibited a relatively important direct phototransformation under simulated sunlight. This drawback may be eliminated by using alternative UV irradiation conditions (λ>320 nm) which reduce the absorption rates by the probe compound itself. As will be shown in the following sub-sections, merry-go-round irradiation conditions with λ>320 nm turned out to be very appropriate for investigating DMABN. A further advantage of DMABN is its relatively simple molecular structure with absence of electric charge at circumneutral pH, and existing information about transient excited and radical species,[33] which are expected to facilitate mechanistic studies.

2.3.2 Characterization of the Indirect Phototransformation of DMABN in the Presence of DOM.

Photoirradiation of sample solutions was performed in this part of the study using the merry-go-round photoreactor setup with emission wavelength > 320 nm, a setup that has proven valuable in a number of previous studies.[1, 14, 20]

Estimation of the contribution of singlet oxygen and hydroxyl radical to the photosensitized transformation of DMABN. A high selectivity for a direct oxidation reaction by ^{3}DOM* is a basic condition that a model compound should fulfill within the objective of the present study. Therefore, it is central to characterize and quantify possible photoinduced side reactions of DMABN in the presence of DOM. An important photooxidant that is always present during DOM photosensitization is singlet (molecular) oxygen ($^1\Delta_g$), a reactive oxygen species that gives rise to photooxidations and photooxygenations of organic compounds in a highly selective manner.[34] The contribution of singlet oxygen to the phototransformation of DMABN was estimated by performing various irradiation experiments (see Table 2.1) comprising the addition of a selective singlet oxygen quencher (sodium azide, NaN$_3$), the use of heavy water as a solvent to increase the steady-state concentration of singlet oxygen by an order of magnitude,[35] the application of RB as a selective photosensitizer for the production of singlet oxygen,[36] and the use of furfuryl alcohol as a selective singlet oxygen probe compound.[37] For a detailed discussion of the rate constants given in Table 2.1 we refer to the SI, Text S2.10. Overall, the rate constants for the phototransformation of DMABN are only marginally affected by the presence of singlet oxygen quenchers or enhancers, even in the presence of RB as the photosensitizer. The maximum second-order rate constant for the reaction of DMABN with singlet oxygen was estimated to be 1.9×10^7 M^{-1} s^{-1} (from H$_2$O experiments) or 1.3×10^6 M^{-1} s^{-1} (from D$_2$O experiments). Also, the fractional contribution of singlet oxygen to the transformation of DMABN photosensitized by PLFA (5 mg$_C$ L^{-1}) was estimated to be lower than 5%. Additional experiments using 2-propanol (10 mM) as a hydroxyl radical scavenger confirmed that this reactive species had a negligible contribution to the transformation of DMABN in PLFA solutions.

Table 2.1. Phototransformation rate constants of DMABN and furfuryl alcohol (FFA) relevant to the characterization of the impact of singlet oxygen on the photosensitized transformation of DMABN.

Solution components [a]	$k_{DMABN}^{obs,c}$ (10⁻⁴ s⁻¹) [b]		$k_{FFA}^{obs,c}$ (10⁻⁴ s⁻¹) [b]		[¹O₂]ss (10⁻¹² M) [c]	
	H₂O	D₂O	H₂O	D₂O	H₂O	D₂O
none [d]	0.14±0.03	n.d. [e]	<0.05	n.d.	<0.04	n.d.
NaN₃ [d,f]	0.99±0.08	n.d.	n.d.	n.d.	n.d.	n.d.
PLFA [d]	5.9±0.6	6.3±0.6	1.9±0.2	18.8±1.2	1.6±0.2	22.7±1.5
PLFA, NaN₃ [d]	4.5±0.7	5.1±0.9	1.1±0.4	1.1±0.4	0.9±0.4	1.4±0.5
Rose Bengal (RB) [g,h]	1.80±0.11	1.92±0.17	11.6±0.4	125±30	9.7±0.3	150±36
RB, NaN₃ [g,h]	2.08±0.18	1.30±0.17	0.95±0.19	0.96±0.2	0.79±0.16	1.2±0.3

Notes:

[a] In addition to DMABN ([DMABN]₀=5.0 µM), FFA ([FFA]₀=5.0 µM) and phosphate (5.0 mM, pH 8.0). Initial concentrations of further components: [PLFA]₀=5.0 mg$_C$ L⁻¹; [RB]₀=2.0 µM; [NaN₃]₀=10.0 mM.

[b] No correction performed for the constants given in the first two rows.

[c] Steady-state concentration of singlet oxygen determined as $k_{FFA}^{obs,c} / k_{FFA,^1O_2}^r$ (see text for details).

[d] Irradiation setup with 500 W MP Hg lamp and filter solution for λ>320 nm.

[e] n.d.: not determined.

[f] Solution did not contain FFA.

[g] Irradiation setup with 150 W MP Hg lamp, filter solution for λ>380 nm and steel wire cloth filter.

[h] All rate constants corrected for the photodegradation RB during irradiation (see SI, Text S2.7).

Photosensitization and inhibition by fulvic acids, and DOM concentration dependence. Figure 2.2 shows the dependence of the phototransformation rate constant of DMABN on DOM concentration. Direct phototransformation was drastically reduced with respect to the solar simulator setup, and photosensitization by DOM was dominant for [DOM]>≈0.2 mg$_C$ L^{-1}. Overall a steady, non-linear increase in rate constant with increasing DOM concentration for both fulvic acids is apparent, while at low DOM concentration (<1.0 mg$_C$ L^{-1}) a linear relationship is observed (see inset in Figure 2.2). The dependence of the rate constants on DOM concentration is similar to that of sulfadiazine in PLFA solutions[20] and of tryptophan in solutions of various humic substances.[21] This behavior was interpreted in terms of the antagonistic photosensitizing and inhibitory effects of DOM on ^{3}DOM*-induced transformation of the target compounds.
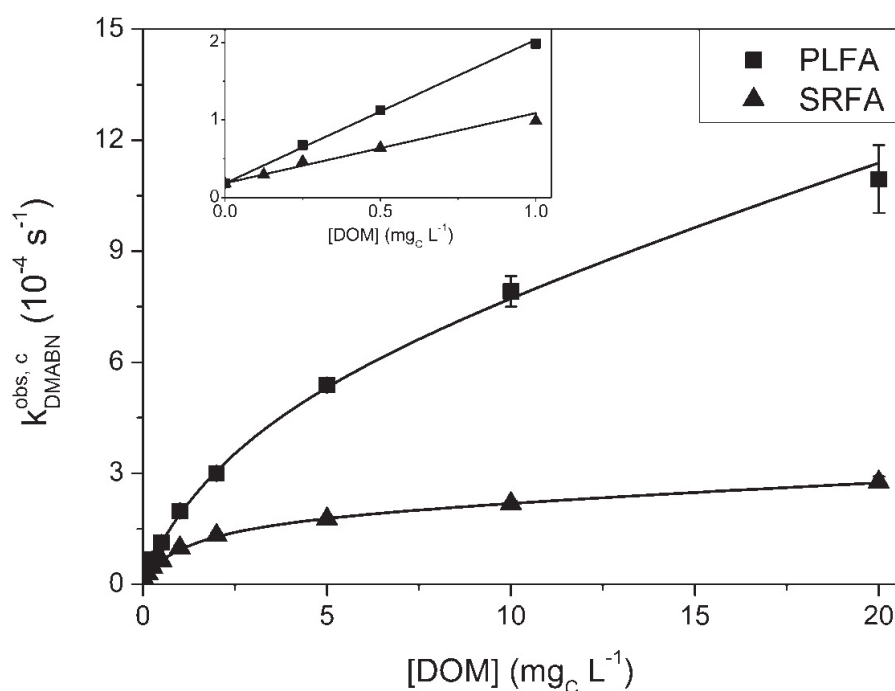

Figure 2.2. Effect of DOM concentration (Pony Lake fulvic acid (PLFA, black squares); Suwannee River fulvic acid (SRFA, black triangles)) on the corrected pseudo-first-order phototransformation rate constant of DMABN (5 µM initial concentration). Results obtained from merry-go-round photoreactor experiments (λ>320 nm). Lines are non-linear fits to equation 2.2. Error bars represent 95% confidence intervals obtained from linear regression. Inset: enlarged view for low DOM concentrations (≤1.0 mg$_C$ L^{-1}) with linear regression lines.

To analyze the rate constant data from Figure 2.2, a two-channel reaction model for inhibition of triplet-induced oxidation [17] was extended to include photosensitization by DOM. The derivation of the kinetic equations for such an extended model is given in detail the SI, Text S2.8. The resulting pseudo-first-order rate constant for the photosensitized transformation, k_{TC}^{sens}, is described by equation 2.2, where the first term on the right-hand side, β[DOM], accounts for a photosensitization directly proportional to the DOM concentration, and the fractional term accounts for inhibition.

$$k_{TC}^{sens}(\text{DOM}) = \beta[\text{DOM}]\frac{1+[\text{DOM}]/[\text{DOM}]_{1/2}(1-f)}{1+[\text{DOM}]/[\text{DOM}]_{1/2}} \tag{2.2}$$

In equation 2.2, β is a proportionality factor that accounts for photoinduced formation of ^{3}DOM*, deactivation of ^{3}DOM* and its reaction with the target compound, f is the fraction of photosensitized reaction intermediates susceptible to inhibition by DOM,[17] and [DOM]$_{1/2}$ is the concentration of DOM required to achieve half of the maximum rate constant reduction obtainable by inhibition. According to equation 2.2, two limiting cases for k_{TC}^{sens} are possible: (a) At low DOM concentration ([DOM]<<[DOM]$_{1/2}$), the

fraction in equation 2.2 becomes unity and the rate constant reduces the mere photosensitization term, as given by equation 2.3. (b) At high DOM concentration ([DOM]>>[DOM]$_{1/2}$), equation 2.4 is obtained.

$$k_{TC}^{sens} = \beta[\text{DOM}] \tag{2.3}$$

$$k_{TC}^{sens} = \beta[\text{DOM}]_{1/2} + \beta[\text{DOM}](1-f) \tag{2.4}$$

Interestingly, for 100% formation of intermediates susceptible to inhibition (i.e., f=1) equation 2.4 reduces to the constant term β[DOM]$_{1/2}$, whereas in all other cases an asymptotic linear increase with increasing DOM concentrations is predicted with β(1-f) as slope.

To fit the data in Figure 2.2, the corrected phototransformation rate constant was assumed to consist of the contributions from direct (k_{TC}^{dir}) and indirect (k_{TC}^{sens}) phototransformation, as given by equation 2.5.

$$k_{TC}^{obs,c} = k_{TC}^{dir} + k_{TC}^{sens} \tag{2.5}$$

Equations 2.2 and 2.3, with the addition of a constant offset accounting for k_{TC}^{dir}, were used to fit the whole rate constant data and the data for [DOM]≤1.0 mg$_C$ L^{-1}, respectively. The assumption of a constant k_{TC}^{dir} is not strictly valid, because k_{TC}^{dir} is probably also affected by DOM inhibition (see the effect of phenol shown in Figure 2.1), but is an acceptable approximation considering the very small value of k_{TC}^{dir}. As demonstrated by the trend lines in Figure 2.2 and the numerical results collected in Table 2.1, both equations provided good fits.

Table 2.1. Parameters for the photosensitizing and inhibitory effects of PLFA and SRFA on the phototransformation of DMABN obtained from data fitting. [a]

Data series	β_1 [b] (10^{-4} L mg_C^{-1} s^{-1}) (DOM$_1$=PLFA)	[DOM$_1$]$_{1/2}$ [c] (mg_C L^{-1})	β_2 [b] (10^{-4} L mg_C^{-1} s^{-1}) (DOM$_2$=SRFA)	[DOM$_2$]$_{1/2}$ [c] (mg_C L^{-1})	[PhOH]$_{1/2}$ (μM)	f [d]	Adjusted R^2
PLFA only data (Figure 2.2)	2.14 ±0.19	3.2 ±1.2	n.a. [e]	n.a.	n.a.	0.86 ±0.06	0.999
SRFA only data (Figure 2.2)			1.21 ±0.15	1.5 ±0.4	n.a.	0.963 ±0.015	0.998
PLFA (5 mg_C L^{-1}) and SRFA data (Figure 2.3)	2.14 (fixed)	4.8 ±0.2	1.21 (fixed)	1.48 ±0.15	n.a.	0.967 ±0.008	0.994
PLFA (5 mg_C L^{-1}) and PhOH data (Figure 2.4)	2.14 (fixed)	3.3 ±1.0	n.a.	n.a.	3.7 ±1.2	0.85 (fixed)	0.961
PLFA (5 mg_C L^{-1}) and PhOD [e] data (Figure 2.4)	2.14 (fixed)	3.4 ±0.3	n.a.	n.a.	4.4 ±0.6	0.85 (fixed)	0.989
PLFA (5 mg_C L^{-1}) and SRFA difference data (Figure 2.4)	2.14 (fixed)	4.5 ±0.3	n.a.	1.5 ±0.3	n.a.	0.93 ±0.02	0.998

Notes:

[a] Errors indicate 95% confidence intervals obtained from the non-linear regressions using equation 2.2 (data from Figure 2.2), equation 2.6 (data from Figure 2.3), or equation 2.7 (data from Figure 2.4).

[b] Proportionality factor accounting for the photosensitizing effect of DOM (see equation 2.2): β_1 for PLFA and β_2 for SRFA.

[c] Concentration of DOM (PLFA or SRFA) required to achieve half of the maximum rate constant reduction obtainable by inhibition (see equation 2.2).

[d] Fraction of photosensitized reaction intermediates susceptible to inhibition by DOM (see equation 2.2).

[e] n.a.: not applicable.

[f] Mono deuterated PhOH, resulting from proton exchange in the solvent D_2O.

Photosensitization and inhibition in solutions with mixed DOMs and in natural water mixtures. In surface freshwaters the composition of DOM is often the result of mixing of waters containing DOM from differing sources. To show exemplarily how such mixing processes may affect the inhibitory properties of DOM, irradiation experiments were performed utilizing a fixed concentration of primarily photosensitizing and weakly inhibitory DOM, and variable concentrations of weakly photosensitizing and strongly inhibitory DOM. PLFA and the DOM in GW were employed as the mainly photosensitizing (and poorly inhibitory) DOMs, according to the results of previous studies.[17-19] To be noted is the mainly autochtonous origin of these materials, which correlates with their relatively low specific absorption coefficient (SUVA254, measured at the wavelength of 254 nm, see SI, Tables S2.1 and S2.2). SRFA and the DOM in EG were selected as strongly inhibitory DOM due to their primarily allochtonous origin. Both exhibit higher specific absorption coefficient than PLFA and the DOM in GW, indicating higher aromaticity.
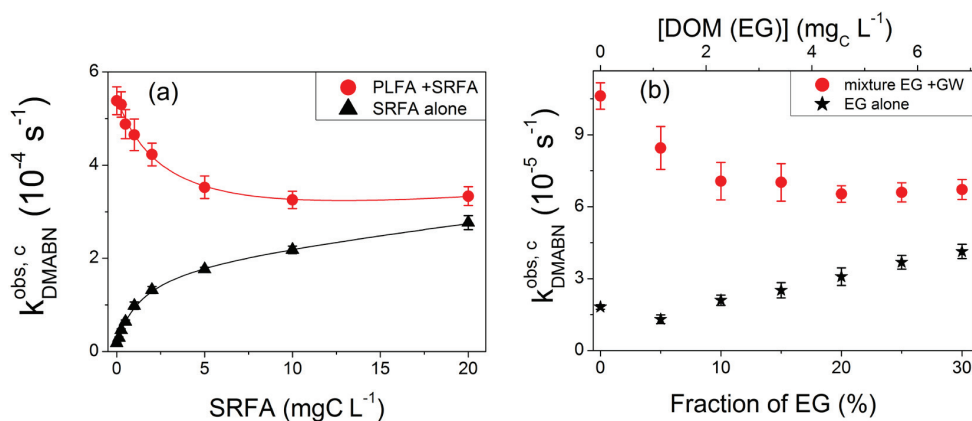

Figure 2.3. Pseudo-first-order phototransformation rate constants of DMABN in (a) solutions containing 0 mg_C L^{-1} (black triangles, same data as in Figure 2.2) or 5 mg_C L^{-1} (red circles) of Pony Lake fulvic acid (PLFA) and varying concentrations of Suwannee River fulvic acid (SRFA), and (b) solutions containing a constant volumetric fraction of GW (0% (black stars) or 68.5% (red circles), the latter corresponding to 2.26 mg_C L^{-1}), varying volumetric fractions of EG and ultrapure water (the remaining volumetric fraction to give 100%). Results obtained from merry-go-round photoreactor experiments (λ>320 nm). Lines are non-linear fits to equation 2.2 (black) and equation 2.6 (red). Error bars represent 95% confidence intervals from linear regressions (equation 2.1).

Figure 2.3 shows that an increase in concentration of strongly inhibiting DOM leads to a decrease in the rate constant for the phototransformation of DMABN. The complete rate constant equation describing photosensitizing and inhibitory effects in a mixture of two different DOMs (derived in analogy to equation 2.2, see SI, Text S2.9) can be formulated as:

$$k_{TC}^{sens}(\mathrm{DOM_1}, \mathrm{DOM_2}) = \left(\beta_1[\mathrm{DOM_1}] + \beta_2[\mathrm{DOM_2}]\right) \frac{1 + \{[\mathrm{DOM_1}]/[\mathrm{DOM_1}]_{1/2} + [\mathrm{DOM_2}]/[\mathrm{DOM_2}]_{1/2}\}(1-f)}{1 + [\mathrm{DOM_1}]/[\mathrm{DOM_1}]_{1/2} + [\mathrm{DOM_2}]/[\mathrm{DOM_2}]_{1/2}} \quad (2.6)$$

Analogous equations can be derived for a higher number of differing DOMs (see SI, Text S2.9, equation S2.20). Rate constant data for solutions containing PLFA ($\equiv$DOM$_1$) and SRFA ($\equiv$DOM$_2$) (Figure 2.3a, red circles) were fit to equation 2.6 with the fixed parameters [PLFA]=5 mg_C L^{-1}, β_1 and β_2 (from the fittings to equation 2.2, see Table 2.1), the three fitting parameters [PLFA]$_{1/2}$, [SRFA]$_{1/2}$ and f, and [SRFA] as the independent variable. The fit was excellent and the obtained values of the fitting parameters (See Table 2.1) were in good agreement with those obtained from single DOM series (Figure 2.2). Attempts to extract reasonably accurate fitting parameters from the data of the natural water mixtures failed, probably due to the restricted range of studied DOM concentrations and the low rate constants. However, qualitative trends are similar as observed for the PLFA/SRFA mixtures. Note that in the absence of a mutual inhibitory effect, the phototransformation rate constants would be additive, and a steady increase would be expected. Such a scenario (with no inhibition) was tested for mixtures of GW and EG by using furfuryl alcohol (FFA) as a target compound. FFA is known to undergo photosensitized oxygenation by singlet molecular oxygen, and its phototransformation should only reflect the photosensitizing properties of DOM, while inhibitory effects should be absent. The observed linear and identical increases (with the same slope) of the phototransformation rate constant of FFA in the presence and absence of GW fully confirmed the expectations (see SI, Figure S2.7).

Inhibitory effect of phenol as a model antioxidant. Phenolic compounds have been shown to cause inhibition of triplet-induced oxidations analogously to DOM and have therefore been used as model inhibitors.[18, 20] To further characterize the inhibitory process in the indirect phototransformation of DMABN, phenol was employed at variable concentrations to inhibit transformation of DMABN photosensitized by 5.0 mg_C L^{-1} of PLFA (see Figure 2.4).
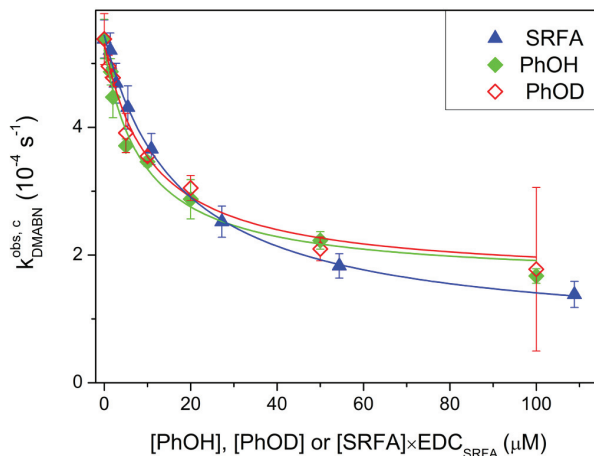

Figure 2.4. Corrected and normalized pseudo-first-order rate constants for the transformation of DMABN photosensitized by Pony Lake fulvic acid (PLFA, 5.0 mg_C L^{-1}) and their dependence on the concentration of added phenol (PhOH, green diamonds) and mono-deuterated phenol (PhOD, open red diamonds). PhOD experiments were performed in D_2O solutions (D atom fraction of ~94%). Results obtained from merry-go-round photoreactor experiments (λ>320 nm). The rate constants were corrected for quenching of ^{3}PLFA* by phenol (see SI, Text S2.6). For comparison, the net inhibitory effect of Suwannee River fulvic acid (SRFA) in terms of concentration of available electrons (see text for calculations) is also shown. Lines are non-linear fits to equation 2.7 (phenol data) or equation 2.6 modified by subtracting term 2.8 (SRFA data, see text). Error bars represents 95% confidence interval from linear regressions (equation 2.1).

The rate constants for DMABN phototransformation decreased nonlinearly with increasing phenol concentration, approaching a reduction of about 60% at 100 μM phenol. Note that the rate constants displayed in Figure 2.4 were corrected for quenching of ^{3}PLFA* by phenol, which was measured using furfuryl alcohol as a probe compound and the methods described in the SI, Text S2.6. The effect of adding deuterated phenol (experiments performed in D_2O) was the same as for phenol. This constitutes an important piece of evidence that the reduction of the oxidation intermediate of DMABN, probably the DMABN$^{\cdot+}$ radical cation, does not involve a hydrogen atom abstraction from the phenolic functional group in the rate-determining reaction step. The data of the phenol series (with phenol (PhOH) or its mono-deuterated form (PhOD)) from Figure 2.4 fitted well to equation 2.7, which was derived from equation 2.6 by setting PLFA≡DOM$_1$ and substituting DOM$_2$ with PhOH (or PhOD). Since phenol has no photosensitizing effect, β_2=0.

$$k_{TC}^{sens}(\mathrm{PLFA, PhOH}) = \beta_1[\mathrm{PFLA}]\frac{1 + \left\{[\mathrm{PLFA}]/[\mathrm{PLFA}]_{1/2} + [\mathrm{PhOH}]/[\mathrm{PhOH}]_{1/2}\right\}(1-f)}{1 + [\mathrm{PLFA}]/[\mathrm{PLFA}]_{1/2} + [\mathrm{PhOH}]/[\mathrm{PhOH}]_{1/2}} \qquad (2.7)$$

Among the obtained fitting parameters, collected in Table 2.1, [PLFA]$_{1/2}$ values were very similar to the fitting of PLFA only data (Figure 2.2, equation 2.2). To compare quantitatively the inhibitory effect of phenol and antioxidant moieties in SRFA, the concentration of the latter antioxidant moieties was calculated by multiplying the electron donating capacity (EDC) of SRFA with its concentration. The published EDC value for pH 7 and an oxidizing potential of E_h=+0.73 V,[38] i.e., 2.848 mmol$_{e-}$ g_{SRFA}^{-1} (corresponding to 5.47 μmol$_{e-}$ mg_C^{-1}, considering the carbon content of SRFA given in the same reference) was used for this purpose. The obtained average [SRFA]$_{1/2}$×EDC value (≈8.2 μmol$_{e-}$ L^{-1}) is about twice as large as [PhOH]$_{1/2}$, indicating an overall lower reactivity of the phenolic moieties of SRFA compared to phenol. Figure 2.4 also shows, for comparison with the phenol data, the rate constants from Figure 2.3 corrected by subtracting the following term, which quantifies the contribution of SRFA to the photosensitized transformation of DMABN:

$$\beta_2[DOM_2]\frac{1+\{[DOM_1]/[DOM_1]_{1/2}+[DOM_2]/[DOM_2]_{1/2}\}(1-f)}{1+[DOM_1]/[DOM_1]_{1/2}+[DOM_2]/[DOM_2]_{1/2}} \tag{2.8}$$

These corrected rate constants, represented by the blue triangles in Figure 2.4, show a similar trend as the lines describing the inhibitory effect of phenol. At low concentrations, the inhibitory effect of SRFA appears to be less important than for PhOH/PhOD, which is reflected in the higher $[SRFA]_{1/2}\times EDC$ value than $[PhOH]_{1/2}$ as discussed above. At higher concentrations, SRFA seems to be at least as an efficient inhibitor as phenol, which may be related to the higher value of f obtained for the fittings regarding SRFA. An accurate quantitative comparison appears to be difficult due to the uncertainty of the various parameters used in the model. Overall, one can affirm that $[SRFA]_{1/2}\times EDC$ is of the same order of magnitude as $[PhOH]_{1/2}$. This confirms the conclusions of a similar comparison performed using sulfonamide data[18] and concurs with the antioxidant hypothesis as the cause of inhibition for the photosensitized transformation of DMABN.

Characterization of product formation. The main peak appearing in the HPLC chromatograms (see SI, Figure S2.8) during the photo-transformation of DMABN was identified as its mono-demethylated derivative, 4-methylaminobenzonitrile (MABN), by comparison of its HPLC retention time and UV absorption spectra with those of commercially available MABN. The kinetics of DMABN depletion and MABN formation during irradiation in the presence of PLFA or RB as photosensitizers are shown in Figure 2.5. The efficiency of formation of MABN from DMABN transformation (moles of MABN formed per mole of DMABN consumed), expressed as the selectivity factor γ, can be estimated by assuming the following system of reactions (see also SI, Scheme S2.3), which considers the transformation of DMABN to either MABN (equation 2.9) or other products (equation 2.10) in a first step, and transformation of MABN to further products (equation 2.11).

$$DMABN \xrightarrow{\ k_1\times\gamma\ } MABN \tag{2.9}$$

$$DMABN \xrightarrow{\ k_1\times(1-\gamma)\ } products_1 \tag{2.10}$$

$$MABN \xrightarrow{\ k_2\ } products_2 \tag{2.11}$$

As shown in the SI, Text S2.13, the kinetics of MABN in a solution initially containing DMABN as the only target compound can be described by the following equation:

$$[MABN]=[DMABN]_0\,\gamma\,\frac{k_1}{k_2-k_1}\left(e^{-k_1t}-e^{-k_2t}\right) \tag{2.12}$$

The pseudo-first-order rate constants k_1 and k_2 for the phototransformation of DMABN and MABN, respectively, were determined in two separate experiments initially containing 5.0 µM of DMABN (see data in Figure 2.5) or MABN (see SI, Figure S2.9). The selectivity factor γ was obtained by fitting the [MABN] data (Figure 2.5) to equation 2.12 (γ was the only fitting parameter). For the kinetic experiments illustrated in Figure 2.5, γ values of 72±4% and 81±2% were obtained for the PLFA and RB systems, respectively.
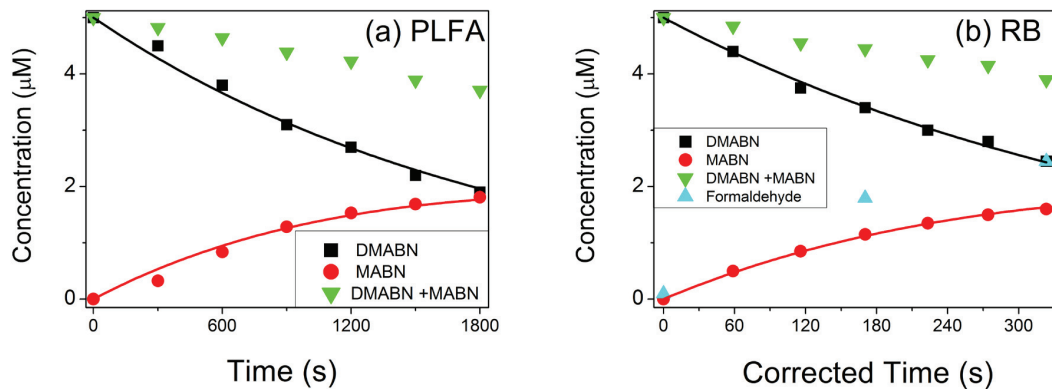
Figure 2.5. Phototransformation kinetics of DMABN (5.0 μM initial concentration) and concomitant *N*-methyl-4-cyanoaniline (MABN) formation in the presence of (a) $5mg_C$ L^{-1} PLFA and (b) 5 μM RB (time axis scale corrected to account for RB photobleaching, see SI, Text S2.7). Results obtained from merry-go-round photoreactor experiments with (a) λ>320 nm, and (b) λ>370 nm. Green triangles represent the sum of DMABN and MABN. Black lines represent non-linear fits to a first-order rate law. Red lines represent non-linear fits to equation 2.12. In (b) blue triangles represent formaldehyde concentration.

The loss of the methyl group upon photosensitized transformation can be rationalized in terms of the reaction mechanisms presented in Scheme 2.1. Derivatives of the *N,N*-dimethylaniline radical cation, such as $DMABN^{·+}$, are known to tautomerize to yield a carbon-centered radical,[39] which can then deprotonate and react with oxygen to form a peroxyl radical.[40] The latter releases superoxide and the so formed imine is hydrolyzed yielding the demethylated aniline and formaldehyde. The formation of formaldehyde was confirmed in the present irradiation experiments using RB as a photosensitizer (Figure 2.5b). Though the mechanism predicts 1:1 formation of MABN and formaldehyde, the concentration of the latter after 30% and 50% transformation of DMABN was higher than the concentration of MABN. This is probably due to the transformation of MABN yielding 4-cyanoaniline and formaldehyde.
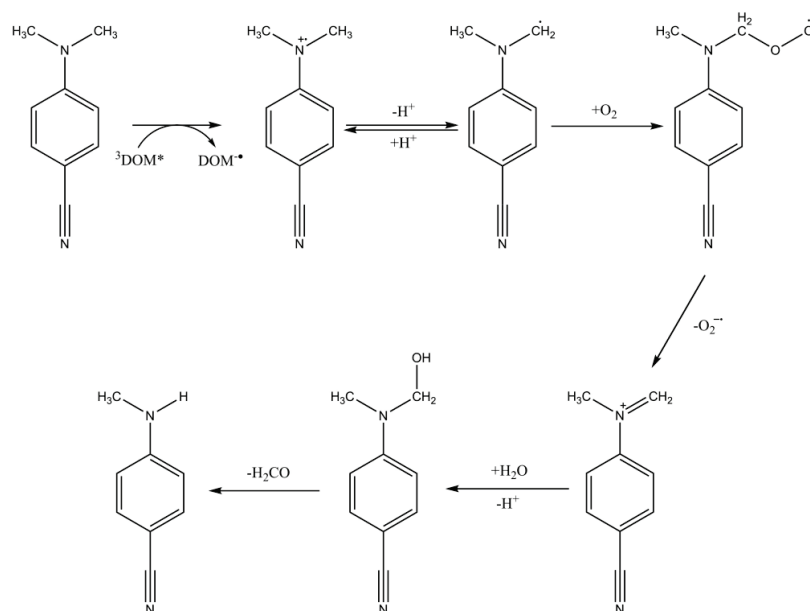
Scheme 2.1. Proposed main reaction pathway for the transformation of DMABN photosensitized by DOM.

Because γ values are lower than unity (by 10–30%), a fraction of DMABN is expected to react through another, still unknown reaction pathway compared to Scheme 2.1. It has to be noted that γ has a different meaning from *f*, which is the fraction of DMABN molecules that can be inhibited in their transformation by the presence of antioxidants. The fact that γ and *f* values are similar does not imply that the non-inhibiting reaction channel corresponds to the process yielding reaction products other than MABN. Supplementary experiments performed with PLFA as the photosensitizer (conditions as for the data in Figure 2.5) with the addition of phenol as an antioxidant revealed that the selectivity factor γ remained constant in the phenol concentration range of 0–50 μM (see SI, Table S2.7). This result concurs with the assumption that antioxidants are exclusively involved in the reduction of $DMABN^{·+}$ to the parent compound and do not affect the subsequent reactions.

2.4 Environmental implications

The previously developed two-channel model accounting for partial inhibition of triplet-induced oxidation[17] was employed successfully in this study to describe the photosensitized transformation kinetics of DMABN in aqueous solutions containing binary mixtures of DOM. Equation 2.6 could be useful in the prediction of rate constants for the photosensitized transformation of aromatic amine contaminants in surface waters that are affected by organic matter input from various origins. Taking the binary mixture of PLFA and SRFA as characterized in this study as an example, one can construct surface plots as shown in Figure 2.6a. In addition to the features already discussed for two-dimensional plots (Figures 2.2 and 2.3), Figure 2.6a also comprises contour lines, which

indicate that a given value of rate constant corresponds to a set of different concentrations of both DOMs. It can be seen that, moving on a contour line from left to right, the concentration of PLFA is only slightly reduced, while there is a big change in SRFA concentration. A situation corresponding to such a scenario was possibly observed for the phototransformation rate constant of sulfadiazine in water samples taken along the course of a river.[20] In that study, only a little increase in sulfadiazine phototransformation rate constant was observed in going from a low DOC pristine water near the source of the river to an increasingly wastewater-impacted river water with higher DOC. An alternative graphical representation of the same data displayed in Figure 2.6a, is shown in Figure 2.6b, in which the fraction X_1=[DOM$_1$]/([DOM$_1$]+[DOM$_2$]) of a the first DOM in the mixture ($0 \leq X_1 \leq 1$) and the total DOM concentration DOC=[DOM$_1$]+[DOM$_2$] were chosen as the independent variables (see SI, Text S2.14). For a given constant fraction X_1, dependencies of k_{TC}^{sens} vs. DOC have a similar curved shape as and are between the two lines shown in Figure 2.2. Moreover, for a constant DOC and varying X_1, convex lines connecting the two extremes in reactivity are observed. We envisage the application of the present concept and graphs to estimate the variability in photoreactivity of compounds such as DMABN (i.e., those affected by DOM-induced photosensitization and inhibition) in surface waters strongly impacted by wastewater effluents from varying degrees of wastewater treatment. However, we would like to point out that the considerations made in this section are restricted to DOM-photosensitized transformations following the sensitization and inhibition models applied in this study. In case of important direct phototransformation or other photosensitized reaction channels, as recently addressed by McNeill and coworkers,[21] a more comprehensive approach has to be adopted.
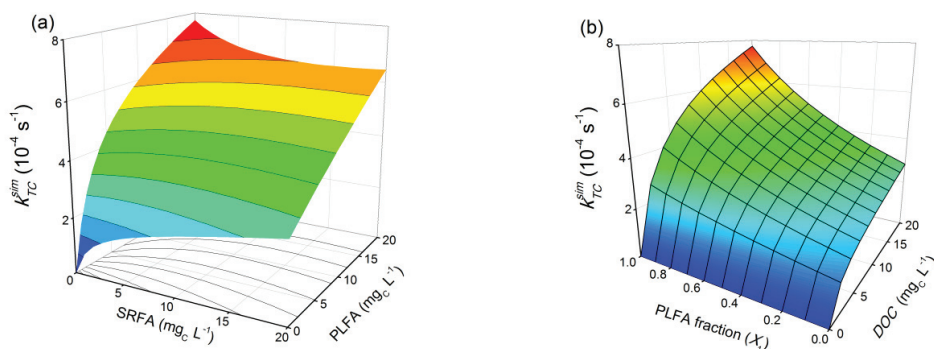

Figure 2.6. Surface plots representing the DOM-concentration dependence of the rate constant (k_{TC}^{sim}) for the transformation of a target contaminant photosensitized and inhibited by a binary mixture of DOM (PLFA and SRFA). Parameter values for PLFA and SRFA determined in this study for DMABN (see Table 2.1, third line) were applied. (a) Representation of equation 2.6, where contour lines (for fixed k_{TC}^{sim} values) are given on the surface plot and shown as projections on the x-y plane; (b) Representation of equation S2.34 (see text and SI, Text S2.14).

2.5   ACKNOWLEDGMENTS

2.6 References for the chapter 2

1. Canonica, S.; Jans, U.; Stemmler, K.; Hoigné, J., Transformation kinetics of phenols in water: Photosensitization by dissolved natural organic material and aromatic ketones. *Environ. Sci. Technol.* **1995,** *29*, (7), 1822-1831.
2. Chin, Y. P.; Miller, P. L.; Zeng, L. K.; Cawley, K.; Weavers, L. K., Photosensitized degradation of bisphenol A by dissolved organic matter. *Environ. Sci. Technol.* **2004,** *38*, (22), 5888-5894.
3. Felcyn, J. R.; Davis, J. C. C.; Tran, L. H.; Berude, J. C.; Latch, D. E., Aquatic photochemistry of isoflavone phytoestrogens: Degradation kinetics and pathways. *Environ. Sci. Technol.* **2012,** *46*, (12), 6698-6704.
4. Kelly, M. M.; Arnold, W. A., Direct and indirect photolysis of the phytoestrogens genistein and daidzein. *Environ. Sci. Technol.* **2012,** *46*, (10), 5396-5403.
5. Canonica, S.; Freiburghaus, M., Electron-rich phenols for probing the photochemical reactivity of freshwaters. *Environ. Sci. Technol.* **2001,** *35*, (4), 690-695.
6. Canonica, S.; Laubscher, H. U., Inhibitory effect of dissolved organic matter on triplet-induced oxidation of aquatic contaminants. *Photochem. Photobiol. Sci.* **2008,** *7*, (5), 547-551.
7. Boreen, A. L.; Arnold, W. A.; McNeill, K., Triplet-sensitized photodegradation of sulfa drugs containing six-membered heterocyclic groups: Identification of an SO_2 extrusion photoproduct. *Environ. Sci. Technol.* **2005,** *39*, (10), 3630-3638.
8. Guerard, J. J.; Chin, Y. P.; Mash, H.; Hadad, C. M., Photochemical fate of sulfadimethoxine in aquaculture waters. *Environ. Sci. Technol.* **2009,** *43*, (22), 8587-8592.
9. Luo, X. Z.; Zheng, Z.; Greaves, J.; Cooper, W. J.; Song, W. H., Trimethoprim: Kinetic and mechanistic considerations in photochemical environmental fate and AOP treatment. *Water Res.* **2012,** *46*, (4), 1327-1336.
10. Guerard, J. J.; Chin, Y. P., Photodegradation of ormetoprim in aquaculture and stream-derived dissolved organic matter. *J. Agric. Food Chem.* **2012,** *60*, (39), 9801-9806.
11. Gerecke, A. C.; Canonica, S.; Müller, S. R.; Schärer, M.; Schwarzenbach, R. P., Quantification of dissolved natural organic matter (DOM) mediated phototransformation of phenylurea herbicides in lakes. *Environ. Sci. Technol.* **2001,** *35*, (19), 3915-3923.
12. Zeng, T.; Arnold, W. A., Pesticide photolysis in prairie potholes: Probing photosensitized processes. *Environ. Sci. Technol.* **2013,** *47*, (13), 6735-6745.
13. Canonica, S.; Hellrung, B.; Wirz, J., Oxidation of phenols by triplet aromatic ketones in aqueous solution. *J. Phys. Chem. A* **2000,** *104*, (6), 1226-1232.
14. Canonica, S.; Hellrung, B.; Müller, P.; Wirz, J., Aqueous oxidation of phenylurea herbicides by triplet aromatic ketones. *Environ. Sci. Technol.* **2006,** *40*, (21), 6636-6641.
15. Erickson, P. R.; Walpen, N.; Guerard, J. J.; Eustis, S. N.; Arey, J. S.; McNeill, K., Controlling factors in the rates of oxidation of anilines and phenols by triplet methylene blue in aqueous solution. *J. Phys. Chem. A* **2015,** *119*, (13), 3233-3243.
16. Jonsson, M.; Lind, J.; Eriksen, T. E.; Merényi, G., Redox and acidity properties of 4-substituted aniline radical cations in water. *J. Am. Chem. Soc.* **1994,** *116*, (4), 1423-1427.
17. Wenk, J.; von Gunten, U.; Canonica, S., Effect of dissolved organic matter on the transformation of contaminants induced by excited triplet states and the hydroxyl radical. *Environ. Sci. Technol.* **2011,** *45*, (4), 1334-1340.
18. Wenk, J.; Canonica, S., Phenolic antioxidants inhibit the triplet-induced transformation of anilines and sulfonamide antibiotics in aqueous solution. *Environ. Sci. Technol.* **2012,** *46*, (10), 5455-5462.
19. Wenk, J.; Aeschbacher, M.; Sander, M.; von Gunten, U.; Canonica, S., Photosensitizing and inhibitory effects of ozonated dissolved organic matter on triplet-induced contaminant transformation. *Environ. Sci. Technol.* **2015,** *49*, (14), 8541-8549.
20. Bahnmüller, S.; von Gunten, U.; Canonica, S., Sunlight-induced transformation of sulfadiazine and sulfamethoxazole in surface waters and wastewater effluents. *Water Res.* **2014,** *57*, 183-192.
21. Janssen, E. M. L.; Erickson, P. R.; McNeill, K., Dual roles of dissolved organic matter as sensitizer and quencher in the photooxidation of tryptophan. *Environ. Sci. Technol.* **2014,** *48*, (9), 4916-4924.
22. Ulrich, M. M.; Muller, S. R.; Singer, H. P.; Imboden, D. M.; Schwarzenbach, R. P., Input and dynamic behavior of the organic pollutants tetrachloroethene, atrazine, and NTA in a lake: A study combining mathematical modeling and field measurements. *Environ. Sci. Technol.* **1994,** *28*, (9), 1674-1685.
23. Wegelin, M.; Canonica, S.; Mechsner, K.; Fleischmann, T.; Pesaro, F.; Metzler, A., Solar water disinfection: Scope of the process and analysis of radiation experiments. *J. Water Supply Res. Technol. - Aqua* **1994,** *43*, (3), 154-169.
24. Huntscha, S.; Singer, H.; Canonica, S.; Schwarzenbach, R. P.; Fenner, K., Input dynamics and fate in surface water of the herbicide metolachlor and of its highly mobile transformation product metolachlor ESA. *Environ. Sci. Technol.* **2008,** *42*, (15), 5507-5513.
25. Dulin, D.; Mill, T., Development and evaluation of sunlight actinometers. *Environ. Sci. Technol.* **1982,** *16*, (11), 815-820.
26. Nash, T., The colorimetric estimation of formaldehyde by means of the Hantzsch reaction. *Biochem. J.* **1953,** *55*, (3), 416-421.
27. Flyunt, R.; Leitzke, A.; Mark, G.; Mvula, E.; Reisz, E.; Schick, R.; von Sonntag, C., Determination of $^{\bullet}OH$, $O_2^{\bullet-}$, and hydroperoxide yields in ozone reactions in aqueous solution. *J. Phys. Chem. B* **2003,** *107*, (30), 7242-7253.
28. Andreozzi, R.; Marotta, R.; Paxeus, N., Pharmaceuticals in STP effluents and their solar photodegradation in aquatic environment. *Chemosphere* **2003,** *50*, (10), 1319-1330.

29. Liu, Q. T.; Williams, H. E., Kinetics and degradation products for direct photolysis of beta-blockers in water. *Environ. Sci. Technol.* **2007,** *41*, (3), 803-810.

30. Jasper, J. T.; Sedlak, D. L., Phototransformation of wastewater-derived trace organic contaminants in open-water unit process treatment wetlands. *Environ. Sci. Technol.* **2013,** *47*, (19), 10781-10790.

31. Alder, A. C.; Schaffner, C.; Majewsky, M.; Klasmeier, J.; Fenner, K., Fate of beta-blocker human pharmaceuticals in surface water: Comparison of measured and simulated concentrations in the Glatt Valley Watershed, Switzerland. *Water Res.* **2010,** *44*, (3), 936-948.

32. Loeff, I.; Rabani, J.; Treinin, A.; Linschitz, H., Charge-transfer and reactivity of nπ* and ππ* organic triplets, including anthraquinonesulfonates, in interactions with inorganic anions: A comparative study based on classical Marcus theory. *J. Am. Chem. Soc.* **1993,** *115*, (20), 8933-8942.

33. Köhler, G.; Getoff, N.; Rotkiewicz, K.; Grabowski, Z. R., Electron photoejection from donor–aryl-acceptor molecules in aqueous solution. *J. Photochem.* **1985,** *28*, (4), 537-546.

34. Larson, R. A.; Marley, K. A., Singlet oxygen in the environment. In *The Handbook of Environmental Chemistry*, Hutzinger, O., Ed. Springer: Berlin, Germany, 1999; Vol. 2, Part L, pp 123-137.

35. Rodgers, M. A. J.; Snowden, P. T., Lifetime of O_2 ($^1\Delta_g$) in liquid water as determined by time-resolved infrared luminescence measurements. *J. Am. Chem. Soc.* **1982,** *104*, (20), 5541-5543.

36. Tratnyek, P. G.; Hoigné, J., Oxidation of substituted phenols in the environment: A QSAR analysis of rate constants for reaction with singlet oxygen. *Environ. Sci. Technol.* **1991,** *25*, (9), 1596-1604.

37. Haag, W. R.; Hoigné, J.; Gassman, E.; Braun, A. M., Singlet oxygen in surface waters. 1. Furfuryl alcohol as a trapping agent. *Chemosphere* **1984,** *13*, (5-6), 631-640.

38. Aeschbacher, M.; Graf, C.; Schwarzenbach, R. P.; Sander, M., Antioxidant properties of humic substances. *Environ. Sci. Technol.* **2012,** *46*, (9), 4916-4925.

39. Baciocchi, E.; Bietti, M.; Gerini, M. F.; Lanzalunga, O., Electron-transfer mechanism in the *N*-demethylation of *N,N*-dimethylanilines by the phthalimide-*N*-oxyl radical. *J. Org. Chem.* **2005,** *70*, (13), 5144-5149.

40. von Sonntag, C.; Schuchmann, H.-P., Peroxyl radicals in aqueous solutions. In *Peroxyl radicals*, Alfassi, Z. B., Ed. John Wiley & Sons: Chichester etc., 1997; pp 173-234.

Chapter 2 , Supporting information for

Probing the photosensitizing and inhibitory effects of dissolved organic matter by using *N,N*-dimethyl-4-cyanoaniline (DMABN)

Frank Leresche, Urs von Gunten, Silvio Canonica

Text S2.1. List of chemicals

a) Target compounds: Ormetoprim (Dr. Ehrenstorfer, 99%), trimethoprim (Sigma, 99%), sulfadimethoxine (Fluka, 98.5%), sulfadiazine (Sigma, 99%), propranolol hydrochloride (Sigma-Aldrich, 99%), sotalol, 4-Cyanoaniline (Fluka, 97%), *N*-methyl-4-cyanoaniline (MABN, from the alternative name 4-methylaminobenzonitrile) (Sigma-Aldrich, 97%), *N,N*-dimethyl-4-cyanoaniline (DMABN, from the alternative name 4-dimethylaminobenzonitrile) (Aldrich, 98%), 4-aminobenzoic acid (Sigma, 99%).

b) Other compounds: Phenol (Fluka, 99%), isopropanol (Fisher Scientific, HPLC grade), *p*-nitroanisole (Aldrich, 97%), pyridine (Aldrich, 99%), sodium azide (Aldrich, 99.99%), phosphoric acid (H_3PO_4, Fluka, analytical grade, 85%), sodium dihydrogen phosphate mono-hydrate ($NaH_2PO_4\bullet H_2O$; Merck, analytical grade, 99%), disodium hydrogen phosphate di-hydrate ($Na_2HPO_4\bullet 2H_2O$; Merck, analytical grade, 99.5%), hydrochloric acid (HCl; Merck, analytical grade, 32%), sodium nitrate ($NaNO_3$; Merck, analytical grade, 99.5%), sodium nitrite ($NaNO_2$; Sigma-Aldrich, analytical grade, 99%), acetonitrile (Acros Organics, HPLC grade), heavy water (D_2O; Aldrich, minimum 99.9%D), formaldehyde (Sigma-Aldrich, 36.6-38% in H_2O with 10-15% methanol), acetylacetone (Sigma-Aldrich, 99%), acetic acid (Sigma-Aldrich, 99.7%), ammonium acetate (Fluka, 98%), furfuryl alcohol (Aldrich, 99%), atrazine (Sigma-Aldrich, 98.8%), rose Bengal (Aldrich, 95%).

Table S2.1. Characteristics of the used fulvic acids from the International Humic Substances Society (IHSS).

	Elemental composition[a] (mass %)					Acidic functional groups[b]		Electron donating capacity (EDC)[c]
	C	H	O	N	S	Carboxyl (meq g_C^{-1})	Phenolic (meq g_C^{-1})	($\mu mol_{e-}\ g_{HS}^{-1}$)
Pony Lake Fulvic Acid (1R109F)	52.47	5.39	31.38	6.51	3.03	Not available	Not available	1203 ±29
Suwannee River Fulvic Acid (1S101F)	52.44	4.31	42.2	0.72	0.44	11.44	2.91	2848 ±85[d]

	Electronic absorption spectral parameters	
	SUVA254[e] (L $mg_C^{-1}\ m^{-1}$)	S$_{300-600}$[f] (nm^{-1})
Pony Lake Fulvic Acid (1R109F)	2.5	0.0158
Suwannee River Fulvic Acid (1S101F)	3.9	0.0156

[a] From the IHSS website: http://www.humicsubstances.org/elements.html, accessed on the 23 February 2015.

[b] Determined by titration.[1]

[c] From Ref. 2, measured using a potential step of 0.71V at pH 7.

[d] Data for another batch of Suwannee River fulvic acid (catalogue number 2S101F).

[e] Specific absorption coefficient at λ=254 nm.

[f] Spectral slope, i.e., negative exponential constant from single-exponential fitting of the absorption spectrum, determined in the wavelength range of 300−600 nm.

Table S2.2. Characteristics of the used natural waters.

	pH [a]	Conductivity [b] (µS cm^{-1})	Alkalinity [c] (mmol L^{-1})	Ammonium [d] (µg$_N$ L^{-1})	Nitrite [e] (µg$_N$ L^{-1})	Nitrate [f] (mg$_N$ L^{-1})	D N [g] (mg$_N$ L^{-1})	DOC [h] (mg$_C$ L^{-1})
Lake Greifensee (GW), collected on 18.11.2014	8.31	408	3.93	97	25.6	0.9	1.4	3.3
Etang de la Gruère (EG), collected on 14.11.2014	7.71	97	0.93	150	6.2	0.8	0.7	22.8

	Electronic absorption spectral parameters	
	SUVA254 [j] (L mg$_C^{-1}$ m^{-1})	S$_{300-600}$ [k] (nm^{-1})
Lake Greifensee (GW), collected on 18.11.2014	2.2	0.0189
Etang de la Gruère (EG), collected on 14.11.2014	5.0	0.0138

[a] Measured using a Metrohm pH meter (model 632) equipped with a Thermo Scientific pH electrode (model Orion 8115SC).

[b] Measured using a Metrohm 712 conductometer.

[c] Measured using a Metrohm 809 Titrando equipped with a Metrohm pH electrode (model Unitrode 6.0258.010).

[d] Measured colorimetrically using Berthelot reaction and a Varian Cary 50 Bio spectrophotometer.

[e] Measured colorimetrically using Griess reaction and a Varian Cary 50 Bio spectrophotometer.

[f] After drying of the water sample, nitrate was reacted in a sulfuric acid solution with sodium salicylate to nitrosalicylic acid, which was then determined colorimetrically in alkaline solution using on a Varian Cary 50 Bio spectrophotometer.

[g] Dissolved Nitrogen, measured using a Shimadzu TOC V-CPH TNM-1 analyzer.

[h] Dissolved Organic Carbon, measured using a Shimadzu TOC L-CSH analyzer.

j Specific absorption coefficient at λ=254 nm.

k Spectral slope, i.e., negative exponential constant from single-exponential fitting of the absorption spectrum, determined in the wavelength range of 300−600 nm.
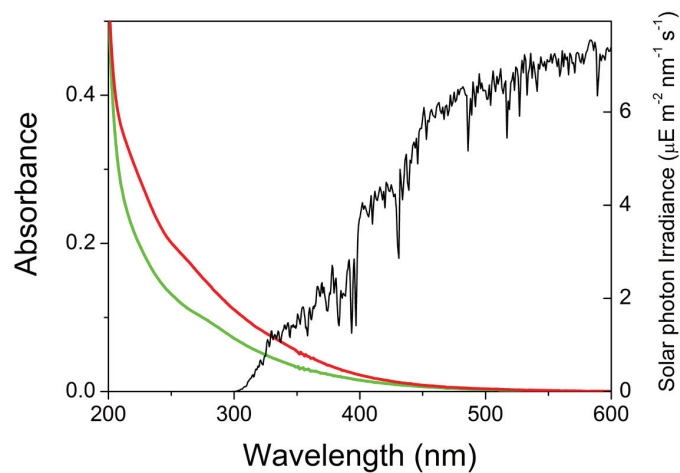
Figure S2.1. UV-visible absorption spectra of Pony Lake (green) and Suwannee River (red) fulvic acids, both measured at a concentration of 5 mg$_C$ L^{-1} in phosphate-buffered pH 8.0 solution and an optical path length of 1 cm. The solar spectral photon irradiance at Air Mass 1.5 (global tilt, calculated using ASTM G173-03 standard & SMART v2.92 data) is also shown.
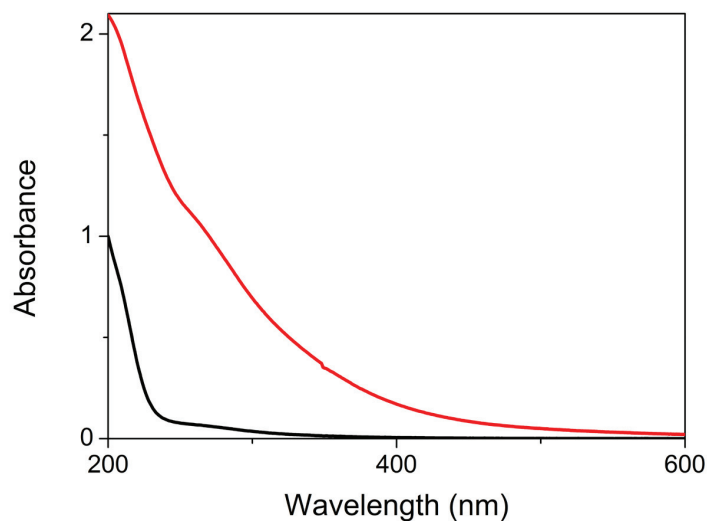

Figure S2.2. UV-visible absorption spectra of the waters used in this study (undiluted, at natural pH). Black: Lake Greifensee water, red: Etang de la Gruère water; optical path length of 1 cm.
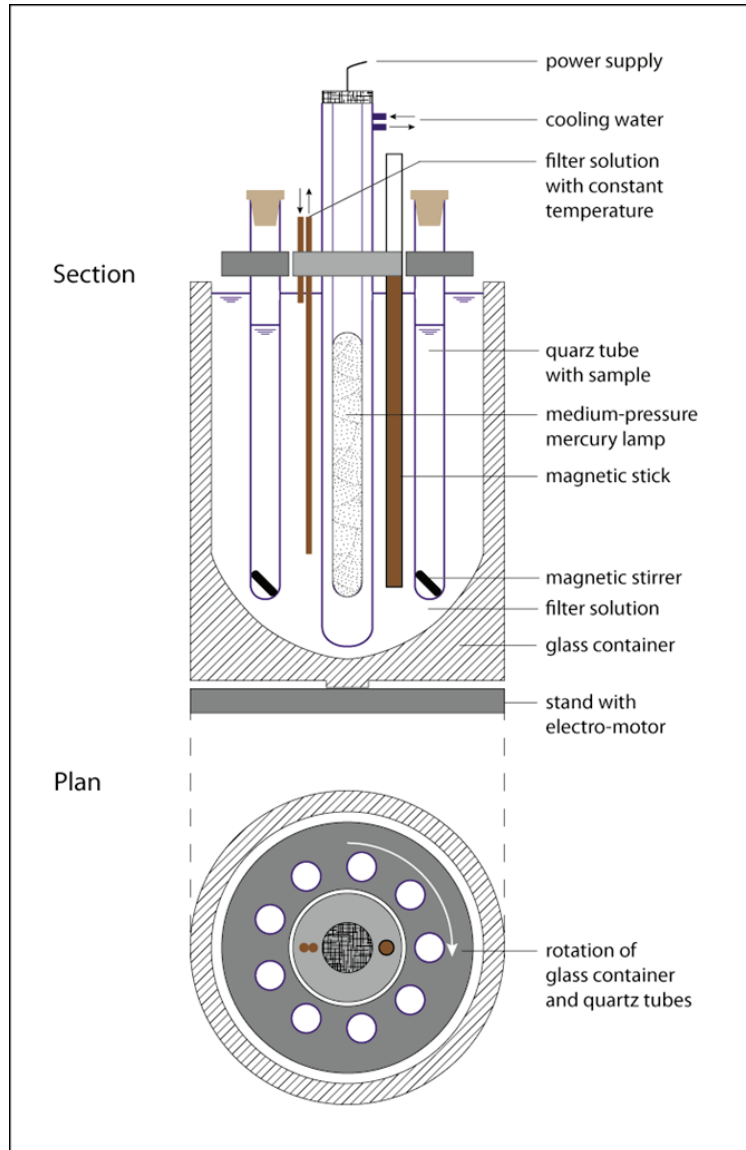
Section

- power supply
- cooling water
- filter solution with constant temperature
- quarz tube with sample
- medium-pressure mercury lamp
- magnetic stick
- magnetic stirrer
- filter solution
- glass container
- stand with electro-motor

Plan

- rotation of glass container and quartz tubes

Figure S2.3. Sketch of the merry-go-round photoreactor. Adapted from Ref. 3, courtesy of Rani Bakkour.
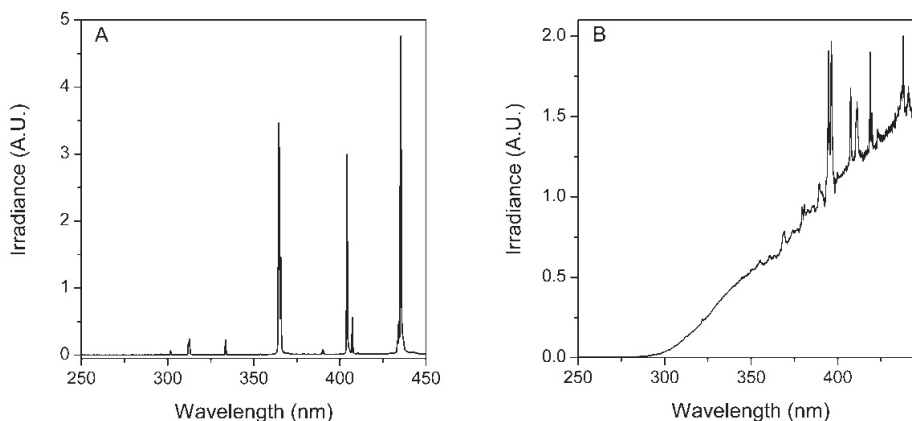
Figure S2.4. Photon irradiance spectra of: (A) The used TQ 718 medium pressure mercury lamp in the Pyrex® glass cooling jacket, and (B) the solar simulator, both measured employing the ILT950-UV spectroradiometer.

Text S2.2. Chemical actinometry and photon fluence rate

The photon fluence rate for irradiations performed using the solar simulator was calculated according to the method employed in Ref. 4, using equation S2.1:

$$E_p^0 (290 - 400nm) = \frac{k_{p,PNA}}{2.303\ \Phi_{PNA}\ \sum_{\lambda=290}^{400nm}(f_{p,\lambda}\ \varepsilon_{PNA,\lambda})} \qquad \text{(S2.1)}$$

Where E_p^0 is the photon fluence rate in the interval 290–400nm (einstein m^{-2} s^{-1}), $k_{p,PNA}$ is the observed phototransformation rate constant of p-nitroanisole (PNA) (s^{-1}), ΦPNA is the quantum yield of the PNA/Pyridine system ($\Phi = 0.44[Pyr] + 0.00028$), assumed to be wavelength independent, $f_{p,\lambda}$ is the normalized emission spectrum of the lamp, and $\varepsilon_{PNA,\lambda}$ is the molar absorption coefficient of PNA at the wavelength λ (m^2 mol^{-1}).

The photon fluence rate of the merry-go-round photoreactor (medium pressure Hg lamp with filter) was calculated similarly, but using the wavelength range of 334–436 nm (see Table S2.3).

Table S2.3. Irradiance and molar extinction coefficient used for the medium pressure Hg lamp system

Wavelength (nm)	Normalized Irradiance	0.15M NaNO$_3$ filter solution Transmittance (2.5cm path length)	Normalized Irradiance with NaNO$_3$ filter $f_{p,\lambda}$	ε_{PNA} (m^2 mol^{-1})
296.7	0.0003	0.0002	-	
302.3	0.001	0.0001	-	
312.9	0.021	0.0008	-	
334.2	0.011	0.568	0.006	854
365.4	0.365	0.992	0.374	221
390.6	0.002	0.992	0.002	29
404.7-407.8	0.204	0.994	0.209	6
435.8	0.396	0.996	0.408	4

Text S2.3. HPLC analytical methods

Concentrations of the compounds in aqueous samples were determined by high-performance liquid chromatography (HPLC) using an Agilent 1100 HPLC chromatograph equipped with a quaternary low-pressure mixing gradient pump, a diode array detector and an Agilent 1200 fluorescent detector or an analogous Dionex 3000 Ultimate system). Chromatographic separation was done using a Nacalai Tesque column, model Cosmosil 5C18-MS-II, with 5 µm particle size, 3 mm internal diameter an 100 mm length. Isocratic conditions were generally employed, except for the quantification of rose Bengal (RB), for which a gradient elution method was used. Details of the elution methods used are given in Table S2.4.

Table S2.4. HPLC analyses parameters.[a]

Compound	Eluent composition (%)			Retention time (min)	Detection wavelength (nm) or Excitation wavelength / Emission wavelength (nm)
	Water	Acetonitrile	Phosphate Buffer[b]		
Propranolol		24	76 (10mM H_3PO_4)	4-5	228/342
Sotalol		10	90 (pH 6)	2.2-2.3	202
4-Aminobenzoic acid		10	90 (10mM H_3PO_4)	2.3	285
4-Cyanoaniline	80	20		4.2-4.6	273
N-Methyl-4-cyanoaniline	50	50		2.2	285 or 290/350
N,N-Dimethyl-4-cyanoaniline	50	50		3.3	298 or 290/488
Sulfadiazine		12	88 (10mM H_3PO_4)	2.8	266
Sulfadimethoxine		15	85 (pH 8)	2.4	268
Trimethoprim		14	86 (10mM H_3PO_4)	2.9-3.1	205
Ormetoprim		14	86 (10mM H_3PO_4)	2.9	200
Phenol	50	50		1.8	200
p-Nitroanisole	50	50		3.3	312
Furfuryl alcohol	80	20		2	215
2-Acetonaphthone	50	50		4.6	247
Rose Bengal	gradient[c]	gradient[c]		2.5-3.5	554

[a] Besides the parameters given in the table, the following conditions were applied: Flow rate 0.5 mL/min, injection volume 20μL, column temperature 30 °C. Dead time was 1.0 min.

[b] 5 mM total concentration if not otherwise specified.

[c] The gradient method for the quantification of rose Bengal was the following (percentage values correspond to the fraction of acetonitrile in the eluent (vol/vol), the remaining being water): t=0–2 min, 17%; t=2–3 min, linear gradient to reach 30%; t=3–4 min, 30%; t=4–5 min, linear gradient to reach 17%; t=5–7.5 min, 17%.

Text S2.4. Hantzsch colorimetric method

Detection of formaldehyde (CH_2O) was done using the Hantzsch colorimetric method.[5] The reagent used was composed of 2 M ammonium acetate, 0.05 M acetic acid and 0.02 M acetylacetone. Five mL of reagent was mixed with 5 mL of sample, whereafter the mixture was kept in a water bath at 50 °C in the dark for 30 minutes. Subsequently, a UV-visible spectrum of the mixture was measured in a quartz cell of 5 cm optical path length. The concentration of formaldehyde was determined using a calibration line, using the absorbance at λ=412nm to measure the amount of formed diacetyldihydrolutidine. The molar absorption coefficient of diacetyldihydrolutidine at λ=412 nm was calculated to be 7590±150 M^{-1} cm^{-1} using formaldehyde standards, in accordance to litera-ture values (7700,[5] 7530[6]). Alternatively, another reagent composed of 0.2 mL acetylacetone, 3 mL acetic acid and 25 g ammonium acetate completed to 100 mL with water was used.[6] Applying this method, 2 mL of reagent was mixed with 5 mL of sample. The rest of the procedure is identical to the description above. This method was more sensitive as the dilution of the sample was lower.

Control experiments were done to detect interferences from rose Bengal or DMABN and showed no interferences of DMABN on formaldehyde measurements. Rose Bengal photodegradation products show to slightly absorb light at the detection wavelength, and the measured absorbance was corrected for this effect using control experiments. Thereby the correction takes into account both formaldehyde formation during rose Bengal photodegradation and the light absorbance of rose Bengal photoproducts.

Text S2.5. Light screening correction

The procedure described in Ref. 7 was taken as the basis for the calculations of the light screening factor. Such a procedure, which assumes the direction of light from the lamp to be horizontal and to enter the sample quartz tube in the plane of its cross-section, is acceptable for relatively small screening effect corrections as occurring in the previous study.[7] Since in the present study higher concentrations of DOM were used, a more realistic model to calculate the light screening factor was used which considered light entering the sample tube from various angles according to the geometry of the reactor (see Figure S2.5). The geometrical parame-ters that have been considered are the height of the lamp, the average height of the sample solution in the tube, and the relative vertical and horizontal position of the lamp and sample tube, respectively. These parameters had the following values:

- Horizontal distance between the centers of the lamp and the sample tubes = 62 mm;

- Height of the lamp = 90 mm

- Average height of the sample solution in the tube = 109 mm (assuming 7 sample withdrawals during the experiment)

- Vertical height difference between the top of the lamp and the average top of the solution = 38 mm.

Additionally, the average internal radius of the sample tubes was: r = 7.4 mm.

Assuming that the lamp is virtually immersed in a water bath, thus neglecting any refractive index effect on the light beams, the lamp was considered as an array of point-sources of equal intensity. Integrating over the height of the lamp and the height of the solution in the sample tube and weighting the differential contributions with a factor inversely proportional to the square of the distance L between the point source and the center of the sample tube at the considered height, the average path length of light through the sample solution was calculated to be by a factor of 1.19 higher than for a horizontal direction of incident light. The screening factor was then calculated according to Ref. [7], with the modification that the path length of light in each sector of the tube considered for the integration was multiplied by 1.19.
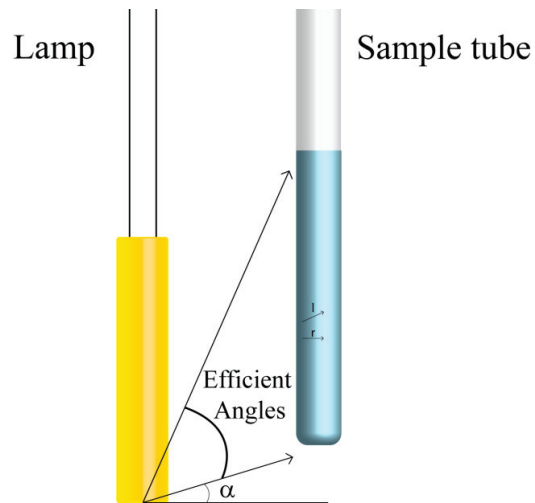
Figure S2.5. Geometrical sketch of the lamp and sample quartz tube in the merry-go-round photoreactor.

Table S2.5. Light attenuation of the fulvic acids or the natural waters.

	Attenuation (%)		
Type of DOM	**1 mg$_C$/L**	**5 mg$_C$/L**	**20 mg$_C$/L**
PLFA	0.77	3.76	13.86
SRFA	1.23	5.94	20.91
PLFA 5mg$_C$/L +SRFA	4.92	9.35	23.49
Natural water	**Water fraction: 30%**	**70%**	**90%**
GW	0.4	1.1	1.6
Natural water	**Water fraction: 10%**	**20%**	**30%**
EG	4.6	8.8	12.8
GW 68.5% + EG	5.7	9.9	13.8

Text S2.6. Determination of the quenching effect of phenol on ^{3}PLFA*

To quantify the quenching of ^{3}PLFA* by phenol (PhOH), the steady-state concentration of singlet oxygen, $\left[^1O_2\right]_{ss}$, was used. The latter is related to the pseudo-first-order transformation rate constant of furfuryl alcohol (FFA), k_{FFA}^{sens}, according to eq. S2.2.

$$\left[^1O_2\right]_{ss} = \frac{k_{FFA}^{sens}}{k_{^1O_2,FFA}^{t}}$$
(S2.2)

Where $k_{^1O_2,FFA}^{t}$ is the second-order rate constant for the transformation of FFA induced by singlet oxygen. Thereby it was assumed that $\left[^1O_2\right]_{ss}$ was proportional to the steady-state concentration of the precursor excited triplet states of PLFA, $\left[^3PLFA^*\right]_{ss}$, and that quenching of singlet oxygen by PhOH was negligible, which is a safe assumption in view of the low rate constants for this reaction.[8] The correction of the rate constants k_{DMABN}^{sens} for the transformation of DMABN photosensitized by ^{3}PLFA* was then performed as follows (eq. S2.3).

$$k_{DMABN}^{sens}\left(corrected\right) = k_{DMABN}^{sens} \frac{\left[^1O_2\right]_{ss}\left(no\ PhOH\right)}{\left[^1O_2\right]_{ss}\left([PhOH]\right)} = k_{DMABN}^{sens} \frac{k_{FFA}^{sens}\left(no\ PhOH\right)}{k_{FFA}^{sens}\left([PhOH]\right)}$$
(S2.3)

For the [PhOH] values for which k_{FFA}^{sens} had not been determined, interpolation was done using equation S2.4, which is based on the kinetic treatment given in Ref. 9.

$$k_{FFA}^{sens}\left([PhOH]\right) = k_{FFA}^{sens}\left(no\ PhOH\right)\frac{A}{A + [PhOH]}$$
(S2.4)

Where the parameter A was determined to be $(1.5\pm0.5)\times10^{-4}$ M. For the maximum PhOH concentration used (100 μM), the decrease in $\left[^3PLFA^*\right]_{ss}$ caused by quenching with phenol was calculated to be −40% with respect to solutions with no phenol added.

Text S2.7. Correction method to account for rose Bengal (RB) photodegradation

As RB was photodegraded during irradiation, causing a reduction of its photosensitizing effect, kinetic data were corrected to account for the decrease in RB concentration during the kinetic runs. We made the assumption that the photosensitizing effect of RB photodegradation products was negligible.

The photodegradation of RB followed first-order kinetics (eq. S2.5) with the corresponding photodegradation rate constant α, which depends on irradiation and other experimental conditions. This rate constant was determined for each experiment in which RB was used as a photosensitizer.

$$[\text{RB}] = [\text{RB}]_0 e^{-\alpha t} \tag{S2.5}$$

For the transformation of a target compound TC photosensitized by RB eq. S2.6 holds.

$$-\frac{d[\text{TC}]}{dt} = k_{TC}^{sens}([\text{RB}])[\text{TC}] \tag{S2.6}$$

In the case of no degradation of RB, [RB] remains constant and equal to its initial concentration, $[\text{RB}]_0$. Eq. S2.6 can thus be integrated to yield eq. S2.7:

$$\ln\frac{[\text{TC}]_t}{[\text{TC}]_0} = -k_{TC}^{sens}([\text{RB}]_0)t \tag{S2.7}$$

In the case of RB photodegradation, its concentration as well as $k_{TC}^{sens}([\text{RB}])$ vary. Direct proportionality between $k_{TC}^{sens}([\text{RB}])$ and [RB] is assumed. Substituting eq. S2.5 into eq. S2.6 one obtains:

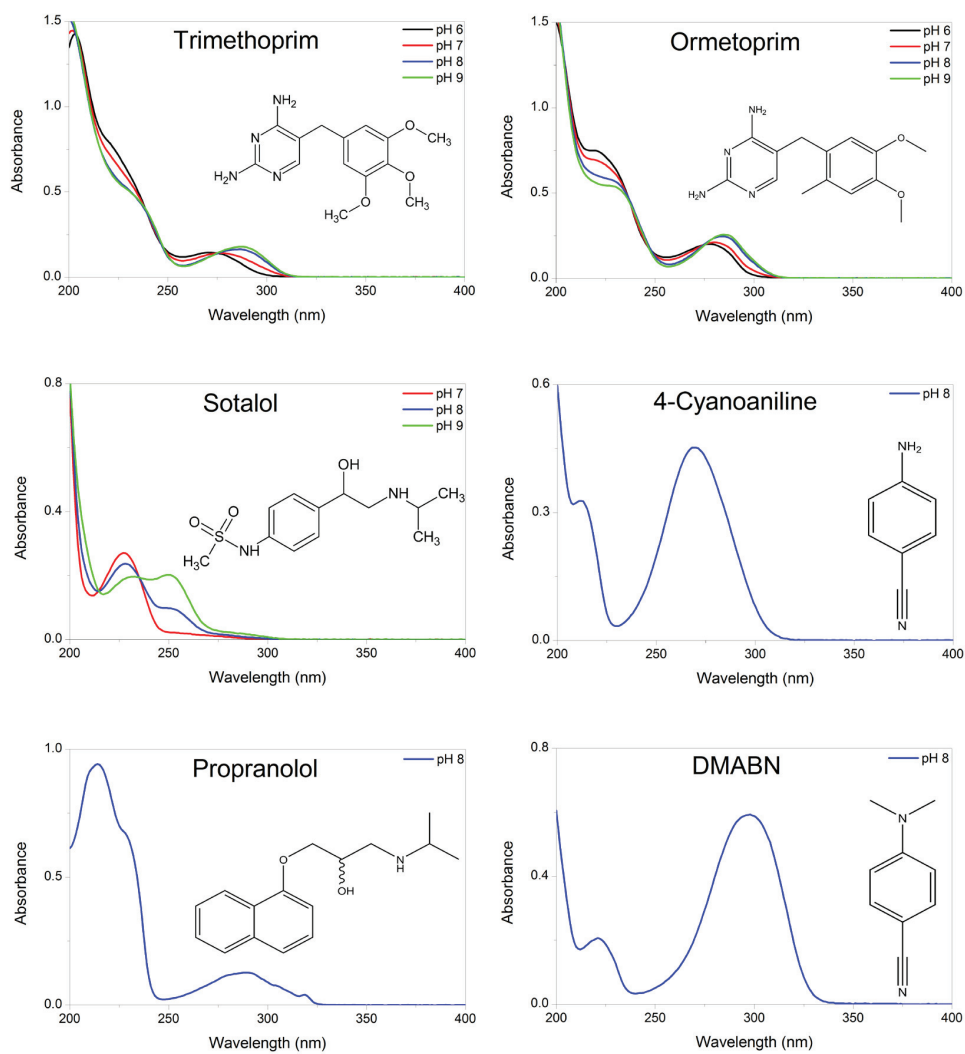$$-\frac{d[\text{TC}]}{dt} = k_{TC}^{sens}([\text{RB}]_0)[\text{TC}]e^{-\alpha t} \tag{S2.8}$$

Rearranging eq. S2.8 one obtains eq. S2.9, which can be integrated to give eq. S2.10.

$$-\frac{d[\text{TC}]}{[\text{TC}]} = k_{TC}^{sens}([\text{RB}]_0)e^{-\alpha t}dt \tag{S2.9}$$

$$\ln\left(\frac{[\text{TC}]_t}{[\text{TC}]_0}\right) = -k_{TC}^{sens}([\text{RB}]_0)\frac{1-e^{-\alpha t}}{\alpha} \tag{S2.10}$$

Using a transformed time $t' = \dfrac{1-e^{-\alpha t}}{\alpha}$ one obtains equation S2.11, which can directly be used to extract $k_{TC}^{sens}([\text{RB}]_0)$ as a fitting parameter from the kinetic data.

$$\ln\left(\frac{[\text{TC}]_{t'}}{[\text{TC}]_0}\right) = -k_{TC}^{sens}([\text{RB}]_0)t' \tag{S2.11}$$

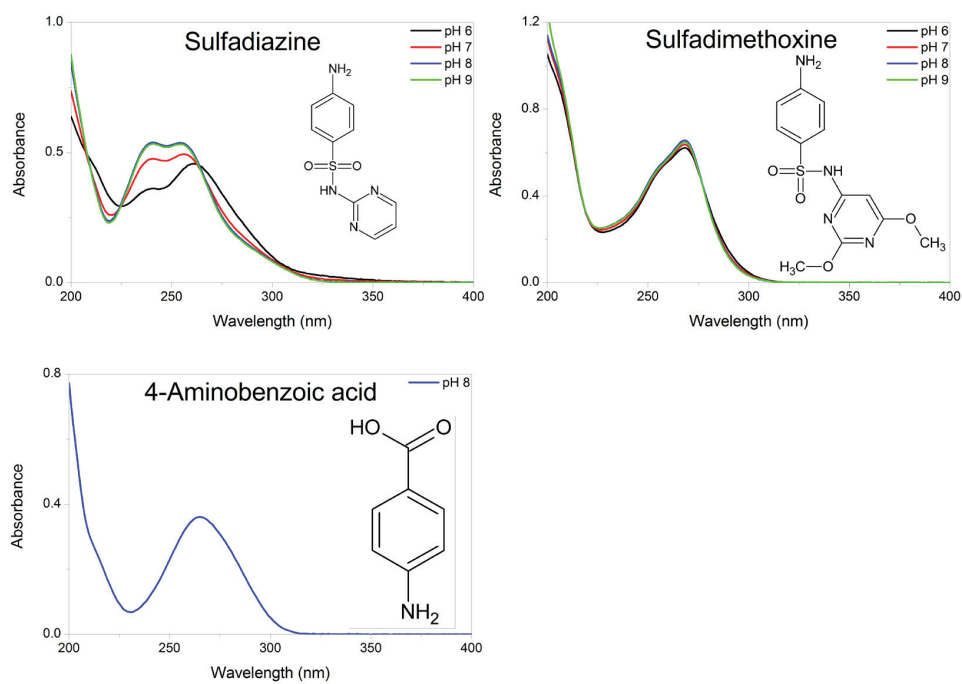(Figure S2.6: Continued on the next page)

Figure S2.6. UV-visible absorption spectra and structures of the investigated compounds (25 µM) in 5 mM phosphate buffer. Note that the buffer slightly absorbs light at wavelengths below 220 nm. Color codes for the spectra: Black for pH 6, red for pH 7, blue for pH 8 and green for pH 9.

Table S2.6. Pseudo-first-order phototransformation rate constants and direct phototransformation quantum yields (Q.Y.) of the selected compounds under simulated solar irradiation. DOM concentrations were 5.0 mg$_C$ L^{-1} for Pony Lake fulvic acid (PLFA) and Suwannee River fulvic acid (SRFA), and 3.0 mg$_C$ L^{-1} for Lake Greifensee water. Samples with added phenol contained initially 10 μM phenol. Initial concentration of the target compounds 5 μM, pH 8.

	Ultrapure water			Pony Lake fulvic acid		Suwannee River fulvic acid		Greifensee water	
	UW	UW	UW +Phenol	PLFA	PLFA +Phenol	SRFA	SRFA +Phenol	GW	GW +Phenol
	Q.Y. (10^{-3})	k$_{obs}$ (10^{-5} s^{-1})		k$_{obs}$ (10^{-5} s^{-1})		k$_{obs}$ (10^{-5} s^{-1})		k$_{obs}$ (10^{-5} s^{-1})	
Propranolol	8.2 ±1.3	4.4 ±0.2	3.57 ±0.10	11.4 ±0.2	9.58 ±0.15	5.42 ±0.05	3.98 ±0.08	9.0 ±0.3	7.8 ±0.3
Sotalol	210 ±30	4.9 ±0.3	2.95 ±0.12	5.7 ±0.3	3.50 ±0.18	1.73 ±0.08	1.53 ±0.07	11.5 ±0.8	6.3 ±0.7
N,N-dimethyl-4-cyanoaniline	1.3 ±0.2	5.3 ±0.3	3.2 ±0.2	13.1 ±0.2	7.67 ±0.13	3.65 ±0.05	2.57 ±0.12	4.8 ±0.3	1.77 ±0.10
Sulfadiazine	1.3 ±0.2	0.80 ±0.03	1.13 ±0.10	4.83 ±0.15	3.1 ±0.3	1.55 ±0.07	1.15 ±0.07	4.2 ±0.3	1.8 ±0.3
4-Cyanoaniline	1.9 ±0.3	0.70 ±0.07	0.60 ±0.08	1.72 ±0.03	1.17 ±0.10	0.718 ±0.018	0.43 ±0.05	1.22 ±0.10	0.45 ±0.03
Sulfadimethoxine	2.1 ±0.4	0.62 ±0.05	0.848 ±0.018	1.22 ±0.03	1.02 ±0.03	0.92 ±0.03	0.87 ±0.02	0.95 ±0.17	0.40 ±0.03
4-Aminobenzoic acid	4.9 ±0.8	1.33 ±0.03	1.16 ±0.02	1.58 ±0.03	1.36 ±0.03	1.19 ±0.03	1.03 ±0.05	1.7 ±0.2	1.2 ±0.8
Trimethoprim	0.23 ±0.05	0.060 ±0.008	0.25 ±0.04	0.69 ±0.04	0.453 ±0.016	0.52 ±0.04	0.55 ±0.05	1.1 ±0.2	0.85 ±0.10
Ormetoprim	0.73 ±0.13	0.248 ±0.02	0.30 ±0.03	1.08 ±0.08	1.33 ±0.17	1.27 ±0.05	0.87 ±0.07	0.28 ±0.05	0.30 ±0.10

Text S2.8. Derivation of equation 2.2

Equation 2.2 can be derived from the kinetic model represented in Scheme S2.1.
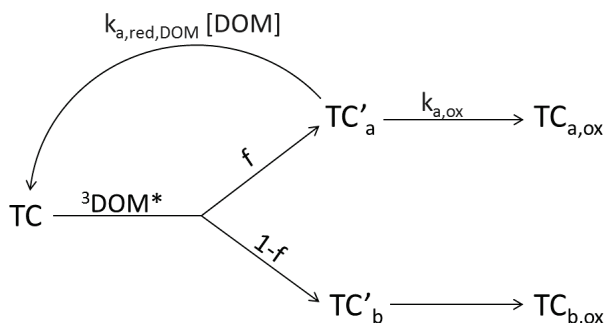
Scheme S2.1. A target contaminant TC reacts with ^{3}DOM* to give (1) an intermediate TC$'_a$, subject to inhibitory effect by DOM, or (2) an intermediate TC'$_b$, not affected by DOM. Of the total reacted TC, a fraction f forms TC'$_a$ while the remaining fraction (1-f) forms TC'$_b$. The intermediate TC$'_a$, will either further react (first-order rate constant $k_{a,ox}$) to give an oxidation product TC$_{a,ox}$, or be reduced back by DOM to the parent compounds TC (second-order rate constant $k_{a,red,DOM}$). The intermediate TC'$_b$ will further react to give an oxidation product TC$_{b,ox}$ (scheme adapted from Ref. 7).

A kinetic equation was previously derived for the rate constant for the photosensitized transformation of TC (eq. S14 in Ref. 7), which can be rewritten as eq. S2.12 substituting P with TC and ^{3}Sens* with ^{3}DOM*.

$$\frac{d[\text{TC}]}{dt} = -k_{^3DOM^*}\left[^3\text{DOM}^*\right][\text{TC}]\left(\frac{fk_{a,ox}}{k_{a,ox} + k_{a,red,DOM}[\text{DOM}]} + (1-f)\right) \tag{S2.12}$$

Where $k_{^3DOM^*}$ is the average second-order rate constant for the transformation of TC by ^{3}DOM*. The corresponding pseudo-first-order rate constant of the photosensitized transformation of TC by DOM, including inhibition by DOM, can be expressed as:

$$k_{TC}^{sens} = k_{^3DOM^*}\left[^3\text{DOM}^*\right]\left(\frac{fk_{a,ox}}{k_{a,ox} + k_{a,red,DOM}[\text{DOM}]} + (1-f)\right) \tag{S2.13}$$

We now introduce a factor β to express the proportionality between $k_{^3DOM^*}\left[^3\text{DOM}^*\right]$ and [DOM] (eq. S2.14).

$$k_{^3DOM^*}\left[^3\text{DOM}^*\right] = \beta[\text{DOM}] \tag{S2.14}$$

This factor β accounts for the formation of ^{3}DOM* from DOM and includes all parameters related to light intensity and its absorption by DOM, and formation quantum yield of ^{3}DOM*. Combining eqs. S2.13 and S2.14 one obtains:

$$k_{TC}^{sens} = \beta[\text{DOM}]\left(\frac{fk_{a,ox}}{k_{a,ox} + k_{a,red,DOM}[\text{DOM}]} + (1-f)\right) \tag{S2.15}$$

Which can be further rearranged to:

$$k_{TC}^{sens} = \beta[\text{DOM}]\left(\frac{f}{1 + \left(k_{a,red,DOM}/k_{a,ox}\right)[\text{DOM}]} + (1-f)\right) \tag{S2.16}$$

As in Ref. 7 we introduce the concept of [DOM]$_{1/2}$ (= $k_{a,ox}/k_{a,red,DOM}$), which is the concentration of DOM needed to halve the production of TC$_{a,ox}$ from TC'$_a$. Substituting $k_{a,ox}/k_{a,red,DOM}$ in eq. S2.16 and making a further rearrangement one obtains eq. S2.17, which corresponds to eq. 2.2.

$$k_{TC}^{sens} = \beta[\text{DOM}]\left(\frac{1+[\text{DOM}]/[\text{DOM}]_{1/2}(1-f)}{1+[\text{DOM}]/[\text{DOM}]_{1/2}}\right)$$

(S2.17)

Text S2.9. Derivation of equation 2.6

Scheme S2.1 was modified to take into account photosensitization and inhibition by two different kinds of DOM, namely DOM_1 and DOM_2 (see Scheme S2.2).
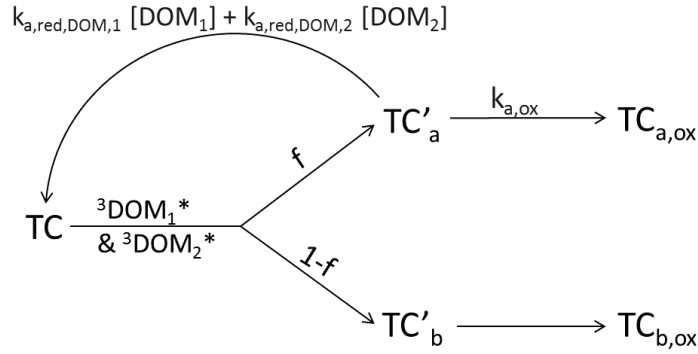
Scheme S2.2. Extension of Scheme S2.1 to include two types of DOM, DOM_1 and DOM_2, present in solution as an ideal mixture (i.e., without any mutual interaction). All symbols are identical or defined analogously as in Scheme S2.1.

In the case of two distinct DOMs, DOM_1 and DOM_2, respectively, both the photosensitizing and inhibitory effects contain the contribution of both DOMs. Therefore, equation S2.12 can be adapted accordingly to this principle to yield eq. S2.18.

$$\frac{d[\text{TC}]}{dt} = -\left(k_{^3DOM_1^*}\left[^3\text{DOM}_1^*\right]+k_{^3DOM_2^*}\left[^3\text{DOM}_2^*\right]\right)[\text{TC}]\times\left(\frac{fk_{a,ox}}{k_{a,ox}+\left(k_{a,red,DOM_1}[\text{DOM}_1]+k_{a,red,DOM_2}[\text{DOM}_2]\right)}+(1-f)\right)$$

(S2.18)

Proceeding as in the preceding section, one can substitute $k_{^3DOM_1^*}\left[^3\text{DOM}_1^*\right]$ with $\beta_1[\text{DOM}_1]$ and $k_{^3DOM_2^*}\left[^3DOM_2^*\right]$ with $\beta_2[\text{DOM}_2]$, as well as $k_{a,ox}/k_{a,red,DOM_1}$ with $[\text{DOM}_1]_{1/2}$ and $k_{a,ox}/k_{a,red,DOM_2}$ with $[\text{DOM}_2]_{1/2}$. After the same type of rearrangements as in the previous section, one obtains for the pseudo-first-order rate constant k_{TC}^{sens} eq. S2.19, which corresponds to eq. 2.6.

$$k_{TC}^{sens} = \left(\beta_1[\text{DOM}_1]+\beta_2[\text{DOM}_2]\right)\left(\frac{1+\left([\text{DOM}_1]/[\text{DOM}_1]_{1/2}+[\text{DOM}_2]/[\text{DOM}_2]_{1/2}\right)(1-f)}{1+[\text{DOM}_1]/[\text{DOM}_1]_{1/2}+[\text{DOM}_2]/[\text{DOM}_2]_{1/2}}\right)$$

(S2.19)

Analogously, one can extend the treatment to consider N distinct types of DOM, DOMi, with i=1–N, to obtain eq. S2.20:

$$k_{TC}^{sens} = \sum_{i=1}^{N}\beta_i[\text{DOM}_i]\left(\frac{1+(1-f)\sum_{i=1}^{N}[\text{DOM}_i]/[\text{DOM}_i]_{1/2}}{1+\sum_{i=1}^{N}[\text{DOM}_i]/[\text{DOM}_i]_{1/2}}\right)$$
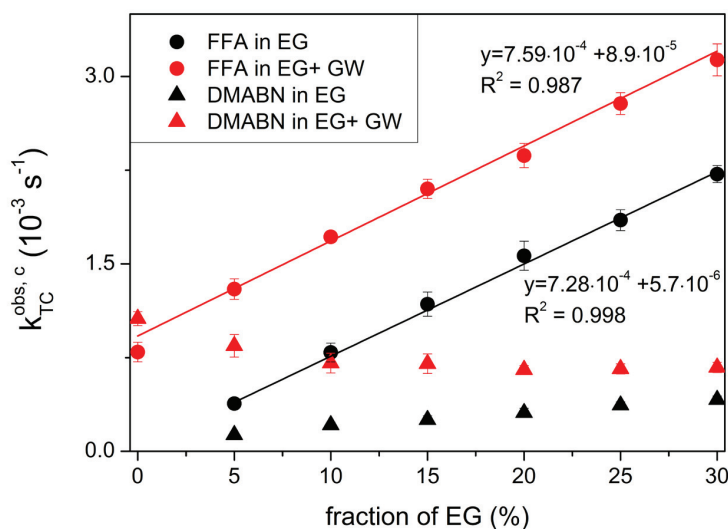
(S2.20)

Figure S2.7. FFA phototransformation rate constant in mixtures of GW and EG. Black circles: FFA phototransformation in EG; Red circles FFA phototransformation in mixtures of GW (68.5%) + EG. For comparison DMABN phototransformation rate constant are also presents (black triangles in EG, red triangle in mixtures of GW + EG). Error bars represents 95% confidence intervals from the regression lines.

Text S2.10. Detailed discussion of the experimental results concerning the role of singlet oxygen in the phototransformation of DMABN.

The most indicative results were obtained by using D_2O as an alternative solvent. The predicted factor of increase in singlet oxygen lifetime (and therefore in the steady-state concentration of singlet oxygen, $[^1O_2]_{ss}$, at equal production rate) for 95% D-atom molar fraction is 8.3 (see SI, Text S2.12). Pseudo-first-order rate constants for transformation of FFA (k_{FFA}^{obs}) photosensitized by PLFA and RB were by a factor of 10.0 and 10.8, respectively, higher in D_2O than in H_2O, confirming the suitability of FFA as a selective singlet oxygen probe compound. In contrast to the results obtained for FFA, no significant increase in transformation rate constants for DMABN was observed in D_2O compared to H_2O for both photosensitizers, which concurs with a negligible reactivity of singlet oxygen with DMABN in these systems. The use of sodium azide as a singlet oxygen quencher yielded mixed results. With RB as a photosensitizer, a very strong reduction in k_{FFA}^{obs} was observed both in H_2O (-92%) and D_2O (-99.2%) upon addition of 10 mM NaN$_3$, which agrees with reductions estimated using published quenching rate constant values. However, with PLFA as a photosensitizer reductions in k_{FFA}^{obs} were only -42% in H_2O and -94% in D_2O. This reduced apparent effectiveness of azide as a singlet oxygen quencher might arise from reaction of FFA with reactive species other than singlet oxygen (e.g., ^{3}PLFA* or the azide radical), analogously as suggested by Al Housari and coworkers.[10] The comparatively small reductions observed in k_{DMABN}^{obs} upon azide addition (for the system with RB in H_2O an increase was even observed) are also supportive of a minor role of singlet oxygen in DMABN phototransformation, which is probably mainly caused by the excited triplet state of RB. The reductions in k_{DMABN}^{obs} observed with these systems might arise from excited triplet state quenching by azide, which has been shown to occur for several excited triplet photosensitizers.[11] To be mentioned here is the accelerated transformation of DMABN in the absence of photosensitizers upon addition of azide, which could originate from quenching of ^{3}DMABN* by azide and consequent formation of the azide radical, which would then react with DMABN.

From the results of experiments using RB as a photosensitizer (Table 2.2, fifth row) it is possible to calculate a maximum second-order rate constant for the reaction of singlet oxygen with DMABN. For doing this, we make the safe assumption that the pseudo-

first-order contribution of singlet oxygen to the transformation of DMABN does not exceed k_{DMABN}^{obs}. Using the second-order rate constants for the reaction of singlet oxygen with FFA (1.2×10^8 M^{-1} s^{-1} in H$_2$O[12] and 8.3×10^7 M^{-1} s^{-1} in D$_2$O[13]) one can calculate the steady-state concentrations of singlet oxygen during the experiments (see Table 2.2), and from this the maximum rate constants for DMABN are obtained: 1.9×10^7 M^{-1} s^{-1} in H$_2$O and 1.3×10^6 M^{-1} s^{-1} in D$_2$O. Finally, the maximum pseudo-first-order rate constants in the PLFA system are obtained by multiplying these second-order rate constants with the corresponding [^{1}O$_2$]$_{ss}$ values (Table 2.2, third row): 3.0×10^{-5} s^{-1} for both H$_2$O and D$_2$O, corresponding to a fraction of 5.0% for H$_2$O and 4.7% for D$_2$O of k_{DMABN}^{obs}. Considering that in D$_2$O the contribution of singlet oxygen is magnified by about a factor of 8 with respect to H$_2$O, the contribution of singlet oxygen to the transformation of DMABN is probably on the order of 1% or less.

Text S2.11. Quantification of the hydroxyl radical ($^\bullet$OH) scavenging effect of isopropanol and the singlet oxygen (^{1}O$_2$) quenching effect of azide (as NaN$_3$)

To calculate the scavenging effect of isopropanol on $^\bullet$OH, the assumption was made that the disappearance of $^\bullet$OH was only due to reaction with PLFA, DMABN or isopropanol at their initial concentrations (therefore neglecting reactions with species possibly formed during irradiation, such as hydrogen peroxide).

The second-order rate constants for the reaction of $^\bullet$OH with each of these compounds are: 1.9×10^9 M^{-1}s^{-1} for isopropanol,[14] $\sim3\times10^4$ L mg$_C^{-1}$ s^{-1} for fulvic acids,[15] and $\sim5\times10^9$ M^{-1}s^{-1} for DMABN (crude assumption).

In a system with 5 mg$_C$/L PLFA, the fractional decrease D in $^\bullet$OH concentration was calculated to be ~92% in the presence of 10 mM isopropanol using equation S2.21:

$$D = 1 - \frac{\sum_i k_{\bullet OH, Q_i}^q [Q_i] (\text{no isopropanol})}{\sum_i k_{\bullet OH, Q_i}^q [Q_i] (\text{with isopropanol})} \qquad (S2.21)$$

Where $k_{\bullet OH, Q_i}^q [Q_i]$ is the contribution of the scavenger Q$_i$ to the pseudo-first-order scavenging rate constant of $^\bullet$OH and $k_{\bullet OH, Q_i}^q$ is the second-order rate constant for the reaction of $^\bullet$OH with Q$_i$.

To calculate the quenching effect of NaN$_3$ on ^{1}O$_2$, the decay rate constant (s^{-1}) of ^{1}O$_2$ in the presence of NaN$_3$ was calculated according to the Stern-Volmer equation, neglecting any quenching contribution by other components in solution:

$$k_{^1O_2}^d = k_{^1O_2}^{d,0} + k_{^1O_2,NaN_3}^q [NaN_3] \qquad (S2.22)$$

Where $k_{^1O_2}^{d,0}$ is the first-order decay rate constant due to the solvent and amounts to 2.4×10^5 s^{-1} for H$_2$O and 1.8×10^4 s^{-1} for D$_2$O,[16] and $k_{^1O_2,NaN_3}^q$ is the second-order rate constant for ^{1}O$_2$ quenching by azide, amounting to 2.3×10^6 M^{-1} s^{-1} in H$_2$O[17] and 3×10^6 M^{-1} s^{-1} in D$_2$O.[18] The fractional decrease in ^{1}O$_2$ steady-state concentration due to the presence of 10 mM NaN$_3$ was calculated to be 90.2% in H$_2$O and 99.4% in D$_2$O.

Text S2.12. Calculation of the ^{1}O$_2$ concentration enhancement factor of D$_2$O

The decay rate constant of ^{1}O$_2$ in an H$_2$O/D$_2$O mixture in the absence of quenchers was calculated using the aforementioned decay rate constants for the pure solvents (see Text S2.11) using the following linear equation:[19]

$$k_{^1O_2, mixture}^{d,0} = X_{H_2O} k_{^1O_2, H_2O}^{d,0} + X_{D_2O} k_{^1O_2, D_2O}^{d,0} \qquad (S2.23)$$

Where X is the molar fraction of each solvent (H$_2$O or D$_2$O).

Since the steady-state concentration of $^1O_2$ is inversely proportional to $k_{^1O_2}^{d,0}$, one obtains the following relationship for the enhancement factor *EF*:

$$EF = \frac{\left[^1O_2\right]_{ss,mixture}}{\left[^1O_2\right]_{ss,H_2O}} = \frac{k_{^1O_2,H_2O}^{d,0}}{k_{^1O_2,mixture}^{d,0}}$$

(S2.24)

For the actual mixtures with D$_2$O-enriched water used in the experiments, i.e., with X_{H_2O} =0.05 and X_{D_2O} =0.95, the calculated increase in $^1O_2$ steady-state concentration for the mixture with respect to pure H$_2$O was by a factor of 8.25 (i.e., *EF*=8.25).

Text S2.13. Derivation of equation 2.12

The photosensitized transformation of DMABN and follow-up reactions can be represented as in Scheme S2.3.
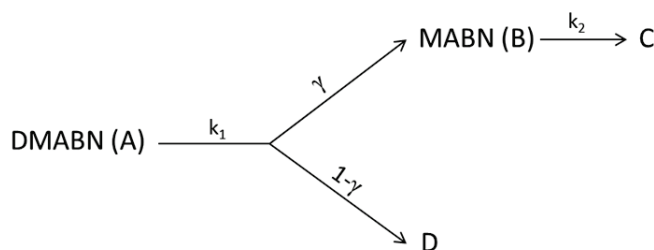
Scheme S2.3. Scheme of a consecutive reaction with a selectivity parameter γ. DMABN (A) is transformed with a reaction rate constant k_1 and a selectivity γ to MABN (B), the rest of reacting DMABN (1-γ) is transformed to other reaction products (D). MABN (B) is also subject to triplet-DOM induced phototransformation with a rate constant k_2 to give further oxidation products (C).

The differential equations describing the kinetics of A and B are as follows:

$$\frac{d[A]}{dt} = -k_1[A]$$

(S2.25)

$$\frac{d[B]}{dt} = \gamma k_1[A] - k_2[B]$$

(S2.26)

Integration of equation S2.25 yields eq. S2.27.

$$[A] = [A]_0 e^{-k_1 t}$$

(S2.27)

Substituting eq. S2.27 into eq. S2.26 one obtains:

$$\frac{d[B]}{dt} = \gamma k_1[A]_0 e^{-k_1 t} - k_2[B]$$

(S2.28)

This differential equation can be integrated by the usual integrating factor method (as for the classical type of consecutive first-order reactions without selectivity parameter, see for instance Ref. 20) to yield eq. S2.29, which is equivalent to eq. 2.12.

$$[B] = \frac{\gamma[A]_0 k_1}{k_2 - k_1}\left(e^{-k_1 t} - e^{-k_2 t}\right)$$

(S2.29)
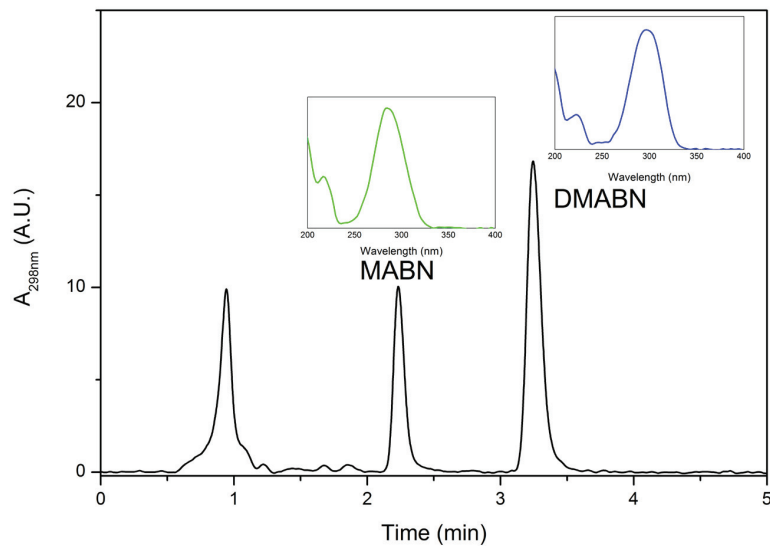
Figure S2.8. Typical HPLC chromatogram showing peaks corresponding to *N*-methyl-4-cyanoaniline (MABN, retention time 2.3 min) and *N,N*-dimethyl-4-cyanoaniline (DMABN, retention time 3.3 min). Insets: UV-visible absorption spectra for each peak. The peak at time 1 min correspond to the injection peak containing the fast eluting DOM. Analytical method as given in Table S2.4. Sample from an irradiation experiment of an aqueous solution containing 5 µM DMABN, 5 mg$_C$ L^{-1} Pony Lake fulvic acid and 5 mM phosphate buffer (pH 8), 20 minutes irradiation time under medium-pressure Hg lamp in the merry-go-round photoreactor equipped with a Pyrex cooling jacket and a 0.15 M NaNO$_3$ solution filter.
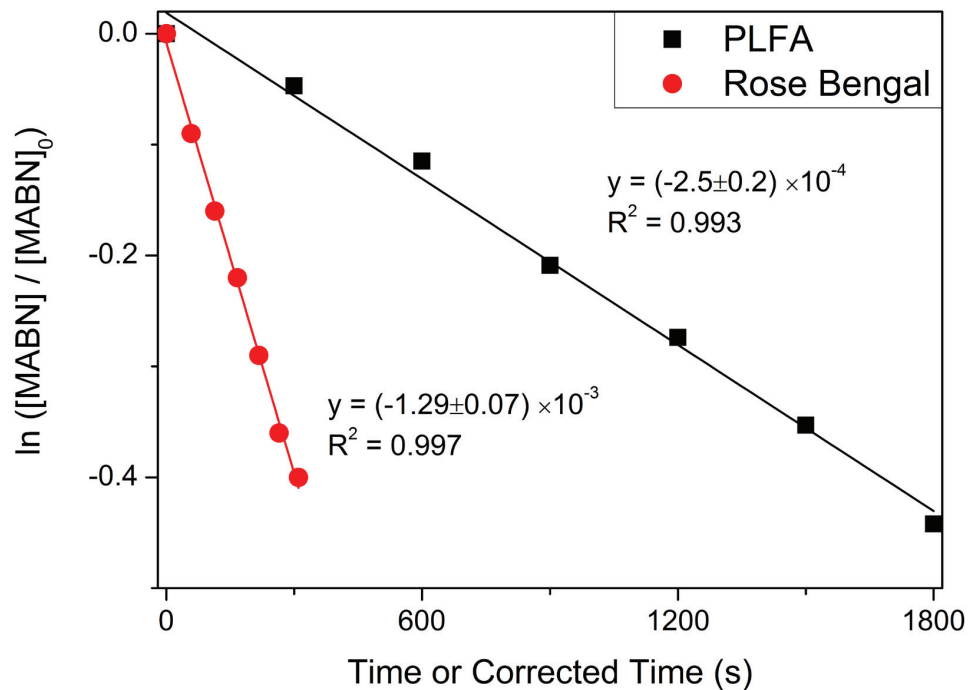
Figure S2.9. Determination of the pseudo-first-order phototransformation rate constant of *N*-methyl-4-cyanoaniline (MABN) in the presence of 5 mg$_C$ L^{-1} Pony Lake fulvic acid (PLFA, black squares) or 5 μM rose Bengal (red circles).

Table S2.7. Selectivity of the demethylation of *N,N*-dimethyl-4-cyanoaniline as function of phenol concentration in the presence of 5mg$_C$ L^{-1} Pony Lake fulvic acid.

	Phenol (μM)			
	0	2	10	50
Selectivity	72 ±4 %	78 ±3 %	78 ±2 %	75.3 ±1.3 %

Text S2.14. Transformation of variables for an alternative form of equation 2.6

As mentioned in the main paper, it may be useful to represent k_{TC}^{sens}, for a mixture of two different DOMs (DOM_1 and DOM_2), as a function of the total DOM concentration and the fraction of one of the DOMs. We define the new variables as follows:

$$DOC = [DOM_1] + [DOM_2] \tag{S2.30}$$

$$X_1 = \frac{[DOM_1]}{[DOM_1] + [DOM_2]} \tag{S2.31}$$

Now we express $[DOM_1]$ and $[DOM_2]$ using the new variables:

$$[DOM_1] = DOC \times X_1 \tag{S2.32}$$

$$[DOM_2] = DOC \times (1 - X_1) \tag{S2.33}$$

Substituting eqs. S2.32 and S2.33 into eq. 2.6 one obtains eq. S2.34, which is represented in the 3D plot of Figure 2.6B.

$$k_{TC}^{sens}(DOC, X_1) =$$

$$DOC \times \left\{ \beta_2 + X_1(\beta_1 - \beta_2) \right\} \times \frac{1 + DOC \times \left\{ \dfrac{1}{[DOM_2]_{1/2}} + X_1 \times \dfrac{[DOM_2]_{1/2} - [DOM_1]_{1/2}}{[DOM_1]_{1/2}[DOM_2]_{1/2}} \right\}(1-f)}{1 + DOC \times \left\{ \dfrac{1}{[DOM_2]_{1/2}} + X_1 \times \dfrac{[DOM_2]_{1/2} - [DOM_1]_{1/2}}{[DOM_1]_{1/2}[DOM_2]_{1/2}} \right\}} \tag{S2.34}$$

References for the supporting information

1. Ritchie, J. D.; Perdue, E. M., Proton-binding study of standard and reference fulvic acids, humic acids, and natural organic matter. *Geochim. Cosmochim. Acta* **2003,** *67*, (1), 85-96.

2. Aeschbacher, M.; Graf, C.; Schwarzenbach, R. P.; Sander, M., Antioxidant properties of humic substances. *Environ. Sci. Technol.* **2012,** *46*, (9), 4916-4925.

3. Wegelin, M.; Canonica, S.; Mechsner, K.; Fleischmann, T.; Pesaro, F.; Metzler, A., Solar water disinfection: Scope of the process and analysis of radiation experiments. *J. Water Supply Res. Technol. - Aqua* **1994,** *43*, (3), 154-169.

4. Bahnmüller, S.; von Gunten, U.; Canonica, S., Sunlight-induced transformation of sulfadiazine and sulfamethoxazole in surface waters and wastewater effluents. *Water Res.* **2014,** *57*, 183-192.

5. Nash, T., The colorimetric estimation of formaldehyde by means of the Hantzsch reaction. *Biochem. J.* **1953,** *55*, (3), 416-421.

6. Flyunt, R.; Leitzke, A.; Mark, G.; Mvula, E.; Reisz, E.; Schick, R.; von Sonntag, C., Determination of $^{\bullet}OH$, $O_2^{\bullet-}$, and hydroperoxide yields in ozone reactions in aqueous solution. *J. Phys. Chem. B* **2003,** *107*, (30), 7242-7253.

7. Wenk, J.; von Gunten, U.; Canonica, S., Effect of dissolved organic matter on the transformation of contaminants induced by excited triplet states and the hydroxyl radical. *Environ. Sci. Technol.* **2011,** *45*, (4), 1334-1340.

8. Tratnyek, P. G.; Hoigné, J., Oxidation of substituted phenols in the environment: A QSAR analysis of rate constants for reaction with singlet oxygen. *Environ. Sci. Technol.* **1991,** *25*, (9), 1596-1604.

9. Halladja, S.; ter Halle, A.; Aguer, J. P.; Boulkamh, A.; Richard, C., Inhihition of humic substances mediated photooxygenation of furfuryl alcohol by 2,4,6-trimethylphenol. Evidence for reactivity of the phenol with humic triplet excited states. *Environ. Sci. Technol.* **2007,** *41*, (17), 6066-6073.

10. al Housari, F.; Vione, D.; Chiron, S.; Barbati, S., Reactive photoinduced species in estuarine waters. Characterization of hydroxyl radical, singlet oxygen and dissolved organic matter triplet state in natural oxidation processes. *Photochem. Photobiol. Sci.* **2010,** *9*, (1), 78-86.

11. Loeff, I.; Rabani, J.; Treinin, A.; Linschitz, H., Charge-transfer and reactivity of nπ* and $\pi\pi$* organic triplets, including anthraquinonesulfonates, in interactions with inorganic anions: A comparative study based on classical Marcus theory. *J. Am. Chem. Soc.* **1993,** *115*, (20), 8933-8942.

12. Haag, W. R.; Hoigné, J.; Gassman, E.; Braun, A. M., Singlet oxygen in surface waters. 1. Furfuryl alcohol as a trapping agent. *Chemosphere* **1984,** *13*, (5-6), 631-640.

13. Latch, D. E.; Stender, B. L.; Packer, J. L.; Arnold, W. A.; McNeill, K., Photochemical fate of pharmaceuticals in the environment: Cimetidine and ranitidine. *Environ. Sci. Technol.* **2003,** *37*, (15), 3342-3350.

14. Buxton, G. V.; Greenstock, C. L.; Helman, W. P.; Ross, A. B., Critical review of rate constants for reactions of hydrated electrons, hydrogen atoms and hydroxyl radicals ($^{\bullet}OH/^{\bullet}O^-$) in aqueous solution. *J. Phys. Chem. Ref. Data* **1988,** *17*, (2), 513-886.

15. Westerhoff, P.; Aiken, G.; Amy, G.; Debroux, J., Relationships between the structure of natural organic matter and its reactivity towards molecular ozone and hydroxyl radicals. *Water Res.* **1999,** *33*, (10), 2265-2276.

16. Wilkinson, F.; Helman, W. P.; Ross, A. B., Rate constants for the decay and reactions of the lowest electronically excited singlet state of molecular oxygen in solution - An expanded and revised compilation. *J. Phys. Chem. Ref. Data* **1995,** *24*, (2), 663-1021.

17. Hasty, N.; Merkel, P. B.; Radlick, P.; Kearns, D. R., Role of azide in singlet oxygen reactions - Reaction of azide with singlet oxygen. *Tetrahedron Lett.* **1972,** *13*, (1), 49-52.

18. Rubio, M. A.; Martire, D. O.; Braslavsky, S. E.; Lissi, E. A., Influence of the ionic strength on $O_2(^1\Delta_g)$ quenching by azide. *J. Photochem. Photobiol. A-Chem.* **1992,** *66*, (2), 153-157.

19. Rodgers, M. A. J.; Snowden, P. T., Lifetime of O_2 $(^1\Delta_g)$ in liquid water as determined by time-resolved infrared luminescence measurements. *J. Am. Chem. Soc.* **1982,** *104*, (20), 5541-5543.

20. Frost, A. A.; Pearson, R. G., *Kinetics and mechanism*. 2nd ed.; John Wiley & Sons, Inc.: New York and London, 1961; p 405.

Chapter 3

Laser Flash Photolysis Study of the Photoinduced Oxidation of

4-(Dimethylamino)benzonitrile (DMABN)

Frank Leresche, Lucie Ludvíková, Dominik Heger, Petr Klán, Urs von Gunten, Silvio Canonica

Abstract

Aromatic amines are aquatic contaminants for which phototransformation in surface waters can be induced by excited triplet states of dissolved organic matter (^{3}DOM*). The first reaction step is assumed to consist of a one-electron oxidation process of the amine to produce its radical cation. In this paper, we present laser flash photolysis investigations aimed at characterizing the photoinduced, aqueous phase one-electron oxidation of 4-dimethylaminobenzonitrile (DMABN) as a representative of this contaminant class. The production of the radical cation of DMABN (DMABN$^{\bullet+}$) after direct photoexcitation of DMABN at 266 nm was confirmed by comparison with previous experimental results. Moreover, the formation of DMABN$^{\bullet+}$ was shown to occur after reaction of several excited triplet photosensitizers (carbonyl compounds) with DMABN. Second-order rate constants for the quenching of the excited triplet states by DMABN were determined to fall in the range of $0.03-5\times10^9$ M^{-1} s^{-1}, and their variations were interpreted in terms of electron transfer theory using a Rehm-Weller relationship. The decay kinetics of DMABN$^{\bullet+}$ was studied under various oxygen concentrations, pHs and excitation conditions. After an initial fast decay, a slower first-order decay component with lifetime values in the range of $25-125$ μs was observed. Kinetic modelling was used to assess the main reactions contributing to the decay of DMABN$^{\bullet+}$ in aerated solutions. Besides the reaction with the superoxide radical anion (O$_2^{\bullet-}$), H-atom shift with subsequent deprotonation and demethylation were suggested to be the main reactions governing the decay kinetics of DMABN$^{\bullet+}$.

3.1 Introduction

Aromatic amines constitute an important class of organic contaminants present in wastewaters and natural waters.[1-4] One of the major pathways contributing to their degradation in the aquatic environment is phototransformation induced by sunlight.[5-9] Besides direct phototransformation following absorption of sunlight by the contaminant, aromatic amines are subject to transformation photosensitized by dissolved organic matter (DOM). The latter is a complex mixture of cross-linked organic compounds derived from the degradation of higher plants or from microbial metabolic activity and ubiquitously present in natural waters.[10-13] Upon photoirradiation, the chromophoric components of DOM are promoted to their excited singlet states and subsequently excited triplet states (^{3}DOM*), which are likely to be the key reactive intermediates in the photosensitized transformation of aromatic amines in surface waters.[8, 14, 15] The initial reaction step in the photosensitized transformation is assumed to be an electron transfer from an aromatic amine to ^{3}DOM*.[16] This can be inferred from the abundant bibliography on the photoreduction of excited triplet carbonyls by amines,[17] arguments on the energetics of the redox reactions between substituted anilines and excited triplet aromatic ketones in aqueous solution,[14] and recent results on the quenching of excited triplet methylene blue by substituted anilines.[15] Formation of a radical cation of the aromatic amine, a primary product of such an electron transfer reaction, is expected.

Studies performed during the last decade in our research group have revealed another important effect of DOM on the photosensitized transformation of anilines, which consists in reducing the rates of transformation. Reduction of transformation intermediates of the anilines by electron-donating (also called antioxidant) moieties of the DOM was hypothesized to cause such an inhibition of transformation, and various pieces of evidence have been presented to support this hypothesis.[7, 14, 18-20]

The effects of DOM on the overall phototransformation rates of substituted anilines are now fairly well understood. However very little is known about the nature and fate of the intermediates produced after the first oxidation step. The main goal of the present study is to characterize the aqueous solution kinetics of such intermediates derived from a model aniline. We selected *N,N*-dimethyl-4-cyanoaniline (abbreviated as DMABN from the alternative name 4-dimethylaminobenzonitrile) for various reasons. Firstly, DMABN was used in a preceding steady-state photolysis kinetic study as a probe compound to assess photosensitized transformation rates of aromatic amines and analogous compounds that undergo DOM-induced inhibition of oxidation in surface waters.[20] Secondly, the results of this study showed that the DOM-photosensitized transformation of DMABN very likely proceeds by direct reaction between DMABN and ^{3}DOM*, whereby singlet oxygen plays a negligible role. Thirdly, DMABN has a doubly substituted aniline functionality, making its radical cation, (DMABN$^{\bullet+}$) more stable than the analogous species with singly substituted or unsubstituted aniline functionalities, which undergo efficient deprotonation. The relative stability of DMABN$^{\bullet+}$ is expected to provide favorable conditions for its direct observation in time-resolved experiments.

DMABN is the archetypal representative of aromatic compounds bearing both an electron-donating and an electron accepting group and exhibiting a dual fluorescence as well as excited-state charge separation in fluid solutions.[21, 22] The excited singlet state characteristics and dynamics of such compounds, in particular DMABN, have been a hot research topic in ultrafast spectroscopy for a few decades.[21, 23-26] Nevertheless, information about the photophysics and photochemistry of DMABN on a microsecond or longer timescale is limited. The transient absorption spectrum observed in the microsecond regime after laser flash photolysis (LFP) of an aqueous solution of DMABN was interpreted as the superposition of various species. These included the excited triplet state of DMABN (^{3}DMABN*, absorption maximum centered at 400 nm and a secondary broad band with maximum at ≈600 nm[27]), the hydrated electron (e_{aq}^-, very broad absorption centered at ≈720 nm), and DMABN$^{\bullet+}$ (absorption maximum at ≈500 nm). While ^{3}DMABN* is formed through intersystem crossing from the lowest excited singlet state of DMABN (^{1}DMABN*, see Equation 3.1) with substantial quantum yields (the value of 0.55 was determined for an ethanol solution[27]), e_{aq}^- and DMABN$^{\bullet+}$ were apparently formed through photoionization of DMABN (Equation 3.2). The photoionization of DMABN was found to be a wavelength-dependent process mainly occurring at irradiation wavelength of <280 nm. This indicated that photoionization did not involve ^{1}DMABN* but some higher excited states of DMABN.[27-29]

$$\text{DMABN} + h\nu \rightarrow {}^1\text{DMABN*} \rightarrow {}^3\text{DMABN*} \tag{3.1}$$

$$\text{DMABN} + h\nu \rightarrow \text{DMABN}^{\bullet+} + e_{aq}^- \tag{3.2}$$

The formation of DMABN$^{\bullet+}$ was implicitly assumed, but not directly observed, in a study on the reduction of excited triplet methylene blue by several aromatic amines.[30] DMABN$^{\bullet+}$ is believed to be the main species formed in natural waters upon oxidation of DMABN by ^{3}DOM*.[20]

The present study focuses on DMABN$^{\bullet+}$ formation and on the characterization of its aqueous solution kinetics under LFP conditions. Modelling of the decay kinetics of DMABN$^{\bullet+}$ was also performed to evaluate its main reaction pathways. To form DMABN$^{\bullet+}$, direct photoexcitation and photosensitized oxidation of DMABN were employed. This allowed a useful intercomparison of the results obtained by these two independent methods.

3.2   Experimental Section

3.2.1   Chemicals and Solutions

All chemicals were commercially available and used as received. A complete list of chemicals is given in the Supplementary Information (SI). Water used for all experiments was obtained from an Aqua Osmotic 02A purification system. All sample solutions, made by diluting stock solutions of the reagents, were buffered using 2 mM phosphate (total concentration) at pH 8.0, except when otherwise mentioned. Stock solutions were made in water except for the photosensitizers 3-methoxyacetophenone, 1-naphthaldehyde, 2-acetonaphthone and 1-acetonaphthone, for which acetonitrile (MeCN) was used as a solvent due to the limited solubility of these compounds in water. The concentration of the cosolvent MeCN in the sample solutions did not exceed 10% (v/v).

3.2.2   Laser Flash Photolysis (LFP) Setup

Nanosecond LFP experiments were conducted using a $4 \times 1 \times 1$ cm quartz cuvette containing the sample solution and laser pulses of the second, third or fourth harmonic from a Nd:YAG laser (EKSPLA, model SL334). The LFP setup was operated in a right-angle arrangement of the pump and probe beams. The laser pulses (pulse energies of 190–210 mJ at λ = 532 nm, 150–180 mJ at λ = 355 nm, and 70–90 mJ at λ = 266 nm; duration ≤170 ps) were dispersed on the 4 cm side of the cell using a cylindrical concave lens. Transient absorption spectra were recorded using an ICCD camera (Andor iStar, model DH740i-18U-03) with an overpulsed xenon arc lamp as a source of the probe light. Kinetic traces were recorded using the software TekScope on a Tektronix digital phosphor oscilloscope (model DPO7104C) at a single wavelength in the 400–670 nm wavelength window (see SI Table S3.3 for the wavelength used in the measurement of each particular transient) with a monochromator using a Hamamatsu photomultiplier tube R928. Absorbance values of the sample solutions were usually adjusted to 0.5–0.8 (for a 1-cm optical path length) at the excitation wavelength. Solutions were purged with a gentle stream of oxygen or N$_2$O for 15 minutes prior to measurements, naturally aerated or degassed by applying three freeze-pump-thaw cycles under reduced pressure (8 Pa). For the determination of second-order quenching rate constants, nominal equilibrium concentration of dissolved gases for an ambient temperature of 21 °C and atmospheric pressure of 99 kPa were assumed. These correspond to 2.80×10^{-4} M and 1.33×10^{-4} M for dissolved oxygen in aerated and O$_2$-purged solution, respectively, and to 2.7×10^{-2} M for dissolved N$_2$O. Electronic absorption spectra of the sample solutions were measured regularly between laser flashes to test for possible photodegradation of the solution components using the later described diode-array spectrophotometer. Experiments were conducted in an air-conditioned room at an ambient temperature of 21±1 °C.

3.2.3   Kinetic Analysis

The kinetic traces were generally fitted to single or multiple exponential decay model functions using the software Flash Fit v. 0.11. In the case of second-order kinetics fits, the corresponding differential equations were solved using the software Matlab, and the Levenberg-Marquard algorithm was applied to determine the best-fit parameters. The uncertainty of the first-order rate constants given in the tables is expressed as 95% confidence interval and was calculated using the values of at least triplicate measurements.

3.2.4   Analytical Instrumentation

Electronic absorption spectra in the ultraviolet (UV) and visible (Vis) range were measured on an Agilent Cary 100 UV-Vis or an Agilent 8654 diode-array spectrophotometer. A BNC pHTestr 10 pH meter equipped with a calibrated glass electrode or an equivalent Eutech Instruments pH600 was used to measure pH.

3.2.5   Kinetic Modelling

The software Kintecus$^{\copyright}$ was employed to model the decay kinetics of DMABN$^{\bullet+}$.[31] Briefly, this software solves the system of differential equations derived from the chemical reaction equations for the chemical system under study using a set of known reaction rate constants and initial concentrations of the chemical species involved. The output comprises the time course of the concentration of each considered species. The systems of reaction equations and corresponding rate constants used in the present study are described in the SI, Texts S3.1 and S3.2.

3.3   Results and Discussion

3.3.1   Direct Photoexcitation of 4-(Dimethylamino)benzonitrile (DMABN)

Direct photoexcitation of DMABN using laser pulses of 266 nm wavelength produced transient absorption spectra that are represented in Figure 3.1. A short-lived transient with a broad absorption band at 600−700 nm wavelength is evident at 5−60 ns delay times in aerated and oxygen-purged solutions, while less apparent in N₂O-purged solution. This transient can be safely assigned to e_{aq}^-, which is known to react with dissolved oxygen and N₂O at diffusion-controlled rates.[29] After the decay of the e_{aq}^- signal, two broad transient bands are apparent in all three solutions. The first of these bands has an absorption maximum at ≈400 nm and decays completely after 800 ns, while the second band has an absorption maximum at ≈500 nm and is especially apparent at long delay times (up to 5 μs). These components can be attributed to the excited triplet state of DMABN (^{3}DMABN*) and to the radical cation of DMABN (DMABN$^{•+}$), respectively.[27] The decay kinetics of the three key species, namely e_{aq}^-, ^{3}DMABN* and DMABN$^{•+}$, is described in more detail below.
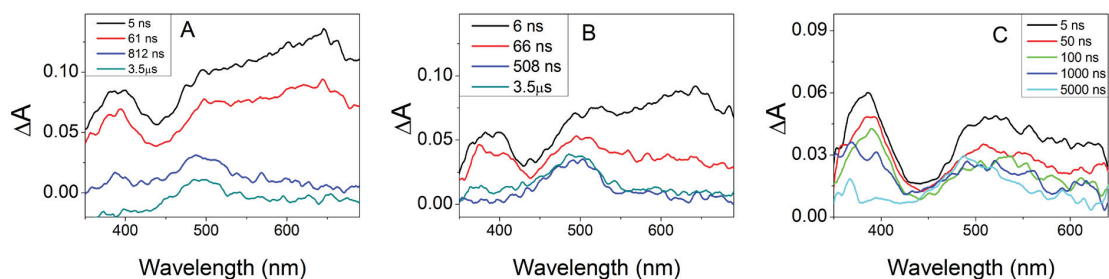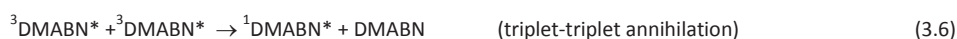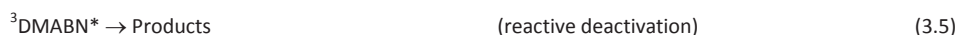

Figure 3.1. Transient absorption spectra obtained upon 266 nm laser flash photolysis of (A) DMABN (83 μM) in aerated solution, (B) DMABN (83 μM) in oxygen-purged solution, and (C) DMABN (133 μM) in N2O-purged solution. The spectra were recorded in the time range of 5 ns to 5 μs after the laser pulse (see legend) using a 5-ns integration window. All measurements were performed in pH 8.0 phosphate-buffered aqueous solutions.

3.3.1.1   Excited Triplet DMABN (3DMABN*)

The decay kinetics of ^{3}DMABN*, measured at the wavelength of 400 nm, was of first order except for degassed solution and exhibited varying decay rate constants (see Table 3.1) depending on the concentration of dissolved gases. In degassed solution the first-order deactivation rate constant of ^{3}DMABN*, corresponding the rate constant that would be observed at infinite dilution of this species, was determined by applying a kinetic model which included a second-order component to consider triplet−triplet annihilation (see SI, Text S3.8). The first-order deactivation rate constant for aerated and oxygen-purged solution was greatly enhanced with respect to degassed solution and nearly proportional to oxygen concentration. From a three-point linear regression a second-order rate constant for quenching of ^{3}DMABN* by oxygen of ≈4.3 × 10^9 M^{-1} s^{-1} was obtained. The deactivation of ^{3}DMABN* in the presence or absence of oxygen can be rationalized in terms of the processes described by Equations 3.3−9, whereby unimolecular deactivation (including contributions by the solvent, Equations 3.3−5) and triplet−triplet annihilation are dominant in degassed solution, while quenching by oxygen (Equations 3.7−9) is largely prevalent in aerated or oxygen-purged solution. A distinction of the processes within the groups of equations 3.3−5 and 3.7−9 is not possible in the frame of this study. However, the processes of reactive deactivation (Equation 3.5) and reactive quenching by oxygen (Equation 3.9) should have minor importance in view of the small quantum yield (1.3×10^{-3}) observed for the direct phototransformation of DMABN under steady-state illumination in aerated solution.[20]

$$^3\text{DMABN*} \rightarrow \text{DMABN} + h\nu \qquad \text{(phosphorescence)} \qquad (3.3)$$

$$^3\text{DMABN*} \rightarrow \text{DMABN} \qquad \text{(intersystem crossing)} \qquad (3.4)$$

$$^3\text{DMABN*} \rightarrow \text{Products} \qquad \text{(reactive deactivation)} \qquad (3.5)$$

$$^3\text{DMABN*} + {}^3\text{DMABN*} \rightarrow {}^1\text{DMABN*} + \text{DMABN} \qquad \text{(triplet-triplet annihilation)} \qquad (3.6)$$

$$^3DMABN^* + O_2 \rightarrow DMABN + {}^1O_2 \qquad \text{(energy transfer)} \qquad (3.7)$$

$$^3DMABN^* + O_2 \rightarrow DMABN + O_2 \qquad \text{(excitation energy loss)} \qquad (3.8)$$

$$^3DMABN^* + O_2 \rightarrow Products \qquad \text{(reactive quenching)} \qquad (3.9)$$

N_2O, used to scavenge e_{aq}^- (see the next sub-section), also contributed to the quenching of $^3DMABN^*$ (Table 3.1 and Equation 3.10), with a second-order rate constant that was estimated to be $\approx 2.4 \times 10^7 \, M^{-1} \, s^{-1}$.

$$^3DMABN^* + N_2O \rightarrow DMABN + N_2O \qquad \text{(excitation energy loss)} \qquad (3.10)$$
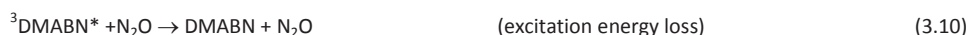
Moreover, the addition of CCl_4 was tested as a possible method to increase the formation rate of $DMABN^{\bullet+}$ (the central transient in this study) according to Equation 3.11.[32] A concentration of 3 mM CCl_4 in aerated solution contributed to an increase in the deactivation rate constant of $^3DMABN^*$ by $7.5 \times 10^5 \, s^{-1}$, yielding a second-order rate constant for quenching by CCl_4 of $\approx 2.5 \times 10^8 \, M^{-1} \, s^{-1}$. The effect of CCl_4-addition on quenching of $^3DMABN^*$ and $DMABN^{\bullet+}$ formation yield was much lower than previously observed for an MeCN solution, which means that this method did not turn out to be convenient to increase the strength of the $DMABN^{\bullet+}$ transient signal.

$$^3DMABN^* + CCl_4 \rightarrow DMABN^{\bullet+} + CCl_4^{\bullet-} \qquad \text{(reductive quenching)} \qquad (3.11)$$
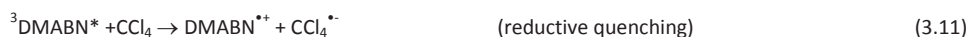
Table 3.1. Fitted first-order rate constants k^d for the deactivation of the main transient species formed upon 266 nm laser flash photolysis of aqueous DMABN (pH 8.0). The rate constants for $DMABN^{\bullet+}$ deactivation obtained from kinetic modelling ($k^{d,sim}$) are also shown.

Dissolved gases	$^3DMABN^*$ k^d $10^5 \, s^{-1}$	e_{aq}^- k^d $10^6 \, s^{-1}$	$DMABN^{\bullet+}$ k^d $10^4 \, s^{-1}$	Sim. $DMABN^{\bullet+}$ $k^{d,sim}$ $10^4 \, s^{-1}$
O_2 (1.33 mM) [a]	59.2 ±0.5	20 ±0.4	3.9 ±0.6	1.03
O_2 (0.28 mM) [b]	18.2 ±0.2	n.m. [c]	2.18 ±0.05	0.933
N_2O (0.027M) [d]	6.47 ±0.02	n.m. [c]	1.24 ±0.07	0.5
None [e]	1.07 ±0.70 [f]	1.8 ±0.3	0.8 ±0.2	0.5

Notes: [a] O_2-purged solution, $[DMABN]_0$=83 μM; [b] Aerated solution, $[DMABN]_0$=133 μM; [c] n.m.: not measured; [d] N_2O-purged solution, $[DMABN]_0$=133 μM; [e] Degassed solution, $[DMABN]_0$=133 μM; [f] Determined by non-exponential fitting as described in the SI, Text S3.8.

3.3.1.2 Hydrated Electron (e_{aq}^-)

Upon LFP of DMABN in oxygenated aqueous solution, the absorption corresponding to e_{aq}^- decayed following first-order kinetics with a rate constant that was proportional to oxygen concentration. The calculated second-order rate constant for this reaction was $(1.5\pm0.3) \times 10^{10} \, M^{-1} \, s^{-1}$, in good agreement with the known rate constant for the reaction of e_{aq}^- with oxygen ($1.9 \times 10^{10} \, M^{-1} \, s^{-1}$) to yield the superoxide radical anion ($O_2^{\bullet-}$, Equation 3.12).[29]

$$e_{aq}^- + O_2 \rightarrow O_2^{\bullet-} \qquad (3.12)$$

In degassed solution, the decay of e_{aq}^- also followed first-order kinetics but was an order of magnitude slower than that in oxygenated solution. It is proposed to be controlled by the reaction of e_{aq}^- with DMABN. This assumption is backed by the high second-order rate constants known for the reaction of e_{aq}^- with compounds similar to DMABN, such as benzonitrile ($1.9 \times 10^{10} \, M^{-1} \, s^{-1}$) and p-methylbenzonitrile ($1.4 \times 10^{10} \, M^{-1} \, s^{-1}$).[29] A comparison of the calculated pseudo-first-order rate constant for the reaction of e_{aq}^- with DMABN (estimated second-order rate constant of $1.4 \times 10^{10} \, M^{-1} \, s^{-1}$), with solvent or buffer components (H^+, OH^-, H_2O, Na^+, $H_2PO_4^-$ and HPO_4^{2-}) and with e_{aq}^- itself (all rate constant values from Ref. [29]), confirmed that the main decay pathway of e_{aq}^- in degassed solutions should be its reaction with DMABN.

In N$_2$O-purged solution, the signal corresponding to e^-_{aq} was not detected on the microsecond time scale (see Figure 3.1C) due to fast scavenging by N$_2$O, which is known to lead to the formation of the hydroxyl radical and elementary nitrogen (Equation 3.13).[33, 34] Under the employed experimental conditions, the pseudo-first-order decay rate constant of e^-_{aq} was estimated to be $\approx 2.5 \times 10^8$ s^{-1}.

$$e^-_{aq} + N_2O + H_2O \rightarrow N_2 + {}^{\bullet}OH + OH^- \tag{3.13}$$

3.3.1.3   Radical Cation of DMABN (DMABN$^{\bullet+}$)

The decay of DMABN$^{\bullet+}$ was found to follow first-order kinetics and to take place on a much longer time scale (lifetimes in the range of 25–125 µs) than the decay of the other species (see Table 3.1). The decay rate constants were determined by fitting the kinetic traces neglecting the data up to a delay time after the laser pulse of 3–9 µs, thus avoiding inclusion of the shorter-lived transients (i.e., e^-_{aq} and ^{3}DMABN*). An example of such a fitting is given in the SI, Figure S3.8. The decay rate constants (Table 3.1) varied as a function of the dissolved gases, being higher in oxygenated or aerated solution than those in N$_2$O-purged or degassed solutions. Various reactions may be hypothesized to contribute to the decay of DMABN$^{\bullet+}$ in oxygen-containing solutions, whereby bimolecular reactions with e^-_{aq} or O$_2^{\bullet-}$ (Equations 3.14 and 3.15) should at first glance yield a second-order kinetic component, because e^-_{aq}, and in O$_2$-containing solution O$_2^{\bullet-}$, are formed in nearly equimolar amounts as DMABN$^{\bullet+}$ upon LFP of DMABN.

$$DMABN^{\bullet+} + e^-_{aq} \rightarrow DMABN \tag{3.14}$$

$$DMABN^{\bullet+} + O_2^{\bullet-} \rightarrow DMABN + O_2 \tag{3.15}$$

The results of kinetic model calculations (Figure 3.2) for aerated or O$_2$-purged solution indicate that (1) the decay of e^-_{aq} is very fast and dominated by its reaction with O$_2$ (Equation 3.12), meaning that e^-_{aq} does not contribute directly to the decay of DMABN$^{\bullet+}$, and (2) the concentration of O$_2^{\bullet-}$, after the initial rise due to the scavenging of e^-_{aq} by O$_2$, remains almost constant, contrary to the simple expectation that it should decay as fast as DMABN$^{\bullet+}$. This almost constant O$_2^{\bullet-}$ concentration agrees well with the observed first-order deacy of DMABN$^{\bullet+}$ and can be rationalized in terms of additional O$_2^{\bullet-}$ production during the transformation of DMABN$^{\bullet+}$ to yield the *N*-demethylated product 4-(methylamino)benzonitrile (MABN). Such a reaction sequence considers an H-atom shift in DMABN$^{\bullet+}$ to yield a carbon-centered radical (abbreviated as DMABNr$^{\bullet}$) on one of the methyl groups upon deprotonation (Equation 3.16),[35] followed by production of O$_2^{\bullet-}$ after reaction with oxygen, finally yielding formaldehyde and MABN (see SI, Model S3.1 and Table S3.1). It is in line with the proposed reaction scheme for the photosensitized conversion of DMABN to MABN. Further, kinetic model calculations indicate that for N$_2$O-purged and degassed solutions the decay of DMABN$^{\bullet+}$ is entirely due to its deprotonation, giving a decay rate constant directly proportional to the deprotonation rate constant. For oxygenated and aerated conditions the model calculations indicate a faster DMABN$^{\bullet+}$ decay, which is controlled by both deprotonation and reaction with O$_2^{\bullet-}$.
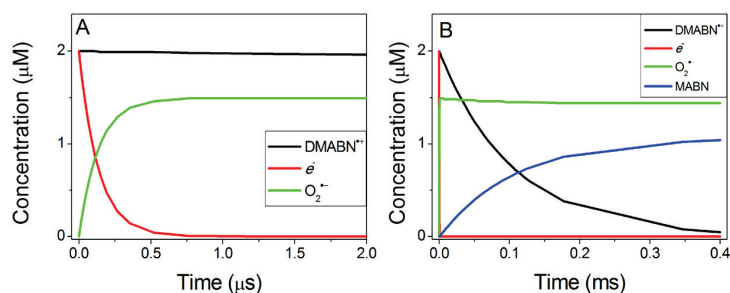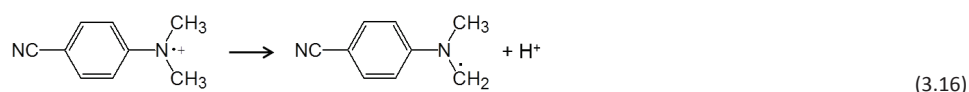
$$\tag{3.16}$$

Figure 3.2. Kinetic modelling of the transient species formed upon 266 nm laser pulse excitation of an aerated solution of DMABN (A) on a microsecond time scale and (B) on a millisecond time scale. Considered species: DMABN$^{\bullet+}$, e^-_{aq}, O$_2^{\bullet-}$ and MABN. Starting reactant concentrations: [DMABN$^{\bullet+}$] = [e^-_{aq}] = 2 µM, [O$_2$] = 2.8×10^{-4} M, [MABN] = 0 µM, pH 8. Starting concentrations of the

transients were set to approximately match the maximum experimental concentration of DMABN$^{\bullet+}$ determined at a delay time of 2μs after the laser pulse.

3.3.1.4 pH Effect

To obtain additional hints about the reactions contributing to the decay of ^{3}DMABN* and DMABN$^{\bullet+}$, their first-order rate constants were investigated in aerated and N$_2$O-purged solutions by varying the pH. For ^{3}DMABN*, the deactivation rate constant was not affected by pH in the range of 4.4–7.8 (Figure 3.3A), while in N$_2$O-purged solution, it was pH-dependent with a marked increase at pH 7.8 compared to the lower pH range. We do not have an explanation for such a pH-dependent quenching of ^{3}DMABN* by N$_2$O. For DMABN$^{\bullet+}$, the decay rate constant increased with pH (same range as above) in both aerated and N$_2$O-purged solution (Figure 3.3B). However, the observed increase is rather steady, with the absence of inflection points as in the case of protonation equilibria, and limited, with a maximum of +46% in aerated solution. This makes it difficult to assign the pH dependence to a well-defined reaction contributing to the decay of DMABN$^{\bullet+}$. Kinetic modelling calculations do not catch the full extent of the effects but indicate that for O$_2$-containing solutions the main factor responsible for the pH effect is the O$_2^{\bullet-}$ concentration, being lower at low pH due to its protonation reaction to the HO$_2^{\bullet}$ radical (pK$_a$.= 4.8).[36] This lower O$_2^{\bullet-}$ concentration may decrease the recombination reaction between DMABN$^{\bullet+}$ and O$_2^{\bullet-}$ (Equation 3.15) thus prolonging the DMABN$^{\bullet+}$ lifetime. For N$_2$O-purged solutions, the calculations indicate a stable DMABN$^{\bullet+}$ lifetime between pH 6 and 8, and an increase of the lifetime in lower pH region, possibly due to protonation of the carbon-centered radical DMABNr$^{\bullet}$ (the reverse reaction of Equation 3.16). However, we think that the accuracy of the kinetic model for O$_2$-free solutions is limited due to the lack of information on the fate of DMABNr$^{\bullet}$ under these conditions.
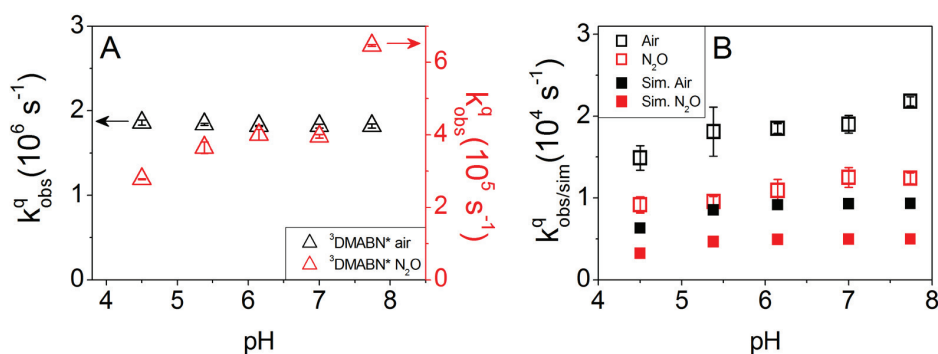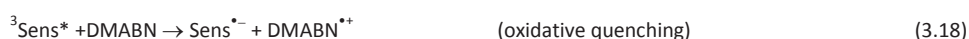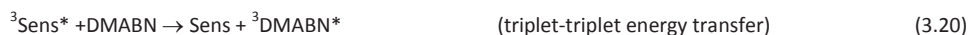

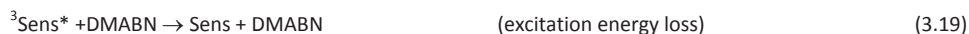**Figure 3.3.** Effect of pH on the first-order rate constants for the decay of (A) ^{3}DMABN* and (B) DMABN$^{\bullet+}$, for aerated (black symbols) and N$_2$O ventilated solutions (red symbols). Modelled rate constants for DMABN$^{\bullet+}$ are shown as filled circles.

3.3.2 Photosensitized Formation of DMABN$^{\bullet+}$

Several photosensitizers were used as a means to oxidize DMABN to DMABN$^{\bullet+}$. Upon irradiation of a photosensitizer (Sens) its excited triplet state (^{3}Sens*) is formed following intersystem crossing from the excited singlet states (Equation 3.17). ^{3}Sens* can act in certain cases as a powerful oxidant. Especially aromatic ketones and quinones possess standard one-electron reduction potentials (E_{red}^{0*}(^{3}Sens*/Sens$^{\bullet-}$)) that are comparable to those of the strongest radical oxidants. [37] The oxidation reaction of DMABN by ^{3}Sens* is expected to produce DMABN$^{\bullet+}$ as well as the radical anion of the photosensitizer (Sens$^{\bullet-}$) within the lifetime of ^{3}Sens* (Equation 3.18). Besides the unimolecular and bimolecular deactivation processes that were listed for ^{3}DMABN* (Equations 3.3–9), oxidizing ^{3}Sens* are expected to undergo the following additional reactions with DMABN: Excitation energy loss (Equation 3.19) and triplet–triplet energy transfer from ^{3}Sens* to DMABN (Equation 3.20). Both reactions 3.18 and 3.19 have been observed during the quenching of excited triplet methylene blue by DMABN in methanol solution with a ratio of 1:3 between electron transfer and physical quenching.[30] While we are not aware of any method that could be used to maximize the yield of DMABN$^{\bullet-}$ formation during quenching (i.e., the ratio of the relative rate constants of reactions 3.18 and 3.19), the energy transfer reaction (Equation 3.20), and consequently the formation of ^{3}DMABN*, can be suppressed by choosing photosensitizers with a lower triplet energy than DMABN.

$$Sens + h\nu \rightarrow {}^1Sens* \rightarrow {}^3Sens* \tag{3.17}$$

$$^3Sens* + DMABN \rightarrow Sens^{\bullet-} + DMABN^{\bullet+} \quad \text{(oxidative quenching)} \tag{3.18}$$

$$^3Sens^* + DMABN \rightarrow Sens + DMABN \qquad \text{(excitation energy loss)} \qquad (3.19)$$

$$^3Sens^* + DMABN \rightarrow Sens + {}^3DMABN^* \qquad \text{(triplet-triplet energy transfer)} \qquad (3.20)$$

To avoid direct excitation of DMABN, the 355 nm and 532 nm excitation wavelengths of the laser were used to selectively produce $^3Sens^*$. The sensitizers were selected to cover a range of one-electron oxidation potentials that could be used to estimate the oxidation potential of DMABN in aqueous solution (presently unknown). Moreover, practical aspects, such as the aqueous solubility of the photosensitizers and the feasibility of their selective excitation were considered.

3.3.2.1 Transient Absorption Spectra

To disentangle the spectra of $^3Sens^*$, $Sens^{\bullet-}$ and $DMABN^{\bullet+}$ present after LFP of solutions containing a given photosensitizer and DMABN, and to select suitable observation wavelength for the kinetic measurements, the following procedure was applied: (1) Generation of the $^3Sens^*$ from a buffered solution of the photosensitizer alone; (2) Generation of $^3Sens^*$, and subsequently $Sens^{\bullet-}$, from a buffered solution containing the photosensitizer and triethanolamine (TEA. Note: The radicals formed from the oxidation of TEA absorb only outside of the considered spectral range [38]); (3) Production of the three species $^3Sens^*$, $Sens^{\bullet-}$ and $DMABN^{\bullet+}$ in a buffered solution of the photosensitizer and DMABN. An illustrative example of this procedure using 2-acetonaphthone (2-AN) as a model photosensitizer, chosen owing to the clear separation of the absorption bands of the various transients, is shown in Figure 3.4. The transient absorption spectrum of the excited triplet state of 2-AN (^{32}-AN*) has a main band centered at ≈440 nm and a secondary band at ≈380 nm (Figure 3.4A), while the spectrum of the radical anion of 2-AN (2AN$^{\bullet-}$) over-laps partly with that of ^{32}-AN* but has its maximum absorption at ≈400 nm (Figure 3.4B). The spectra shown in Figure 3.4C contain a dominating superposition of ^{32}-AN* and 2-AN$^{\bullet-}$ at short delay times (up to ≈500 ns) after the laser pulse, but at longer delay times a band centered at ≈500 nm clearly emerged. This was assigned to $DMABN^{\bullet+}$ based on its similarities to the spectra of $DMABN^{\bullet+}$ observed from direct photoexcitation of DMABN in this work (Figure 3.1) and in other studies.[27, 32] Note that the presence of oxygen is beneficial to the observation of $DMABN^{\bullet+}$, because it accelerates the decay of $Sens^{\bullet-}$ (in this case 2-AN$^{\bullet-}$) according to Equation 3.21, leaving $DMABN^{\bullet+}$ as the only absorbing species in the considered spectral range at long delay times.

$$Sens^{\bullet-} + O_2 \rightarrow Sens + O_2^{\bullet-} \qquad (3.21)$$

The transient absorption spectra shown in Figure 3.4 were utilized to evaluate the optimal observation wavelength to be used for the measurement of kinetic traces and the determination of decay rate constants of the various species. Figure 3.4D displays an example of Stern-Volmer plot used in the determination of second-order rate constants for the quenching of ^{32}-AN* by DMABN.
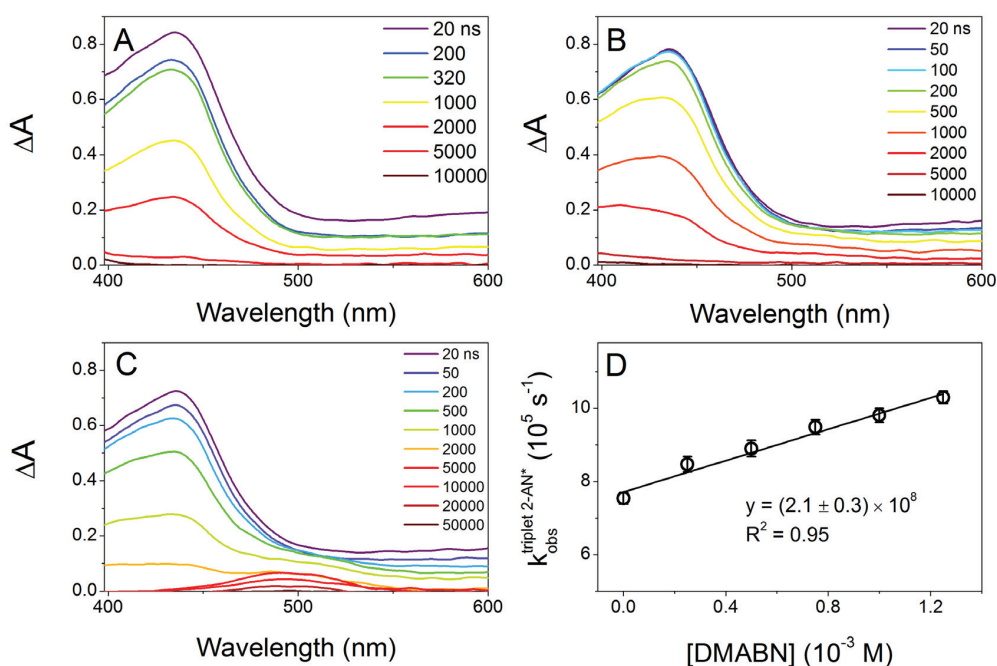
Figure 3.4. A–C: Transient absorption spectra following 355 nm laser pulse excitation of: (A) 2-Acetonaphthone (2-AN, 500 μM); (B) 2-AN (500 μM) and triethanolamine (TEA, 10 mM); (C) 2-AN (500 μM) and DMABN (500 μM). All solutions in pH 8.0 aerated water containing 0.9% (v/v) acetonitrile. (D) A Stern-Volmer plot of the first-order decay rate constant of the triplet state of 2-AN (obtained at the observation wavelength of 520 nm) vs. DMABN concentration. Error bars represent 95% confidence intervals from at least quadruplicate measurements. Spectra were recorded in the time range from 20 ns to 50 μs after the laser pulse using a 5-ns integration window.

3.3.2.2   Quenching of Excited Triplet Photosensitizers by DMABN

For photosensitizers having oxidizing excited triplet states, quenching rate constants can be used as an indicator of the efficacy in producing the oxidized substrate. For the sake of DMABN$^{\bullet+}$ production at sufficiently high concentration to allow an accurate evaluation of its decay kinetics, high ^{3}Sens* second-order quenching rate constants are advantageous. Under these conditions the oxidation potential of DMABN, currently unknown in aqueous solution, can be estimated as is shown below. Table 3.2 collects the second-order quenching rate constants obtained in this study for six photosensitizers exhibiting E_{red}^{0*} values in the range of 1.26−1.86 V vs. standard hydrogen electrode (SHE). The quenching rate constants vary over about two orders of magnitude and increase non-linearly with increasing E_{red}^{0*}. Literature values of the triplet energies of the photosensitizers are also collected in Table 3.2 to evaluate the possibility of energy transfer as a side-reaction (Equation 3.20). Only 3-methoxyacetophenone has a triplet energy that is higher than that one of DMABN (3.14 eV),[39] but no evidence for the formation of ^{3}DMABN* could be found in transient absorption spectra using this photosensitizer. For all other photosensitizers energy transfer can be excluded *a priori*.

Table 3.2. Ground-state reduction potentials (E_{red}^0), triplet-state reduction potentials (E_{red}^{0*}), triplet energies (E_T) and measured second-order triplet quenching rate constants by DMABN ($k_{3\mathrm{Sens*,DMABN}}^\mathrm{q}$) for the studied photosensitizers.

Photosensitizer (Sens)	$E^{\circ\prime}{}_{red}$ [a]	$E^{\circ\prime*}{}_{red}$ [a]	E_T [a]	$k^\mathrm{q}_{3\mathrm{Sens*,DMABN}}$ [b]
	V vs. SHE	V vs. SHE	eV	10^9 M^{-1} s^{-1}
9,10-Anthraquinone-1,5-disulfonate	-0.5	1.86	2.36	5.02 ±0.16
3-Methoxyacetophenone	-1.43 [c]	1.71 [c]	3.14 [c]	4.0 ±0.2 [d]
Thionine	-0.25	1.45	1.70	4.6 ±0.3
1-Naphthaldehyde [c]	-1.11	1.34	2.45	3.4 ±0.3 [e]
2-Acetonaphthone [c]	-1.25	1.34	2.59	0.21 ±0.03 [e]
1-Acetonaphthone [c]	-1.26	1.26	2.52	0.031 ±0.017 [e]

Notes: [a]Standard one-electron reduction potentials of the photosensitizers in their electronic ground state (E_{red}^0) and excited triplet state (E_{red}^{0*}) as well as triplet energies (E_T) obtained from Ref. [37] unless otherwise noted; [b]Measured in aerated aqueous solution at pH 8.0. Errors represent 95% confidence intervals obtained from the linear regression lines (Stern-Volmer plots); [c]From Ref. [39]; [d]Solutions containing 10% (v/v) acetonitrile; [e]Solutions containing ≈1% (v/v) acetonitrile.

In the following we analyze the rate constants for triplet quenching by DMABN in the frame of electron transfer theory, and more precisely by using the Rehm-Weller relationship (equation 3.22).[40-42]

$$k^\mathrm{q} = \frac{k_\mathrm{d}}{1 + \frac{k_\mathrm{d}}{K_\mathrm{d}Z}\left\{\exp\left[\left(\sqrt{\left(\frac{\Delta_\mathrm{r}G_\mathrm{et}^0}{2}\right)^2 + \left(\frac{\lambda}{4}\right)^2} + \left(\frac{\Delta_\mathrm{r}G_\mathrm{et}^0}{2}\right)\right)/RT\right] + \exp\left(\frac{\Delta_\mathrm{r}G_\mathrm{et}^0}{RT}\right)\right\}} \tag{3.22}$$

The parameters are defined as follows: k_d is the diffusion-controlled second-order reaction rate constant, $K_\mathrm{d} = k_\mathrm{d}/k_{-\mathrm{d}}$ is the equilibrium constant for the formation of the encounter complex, Z is the universal collision frequency factor, R is the universal gas constant, T is the absolute temperature, λ is the reorganization energy, and $\Delta_\mathrm{r}G_\mathrm{et}^0$ is the standard molar free energy change of the electron transfer reaction, i.e., the standard molar free energy difference between successor complex and precursor complex, which was approximated using Equation 3.23.

$$\Delta_\mathrm{r}G_\mathrm{et}^0 \cong F \times \left(E_\mathrm{red}^0\left(\mathrm{DMABN}^{\bullet+}/\mathrm{DMABN}\right) - E_\mathrm{red}^{0*}\left(^3\mathrm{Sens}^*/\mathrm{Sens}^{\bullet-}\right)\right) \tag{3.23}$$

For the fittings of the quenching rate constant data to Equation 3.23 was inserted in Equation 3.22, and $E_{\text{red}}^{0*}(^3\text{Sens*/Sens}^{\bullet-})$ was used as the x-variable while $E_{\text{red}}^0(\text{DMABN}^{\bullet+}/\text{DMABN})$ was employed as a fit parameter, whereby a similar procedure as in Ref. [43] was applied, keeping the ratio $k_d/(K_d \times Z)$ fixed at 0.1. The fit parameters were $E_{\text{red}}^0(\text{DMABN}^{\bullet+}/\text{DMABN})$ and λ, while k_d was fixed at 5.0×10^9 M^{-1} s^{-1}. Fits to the Rehm-Weller equation are represented in Figure 3.5, whereby fits with various fixed values of λ are also shown. The best fit to the Rehm-Weller equation gives a value of 0 kJ/mol for λ, but uncertainty in the fitting parameters are large due to the limited number of data points. Using a fixed value of λ=20 kJ mol^{-1} (a value which was obtained for the quenching of excited triplet methylene blue by a series of substituted anilines [15]) also yields a reasonably good fit yielding $E_{\text{red}}^0(\text{DMABN}^{\bullet+}/\text{DMABN})$ =1.33±0.08 V vs. SHE (used as the only fitting parameter). This value is slightly higher (by 0.14 V) than a crude estimation obtained by adding the difference between the oxidation potentials of 4-cyanoaniline (1.32 V)[45] and aniline (1.00 V)[45] to the oxidation potential of *N,N*-dimethylaniline (0.87 V),[46] all measured in aqueous solution. Note that the value determined in MeCN for $E_{\text{red}}^0(\text{DMABN}^{\bullet+}/\text{DMABN})$ is 1.11 V,[44] which is significantly lower than our estimated value in water obtained from the Rehm-Weller fitting.
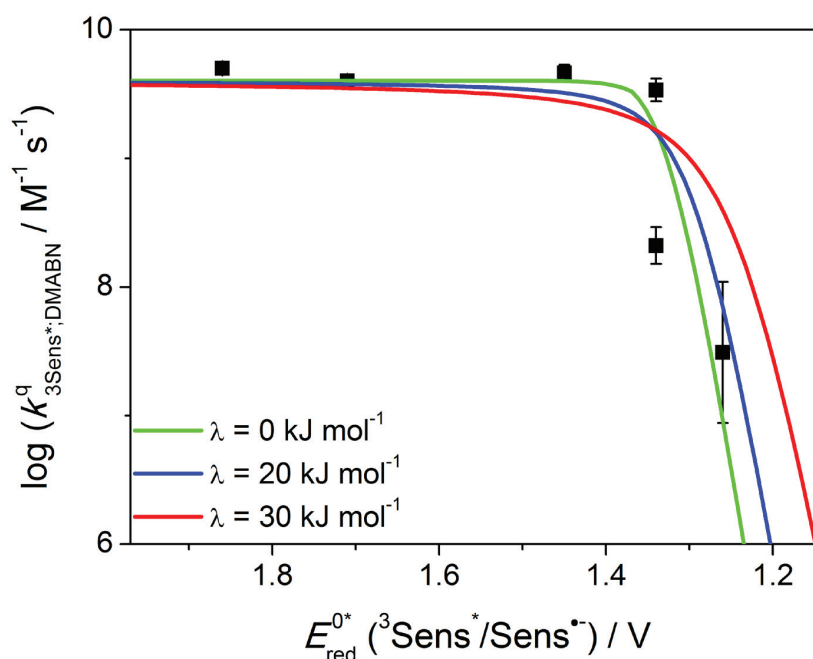

Figure 3.5. Measured second-order rate constant for the quenching of excited triplet photosensitizers by DMABN ($k^{\text{q}}_{^3\text{Sens*,DMABN}}$) (black squares) plotted on a logarithmic scale against $E_{\text{red}}^{0*}(^3\text{Sens*/Sens}^{\bullet-})$, the one-electron reduction potential of the excited triplet photosensitizers. The lines represent fits to the Rehm-Weller model with reorganization energy (λ) values as given in the legend. The fitting procedure is explained in the text. Errors bars represent 95% confidence intervals obtained from Stern-Volmer plots (see Figures 3.4D and S3.7).

3.3.2.3   Factors Controlling the Decay of DMABN$^{\bullet+}$

Figure 3.6A shows the dependence of the pseudo-first-order decay rate constant of DMABN$^{\bullet+}$ on the concentration (or "effective concentration", see definition below) of 1-naphthaldehyde (1-NA), which was used as a photosensitizer. Experimental details on the determination of these constants are given in the SI, Text S3.7. In the present series of experiments, the concentration of 1-NA was varied in the range of 50–300 μM, and additionally the laser pulse intensity was decreased by means of metal-grid filters for an experimental series conducted at 50 μM 1-NA concentration. The "effective concentration" of 1-NA was thus calculated by multiplying the concentration of 50 μM by the transmittance of the filter. Assuming a constant laser pulse energy over the whole experimental series, concentration and "effective concentration" should be directly proportional to the "initial" concentration of ^{3}1-NA* (the concentration of ^{3}1-NA* formed by the laser pulse). It is apparent from Figure 3.6A that the decay rate constant of DMABN$^{\bullet+}$ increases non-linearly with the concentration and the "effective concentration" of 1-NA, and thus with the "initial" concentration of ^{3}1-NA*.

To further elucidate the reactions controlling the decay of DMABN$^{\bullet+}$ under the conditions of photosensitization, kinetic modelling was employed. In addition to the reactions discussed in sub-section 3.1.3., DMABN$^{\bullet+}$ can be assumed to undergo a one-electron reduction by Sens$^{\bullet-}$ (Equation 3.24).

$$DMABN^{\bullet+} + Sens^{\bullet-} \rightarrow DMABN + Sens \qquad (3.24)$$

This reaction is expected to be nearly diffusion-controlled, but in aerated solution it would be overruled by the fast reaction between DMABN$^{\bullet+}$ and O$_2^{\bullet-}$ (Equation 3.15) at relatively short delay times ($>\approx 3$ μs) after the laser pulse, because Sens$^{\bullet-}$ should be scavenged by oxygen for most photosensitizers to give O$_2^{\bullet-}$ (Equation 3.21). Kinetic modelling was performed according to the details given in the SI, Model S3.2 and Table S3.2 and confirmed this qualitative evaluation. The results of the kinetic modelling provide values of the rate constant for the decay of DMABN$^{\bullet+}$ that are comparable to those determined experimentally (see Figure 3.6A). Using modelling, a larger range of the initial ^{3}1-NA* concentration than that experimentally available is accessible, which suggests that the decay constant of DMABN$^{\bullet+}$ is further reduced for small concentrations of ^{3}1-NA*. Further details of the modelling results indicate that the reaction of O$_2^{\bullet-}$ with DMABN$^{\bullet+}$ (Equation 3.15) is the dominant pathway for the disappearance of DMABN$^{\bullet+}$ for an ^{3}1-AN* starting concentration above 2 μM, while for lower starting concentrations the deprotonation reaction (Equation 3.16) dominates (see Figure 3.6B to 3.6D).
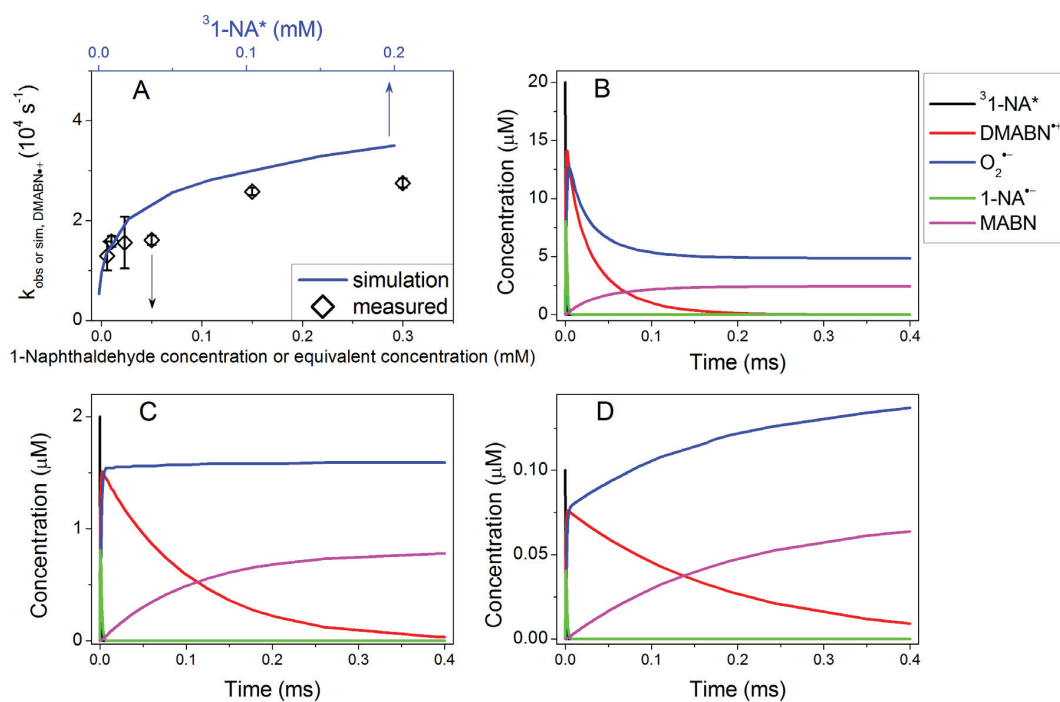

Figure 3.6. (A) Measured first-order decay rate constant of DMABN$^{\bullet+}$ (black open diamonds) vs. the concentration or "effective concentration" of 1-naphthaldehyde (1-NA) (see text for explanations). The values obtained from kinetic modelling are also shown as a blue line, which is plotted vs. the initial ^{3}1-NA* concentration (upper x-axis). Errors bars represent 95% confidence interval from the mean of at least triplicates measurements. (B–D) Kinetic modelling results showing the concentration time course of: ^{3}1-NA*, DMABN$^{\bullet+}$, O2$^{\bullet-}$, the radical anion of 1-NA (1-NA$^{\bullet-}$) and 4-(methylamino)benzonitrile (MABN). Modelling calculations performed with varying initial ^{3}1-NA* concentration: (B) 20 μM, (C) 2 μM, and (D) 100 nM. All measurements or kinetic model calculations were obtained for aerated solution at pH 8.

3.4 Conclusions

This study focused on the decay kinetics of the radical cation of DMABN (DMABN$^{\bullet+}$), which was produced upon direct and sensitized laser flash excitation in aqueous solution. The lifetime of DMABN$^{\bullet+}$ appeared to be limited by H-atom shift and subsequent deprotonation in oxygen-free solution, with a decay rate constant estimated to be on the order of $\approx 5 \times 10^3$ s^{-1}. In the presence of

dissolved oxygen, the decay of DMABN$^{\bullet+}$ was also significantly affected by its reaction with the superoxide radical anion (O$_2^{\bullet-}$), leading to the reformation of DMABN. However, we expect that this reaction should be negligible for irradiation conditions occurring in the aquatic environment because of the very low concentration O$_2^{\bullet-}$ (10^{-12}–10^{-9} M)[47] found under these conditions. The reaction of DMABN$^{\bullet+}$ with dissolved organic matter, an important natural water component, will be the subject of a follow-up study intended to assess the phototransformation rates of DMABN and analogous aquatic contaminants in surface waters.

3.5 Acknowledgements

3.6 References for chapter 3

1. W. W. Stone, R. J. Gilliom and K. R. Ryberg, *Environ. Sci. Technol.*, 2014, **48**, 11025-11030.
2. C. Moschet, I. Wittmer, J. Simovic, M. Junghans, A. Piazzoli, H. Singer, C. Stamm, C. Leu and J. Hollender, *Environ. Sci. Technol.*, 2014, **48**, 5423-5432.
3. T. A. Ternes, *Water Res.*, 1998, **32**, 3245-3260.
4. X. S. Miao, F. Bishay, M. Chen and C. D. Metcalfe, *Environ. Sci. Technol.*, 2004, **38**, 3533-3541.
5. K. Othmen and P. Boule, *J. Photochem. Photobiol. A- Chem.*, 1999, **121**, 161-167.
6. D. Vialaton, J. F. Pilichowski, D. Baglio, A. Paya-Perez, B. Larsen and C. Richard, *J. Agr. Food Chem.*, 2001, **49**, 5377-5382.
7. S. Canonica and H. U. Laubscher, *Photochem. Photobiol. Sci.*, 2008, **7**, 547-551.
8. A. L. Boreen, W. A. Arnold and K. McNeill, *Environ. Sci. Technol.*, 2005, **39**, 3630-3638.
9. J. J. Guerard, P. L. Miller, T. D. Trouts and Y. P. Chin, *Aquat. Sci.*, 2009, **71**, 160-169.
10. J. A. Leenheer and J. P. Croué, *Environ. Sci. Technol.*, 2003, **37**, 18A-26A.
11. C. Richard and S. Canonica, in *Handbook of Environmental Chemistry*, ed. O. Hutzinger, Springer-Verlag Berlin, Heidelberger Platz 3, D-14197 Berlin, Germany, 2005, vol. 2, pp. 299-323.
12. J. Hoigné, B. C. Faust, W. R. Haag, F. E. Scully and R. G. Zepp, *ACS Sym. Ser.*, 1989, **219**, 363-381.
13. D. Vione, M. Minella, V. Maurino and C. Minero, *Chem. Eur. J.*, 2014, **20**, 10590-10606.
14. J. Wenk and S. Canonica, *Environ. Sci. Technol.*, 2012, **46**, 5455-5462.
15. P. R. Erickson, N. Walpen, J. J. Guerard, S. N. Eustis, J. S. Arey and K. McNeill, *J. Phys. Chem. A*, 2015, **119**, 3233-3243.
16. R. G. Zepp, P. F. Schlotzhauer and R. M. Sink, *Environ. Sci. Technol.*, 1985, **19**, 74-81.
17. S. G. Cohen, A. Parola and G. H. Parsons, *Chem. Rev.*, 1973, **73**, 141-161.
18. J. Wenk, U. von Gunten and S. Canonica, *Environ. Sci. Technol.*, 2011, **45**, 1334-1340.
19. J. Wenk, M. Aeschbacher, M. Sander, U. von Gunten and S. Canonica, *Environ. Sci. Technol.*, 2015, **49**, 8541-8549.
20. F. Leresche, U. von Gunten and S. Canonica, *Environ. Sci. Tech.*, 2016, **50**, 10997-11007.
21. Z. R. Grabowski, K. Rotkiewicz and W. Rettig, *Chem. Rev.*, 2003, **103**, 3899-4031.
22. A. Demeter and K. A. Zachariasse, *Journal of Physical Chemistry A*, 2008, **112**, 1359-1362.
23. W. Rettig, *J. Lumines.*, 1981, **26**, 21-46.
24. S. I. Druzhinin, N. P. Ernsting, S. A. Kovalenko, L. W. Lustres, T. A. Senyushkina and K. A. Zachariasse, *Journal of Physical Chemistry A*, 2006, **110**, 2955-2969.
25. J. Catalán, *Phys. Chem. Chem. Phys.*, 2013, **15**, 8811-8820.
26. S. I. Druzhinin, V. A. Galievsky, A. Demeter, S. A. Kovalenko, T. Senyushkina, S. R. Dubbaka, P. Knoche, P. Mayer, C. Grosse, D. Stalke and K. A. Zachariasse, *Journal of Physical Chemistry A*, 2015, **119**, 11820-11836.
27. G. Köhler, G. Grabner and K. Rotkiewicz, *Chem. Phys.*, 1993, **173**, 275-290.
28. G. Köhler, N. Getoff, K. Rotkiewicz and Z. R. Grabowski, *J. Photochem.*, 1985, **28**, 537-546.
29. G. V. Buxton, C. L. Greenstock, W. P. Helman and A. B. Ross, *J. Phys. Chem. Ref. Data*, 1988, **17**, 513-886.
30. R. H. Kayser and R. H. Young, *Photochem. Photobiol.*, 1976, **24**, 395-401.
31. J. C. Ianni, Kintecus Windows version 5.20, 2014. www.kintecus.com (accessed August 2016)
32. R. J. Visser, P. C. M. Weisenborn, J. Konijnenberg, B. H. Huizer and C. A. G. O. Varma, *J. Photochem.*, 1986, **32**, 217-233.
33. F. S. Dainton and D. B. Peterson, *Proc. R. Soc. Lon. Ser-A*, 1962, **267**, 443-463.
34. D. Zehavi and J. Rabani, *J Phys Chem-Us*, 1971, **75**, 1738-1744.
35. E. Baciocchi, M. Bietti, M. F. Gerini and O. Lanzalunga, *J. Org. Chem.*, 2005, **70**, 5144-5149.
36. B. H. J. Bielski, D. E. Cabelli, R. L. Arudi and A. B. Ross, *J. Phys. Chem. Ref. Data*, 1985, **14**, 1041-1100.
37. I. Loeff, J. Rabani, A. Treinin and H. Linschitz, *J. Am. Chem. Soc.*, 1993, **115**, 8933-8942.
38. K. Kalyanasundaram, J. Kiwi and M. Gratzel, *Helv. Chim. Acta*, 1978, **61**, 2720-2730.
39. H. Shizuka and H. Obuchi, *J. Phys. Chem.*, 1982, **86**, 1297-1302.
40. D. Rehm and A. Weller, *Ber. Bunsenges. Phys. Chem.*, 1969, **73**, 834-839.
41. D. Rehm and A. Weller, *Israel J. Chem.*, 1970, **8**, 259-271.
42. R. A. Marcus, *J. Chem. Phys.*, 1956, **24**, 966-978.
43. S. Canonica, B. Hellrung and J. Wirz, *J. Phys. Chem. A*, 2000, **104**, 1226-1232.
44. R. J. Visser and C. A. G. O. Varma, *J. Chem. Soc. Farad. Trans. 2*, 1980, **76**, 453-471.
45. M. Jonsson, J. Lind, T. E. Eriksen and G. Merenyi, *J. Am. Chem. Soc.*, 1994, **116**, 1423-1427.
46. G. Merényi and J. Lind, in *N-centered radicals*, ed. Z. B. Alfassi, John Wiley & Sons Ltd, Chichester, 1998, ch. 20, pp. 599-613.
47. J. M. Burns, W. J. Cooper, J. L. Ferry, D. W. King, B. P. DiMento, K. McNeill, C. J. Miller, W. L. Miller, B. M. Peake, S. A. Rusak, A. L. Rose and T. D. Waite, *Aquat. Sci.*, 2012, **74**, 683-734.

Chapter 3 , Supporting information for

Laser Flash Photolysis Study of the Photoinduced Oxidation of

4-Dimethylaminobenzonitrile (DMABN)

Frank Leresche, Lucie Ludvíková, Dominik Heger, Petr Klán, Urs von Gunten, Silvio Canonica

Text S3.1. List of Chemicals

4-(Dimethylamino)benzonitrile (DMABN, Aldrich, 98%), $NaH_2PO_4 \bullet 2H_2O$ (Lachner, 100%), $Na_2HPO_4 \bullet 12H_2O$ (Lachner, 99.3%), H_3PO_4 (Lachema, 85%), $NaNO_2$ (Lachema, 98%), acetonitrile (Sigma Aldrich, HPLC grade), triethanolamine (TEA, Sigma, 99%), CCl_4 (Sigma, 99%), O_2 (Siad, technical 2.5), N_2O (Siad, 99.99%).

Photosensitizers: 9,10-Anthraquinone-1,5-disulfonate (AQdS, ABCR 98%), 2-acetonaphthone (2-AN, Sigma-Aldrich, 99%), 1-acetonaphthone (1-AN, Sigma-Aldrich, 97%), 1-naphthaldehyde (1-NA, Aldrich, 95%), thionine acetate salt (THI, Sigma, for microscopy), 3-methoxyacetophenone (3-MA, Fluka 97%).

Model S3.1. Kinetic modelling of the decay of hydrated electron and radical cation of DMABN (DMABN$^{\bullet+}$) for various conditions regarding dissolved gases (O_2, N_2O, degassed) and pH values.

Model compilation

The kinetic modelling was performed using the software Kintecus[1]. The following concentrations were used:

[DMABN] = 133μM;

Starting concentration of [DMABN$^{\bullet+}$] and [e_{aq}^-] (hydrated electron) = 2μM

For O_2-purged solution: [O_2] = 1.23 mM

For aerated solution: [O_2] = 258 μM

For N_2O-purged solution: [N_2O] = 27 mM

The concentration of [$H_2PO_4^-$] and [HPO_4^{2-}] was adjusted to the given pH using the pK_a value of 7.21 and [$H_2PO_4^-$] + [HPO_4^{2-}] = 2 mM. The rate constants for acid–base speciation were calculated from the corresponding pK_a using a rate constant for the protonation reaction of 5×10^9 M^{-1} s^{-1}.

The concentration of [H^+] and [OH^-] were calculated from the pH and fixed as constants during the calculations.

The modeled decay rate constants were retrieved from the Kintecus model results by fitting ln(c/c_{start}) vs time. The fittings were performed excluding the initial part of the decay to avoid incorporating fast second-order kinetic components, and using c_{start} = $0.5\times c_0$, where c_0 is the concentration of a given species at the beginning of the kinetic model calculation.

Model explanations

The starting concentration of [DMABN$^{\bullet+}$] and of the hydrated electron [e_{aq}^-] were chosen according to the initial transient absorption of the laser flash photolysis experiments. In aerated or O_2-purged solution, the main decay pathway for e_{aq}^- is its reaction with oxygen to form the superoxide radical anion ($O_2^{\bullet-}$, equation A1). The relative importance of a particular reaction was assessed by inserting dummy reaction products in the equations (e.g. for Equation A1, one could insert such a dummy reaction product X by writing the equation as: e_{aq}^- + O_2 ==> $O_2^{\bullet-}$ +X), and monitoring the formation of this dummy product (which was not subject to any other reaction).

In experiments with degassed solutions the main decay pathway for the hydrated electron is most probably its reaction with DMABN to form a radical anion of DMABN (Equation A9). [2] The fate of such a radical is not known to our knowledge. The reactivity of the hydrated electron with water or with constituents of the buffer was of minor importance in our system (Equations A4–A8; A10–A12).

The fate of the radical cation of DMABN (DMABN$^{\bullet+}$) is either reaction with the superoxide radical anion (Equation A13) or the hydrated electron (Equation A2) to give back the parent compound DMABN, or deprotonation (Equation A14) followed by reaction with oxygen and elimination of superoxide radical anion yielding an imine intermediate (equation A16) that will undergo hydrolysis yielding the demethylated product of DMABN, 4-(methylamino)benzonitrile (MABN). This set of reactions (Equations A14; A16 and A17) was written to mimic the photodegradation pathway of DMABN in aerated solution. [3] For degassed solutions, the phototransformation pathway of DMABN is not known, and Equation A18 was written to reflect the observed disappearance of DMABN$^{\bullet+}$ in these experiments.

In the presence of oxygen, the reaction of DMABN$^{\bullet+}$ with $O_2^{\bullet-}$ (Equation A13) was found to be more important than its reaction with e_{aq}^- (Equation A2). The former reaction could explain the longer observed lifetime of DMABN$^{\bullet+}$ at lower pH, for which the concentration of $O_2^{\bullet-}$ is lowered by its protonation (Equation A20) and disproportionation (Equation A23).

Table S3.1. Proposed kinetic model following the direct photoionization of DMABN

No	Reaction	Rate constant	Comment	Ref.
Hydrated electron (e_{aq}^-) reactions				
A1	$e_{aq}^- + O_2 ==> O_2^{\bullet-}$	$2\times10^{10}\,(M^{-1}\,s^{-1})$		4
A2	$e_{aq}^- + DMABN^{\bullet+} ==> DMABN$	$1\times10^{10}\,(M^{-1}\,s^{-1})$	Estimation	
A3	$e_{aq}^- + N_2O ==> OH^\bullet + N_2 + OH^-$	$9.1\times10^9\,(M^{-1}\,s^{-1})$		5
A4	$e_{aq}^- + e^- ==> H_2 + 2\,OH^-$	$5.5\times10^9\,(M^{-1}\,s^{-1})$		6
A5	$e_{aq}^- + Na^+ ==> Na$	$2\times10^4\,(M^{-1}\,s^{-1})$		6
A6	$e_{aq}^- + H^+ ==> H^\bullet$	$2.3\times10^{10}\,(M^{-1}\,s^{-1})$		6
A7	$e_{aq}^- + H^\bullet ==> H_2 + OH^-$	$2.5\times10^{10}\,(M^{-1}\,s^{-1})$		6
A8	$e_{aq}^- + OH^\bullet ==> OH^-$	$3\times10^{10}\,(M^{-1}\,s^{-1})$		6
A9	$e_{aq}^- + DMABN ==> DMABN^{\bullet-}$	$1.4\times10^{10}\,(M^{-1}\,s^{-1})$	Value for 4-methyl-benzonitrile	6
A10	$e_{aq}^- + H_2O ==> H^\bullet + OH^-$	$20\,(M^{-1}\,s^{-1})$		6
A11	$e_{aq}^- + H_2PO_4^- ==> H^\bullet + HPO_4^{2-}$	$1.9\times10^7\,(M^{-1}\,s^{-1})$		6
A12	$e_{aq}^- + HPO_4^{2-} ==> H^\bullet + PO_4^{3-}$	$1.4\times10^5\,(M^{-1}\,s^{-1})$		6
DMABN$^{+\bullet}$ reactions				
A13	$DMABN^{+\bullet} + O_2^{\bullet-} ==> DMABN + O_2$	$3\times10^9\,(M^{-1}\,s^{-1})$	Estimation	
A14	$DMABN^{+\bullet} ==> DMABNr^\bullet + H^+$	$5\times10^3\,(s^{-1})$	Estimation	
A15	$DMABNr^\bullet + H^+ ==> DMABN^{\bullet+}$	$5\times10^9\,(M^{-1}\,s^{-1})$	Estimation	
A16	$DMABNr^\bullet + O_2 ==> DMABNim + O_2^{\bullet-}$	$5\times10^9\,(M^{-1}\,s^{-1})$	Estimation	
A17	$DMABNim + H_2O ==> MABN + H_2CO + H^+$	$1\times10^9\,(M^{-1}\,s^{-1})$	Estimation	
A18	$DMABNr^\bullet ==> MABN$	$3\times10^5\,(s^{-1})$	Reaction added for degassed and N$_2$O-purged solutions	
Other reactions				
A19	$H^\bullet + OH^\bullet ==> H_2O$	$7\times10^9\,(M^{-1}\,s^{-1})$		6
A20	$O_2^{-\bullet} + H^+ ==> HO_2^\bullet$	$5\times10^9\,(M^{-1}\,s^{-1})$	From pK_a 4.8	4
A21	$HO_2^\bullet ==> O_2^{\bullet-} + H^+$	$7.5\times10^4\,(s^{-1})$		4
A22	$HO_2^\bullet + HO_2^\bullet ==> H_2O_2 + O_2$	$8.3\times10^5\,(M^{-1}\,s^{-1})$		4
A23	$HO_2^\bullet + O_2^{\bullet-} ==> HO_2^- + O_2$	$9.7\times10^7\,(M^{-1}\,s^{-1})$		4
A24	$H_2O_2 ==> HO_2^- + H^+$	$1.2\times10^{-2}\,(s^{-1})$	From pK_a 11.62	7
A25	$HO_2^- + H^+ ==> H_2O_2$	$5\times10^9\,(M^{-1}\,s^{-1})$		7
A26	$DMABN + OH^\bullet ==> DMABNOH$	$5\times10^9\,(M^{-1}\,s^{-1})$	Estimation	

Model S3.2. Kinetic modelling to determine the lifetime of the radical cation of DMABN (DMABN$^{\bullet+}$) formed through photosensitization using 1-naphthaldehyde (1-NA)

Model compilation

The modelling was performed using the software Kintecus[1]. The following conditions were used:

[DMABN] = 500µM; [O$_2$] = 280 µM; [H$^+$] = 10 nM; [OH$^-$] = 1 µM.

The rate constant for deprotonation reactions were calculated from the acid-base equilibrium constants using a rate constant for the protonation reaction of 5×10^9 M^{-1} s^{-1}.

The modeled decay rate constants were retrieved from the Kintecus model results by fitting ln(c/c_{start}) vs time. The fittings were performed excluding the initial part of the decay to avoid incorporating fast second-order kinetic components, and using $c_{start} = 0.5 \times c_0$, where c_0 is the concentration of a given species at the beginning of the kinetic model calculation.

Model explanations

The decay of the triplet state of 1-NA (^{3}1-NA*) is dominated in the model by its reaction with DMABN (Equation B1), with a non-negligible (21%) contribution of quenching by O$_2$ (Equation B2).

As the fraction of ^{3}1-NA* undergoing quenching by DMABN through energy loss (Equation 3.19 in the main paper) is not known, Equation B1 was written by neglecting this deactivation channel of ^{3}1-NA* and assuming that the rate constants for quenching of ^{3}1-NA* by DMABN and for reactive quenching leading to DMABN$^{\bullet+}$ formation are identical.

Similarly, the model does not take into account other deactivation pathways for ^{3}1-NA* such as triplet–triplet annihilation and the various unimolecular deactivation channels, but these should be negligible under the present experimental conditions.

Regarding the quenching of ^{3}1-NA* by O$_2$, no distinction between the energy transfer pathway yielding ^{1}O$_2$ and the energy loss pathway was done, because ^{1}O$_2$ is not expected to react with any of the relevant species in solution. Moreover, a possible reactive quenching (leading to the transformation of 1-NA) was neglected.

The decay of the radical cation of DMABN (DMABN$^{\bullet+}$) is affected by its two reactions with the radical anion of 1-NA (1-NA$^{\bullet-}$) and O$_2^{\bullet-}$ (Equations B5 and B6) and by its deprotonation (Equation B7). The relative importance of these three reactions depends on the starting ^{3}1-NA* concentration: For [^{3}1-NA*] > 2 µM the reduction reactions to recover DMABN were dominant, whereas for [^{3}1-NA*] < 2 µM the deprotonation reaction, finally leading to the formation of MABN, prevailed. Moreover, the reaction between DMABN$^{\bullet+}$ and O$_2^{\bullet-}$ was always more important for the fate of DMABN$^{\bullet+}$ than its reaction with 1-NA$^{\bullet-}$.

The modelling results also showed that the decay of O$_2^{\bullet-}$ was almost exclusively due to its reaction with DMABN$^{\bullet+}$ (Equation B6), whereas the protonation and disproportionation reactions of O$_2^{\bullet-}$ (Equations B11 and B14) played only a minor role.

Table S3.2. Proposed kinetic model for the influence of the starting concentration of the triplet state of 1-naphthaldehyde (^{3}1-NA*) on the lifetime of the radical cation of DMABN (DMABN$^{\bullet+}$)

| No	Reaction	Rate constant	Comment	Ref.
Triplet state of 1-Naphthaldehyde decay and singlet oxygen				
B1	^{3}1-NA* +DMABN ==> DMABN$^{\bullet+}$ +1-NA$^{\bullet-}$	3.4×10^9 (M^{-1} s^{-1})	This paper	
B2	^{3}1-NA +O$_2$ ==> 1-NA + products	1.8×10^9 (M^{-1} s^{-1})	Estimation from ^{3}1-NA* lifetime	
B3	(not used)			
B4	1-NA$^{\bullet-}$ +O$_2$ ==> 1-NA +O$_2$$^{\bullet-}$	3.4×10^9 (M^{-1} s^{-1})	Estimation	
Recombination reactions of DMABN$^{\bullet+}$				
B5	DMABN$^{\bullet+}$ +1-NA$^{\bullet-}$ ==> DMABN +1-NA	4×10^9 (M^{-1} s^{-1})	Estimation	
B6	DMABN$^{\bullet+}$ +O$_2$$^{\bullet-}$ ==> DMABN +O$_2$	3×10^9 (M^{-1} s^{-1})	Estimation	
Decay reactions of DMABN$^{+\bullet}$				
B7	DMABN$^{\bullet+}$ ==> DMABNr$^{\bullet}$ +H$^+$	5×10^3 (s^{-1})	Estimation	
B8	DMABNr$^{\bullet}$ +H$^+$ ==> DMABN$^{\bullet+}$	5×10^9 (M^{-1} s^{-1})	Estimation	
B9	DMABNr$^{\bullet}$ +O$_2$ ==> DMABNim +O$_2$$^{\bullet-}$	5×10^9 (M^{-1} s^{-1})	Estimation	
B10	DMABNim +H$_2$O ==> MABN +H$_2$CO +H$^+$	1×10^9 (M^{-1} s^{-1})	Estimation	
Other reactions				
B11	O$_2$$^{\bullet-}$ +H$^+$ ==> HO$_2$$^{\bullet}$	5×10^9 (M^{-1} s^{-1})	From pK_a 4.8	[4]
B12	HO$_2$$^{\bullet}$ ==> O$_2$$^{\bullet-}$ +H$^+$	7.5×10^4 (s^{-1})		[4]
B13	HO$_2$$^{\bullet}$ + HO$_2$$^{\bullet}$ ==> H$_2$O$_2$ +O$_2$	8.3×10^5 (M^{-1} s^{-1})		[4]
B14	HO$_2$$^{\bullet}$ +O$_2$$^{\bullet-}$ ==> HO$_2$$^-$ +O$_2$	9.7×10^7 (M^{-1} s^{-1})		[4]
B15	H$_2$O$_2$ ==> HO$_2$$^-$ + H$^+$	1.2×10^{-2} (s^{-1})	From pK_a 11.62	[7]
B16	HO$_2$$^-$ +H$^+$ ==> H$_2$O$_2$	5×10^9 (M^{-1} s^{-1})		
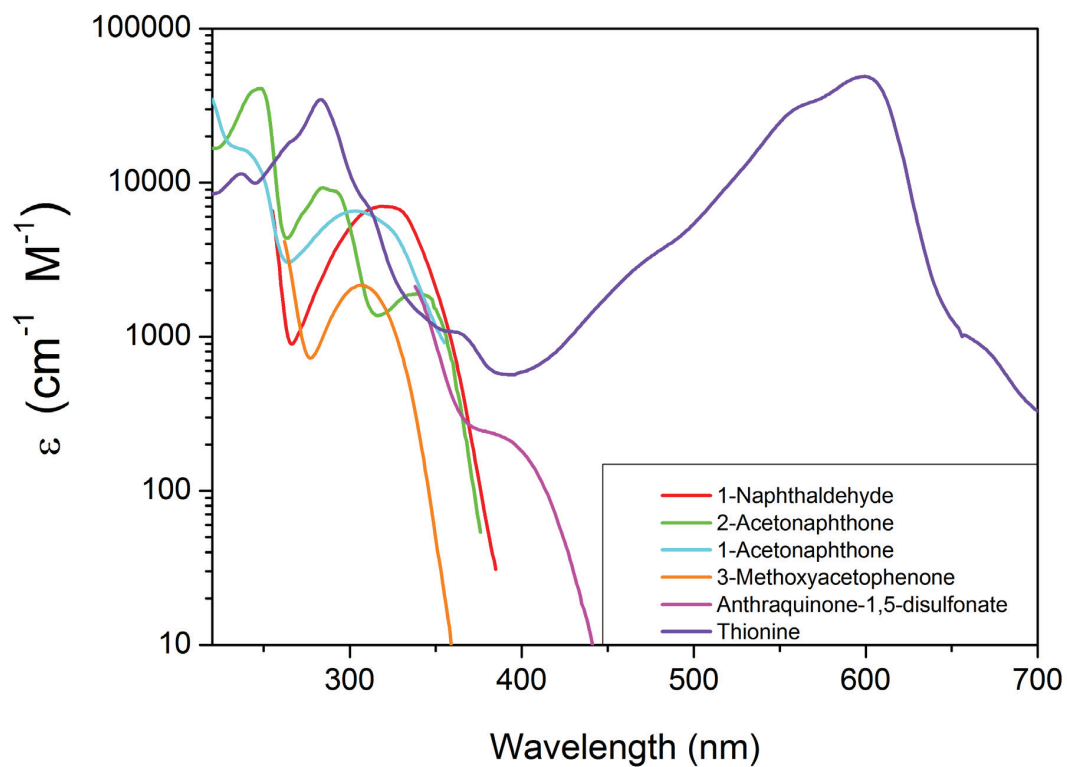
Figure S3.1. Spectral molar absorption coefficients of the photosensitizers used during the experiments, measured in pH 8 phosphate-buffered aqueous solution (containing small amount of acetonitrile as a co-solvent in the case of 1-naphthaldehyde (0.6% v/v) and 3-methoxyacetophenone (10% v/v)).

Table S3.3. Observation wavelengths used in LFP kinetic measurements to determine the decay rate constants of transient species.

Transient Species	Observation wavelength (nm)
Excitation Wavelength 266nm	
^{3}DMABN*	400 & 600
DMABN$^{\bullet+}$	500
Hydrated electron (e_{aq}^-)	600 & 700
Excitation Wavelength 355 or 532 nm	
DMABN$^{\bullet+}$	500 & 520
9,10-Anthraquinone-1,5-disulfonate triplet (^{3}AQdS*)	420 & 470
9,10-Anthraquinone-1,5-disulfonate radical anion (AQdS$^{\bullet-}$)	500
2-Acetonaphthone triplet (^{3}2-AN*)	440
2-Acetonaphthone radical anion (2-AN$^{\bullet-}$)	400
1-Naphthaldehyde triplet (^{3}1-NA*)	600
1-Naphthaldehyde radical anion (1-NA$^{\bullet-}$)	400
3-Methoxyacetophenone triplet (^{3}3-MOAP*)	400
Thionine triplet (^{3}THI*)	670
Thionine radical anion (THI$^{\bullet-}$)	400
1-Acetonaphthone triplet (^{3}1-AN*)	500

Figure S3.2. Transient absorption spectra following a 355nm laser pulse in pH 8 aerated conditions of solutions containing: (A) 1-Naphthaldehyde (1-NA, 300 µM). (B) 1-NA (300 µM) + triethanolamine (TEA, 10 mM). (C) 1-NA 300 µM + DMABN (500 µM).

Text S3.2. Transient species observed in the 1-naphthaldehyde (1-NA) system

The absorption spectrum of triplet 1-NA (^{3}1-NA*) has a broad maximum centered at ≈500 nm (Figure S3.2.A). [8, 9] A band centered at the ≈420 nm can be attributed to the radical anion of 1-NA (Figure S3.2.B). The DMABN$^{•+}$ band can be observed at ≈500 nm on a long timescale in the 1-NA + DMABN system (Figure S3.2.C).

Figure S3.3. Transient absorption spectra following 355 nm laser pulse excitation in pH 8 aerated conditions of solutions containing: (A) 1-Acetonaphthone (1-AN, 250 µM). (B) 1-AN (250 µM) + DMABN (500µM).

Text S3.3. Transient species observed in the 1-acetonaphthone (1-AN) system

The absorption spectrum of triplet 1-AN (^{3}1-AN*) has a maximum centered at ≈500 nm (Figure S3.3.A). No additional species were observable in the 1-AN + DMABN system (Figure S3.3.B), probably because of the low reactivity of DMABN towards ^{3}1-AN*.
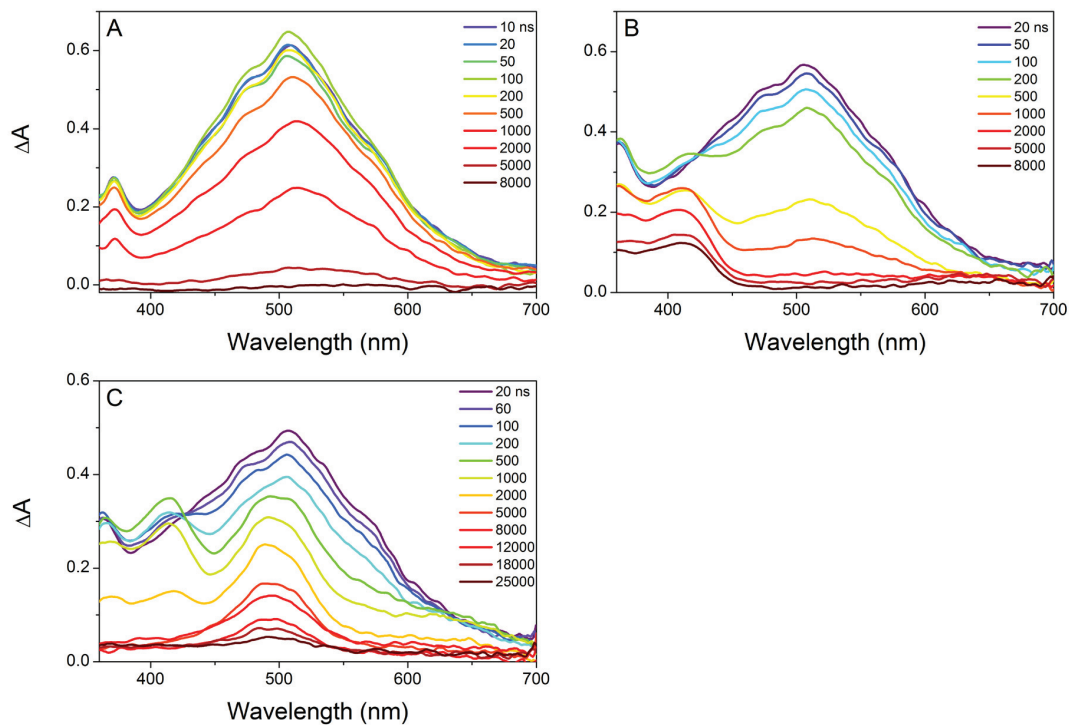
Figure S3.4. Transient absorption spectra following 355 nm laser pulse excitation in pH 8 aerated conditions of solutions containing: (A) 9,10-Anthraquinone-1,5-disulfonate (AQdS, 1 mM). (B) AQdS (1 mM) + NaNO$_2$ (10 mM). (C) AQdS (1 mM) + DMABN (400 μM).

Text S3.4. Transient species observed in the 9,10-anthraquinone-1,5-disulfonate (AQdS) system

The absorption spectrum of triplet AQdS (^{3}AQdS*) exhibits a maximum at ≈400 nm (Figure S3.4.A). The radical anion of AQdS (AQdS$^{\bullet-}$) was produced by electron transfer from nitrite to ^{3}AQdS* and shows an absorption band centered at ≈520 nm (Figure S3.4.B). [10]

The absorption spectrum of DMABN$^{\bullet+}$ overlaps with the one of AQdS$^{\bullet-}$ (Figure S3.4.C), making the AQdS system unpractical for the measurement of DMABN$^{\bullet+}$.
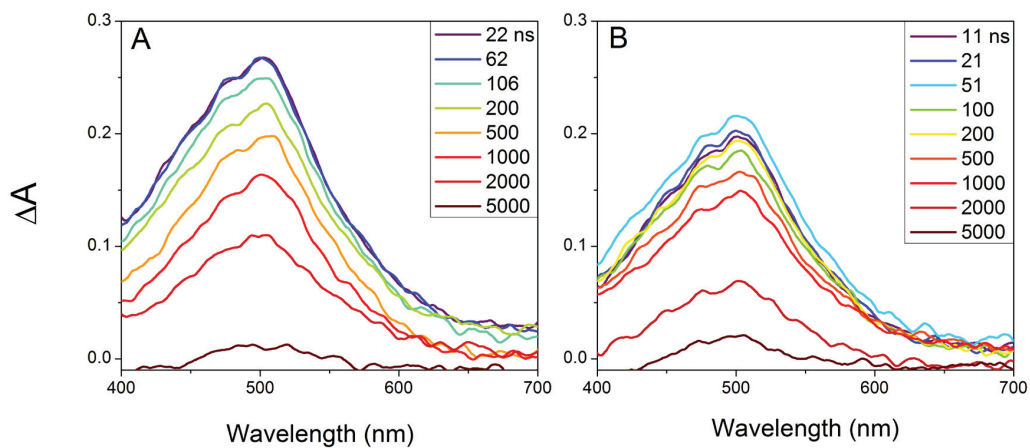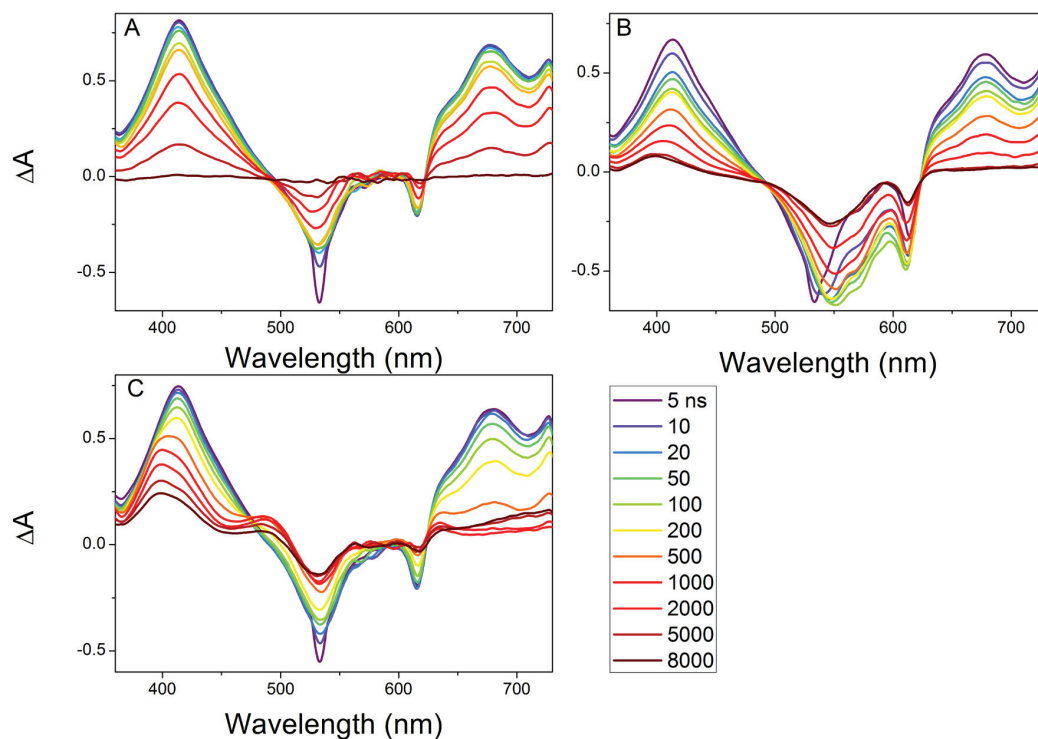
Figure S3.5. Transient absorption spectra following 532 nm laser pulse excitation in pH 8 aerated conditions of solutions containing: (A) Thionine (THI, 35 µM). (B) THI (35 µM) + TEA (10 mM). (C) THI (35 µM) + DMABN (500 µM).

Text S3.5. Transient species observed in the thionine (THI) system

Upon LFP of a thionine solution, the triplet its triplet absorption spectrum as well as a bleaching of its ground-state absorption can be observed (Figure S3.5.A), since THI absorbs light across the whole observation spectral window (Figure S3.1).Therefore, the observed traces are differential spectra. In the presence of triethanolamine (TEA), the radical anion of THI can be observed with an absorption band at ≈400 nm (Figure S3.5.B). DMABN$^{\bullet+}$ can be observed on a long timescale in the THI + DMABN system (Figure S3.5.C).
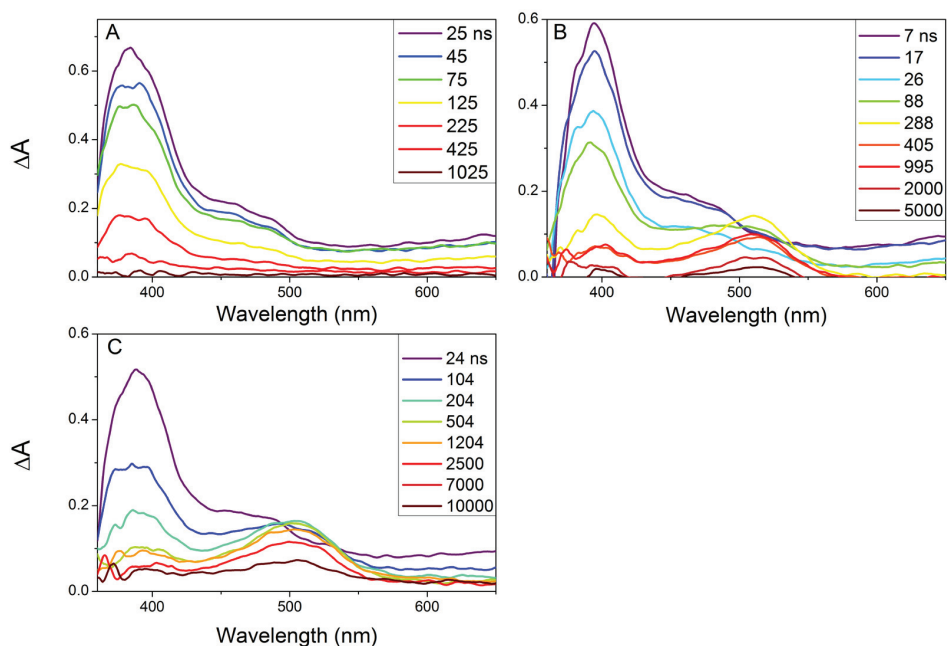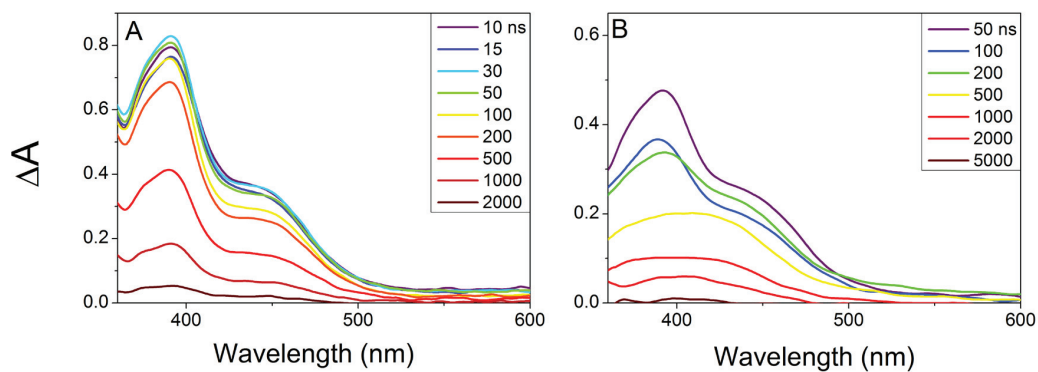
Figure S3.6. Transient absorption spectra following 355 nm laser pulse excitation in pH 8 aerated conditions of solutions containing: (A) 3-Methoxyacetophenone (3-MOAP, 10 mM). (B) 3-MOAP (10 mM) + TEA (10 mM). The solutions contain 10% (v/v) acetonitrile as co-solvent.

Text S3.6. Transient species observed in the 3-methoxyacetophenone (3-MOAP) system

The absorption spectrum of triplet 3-MOAP (^{3}3-MOAP*) exhibits a maximum at ≈400 nm and a shoulder at ≈440 nm (Figure S3.6.A). [11] The spectrum of the radical anion of 3-MOAP overlaps with the one of the triplet with an absorption centered at 420 nm. (Figure S3.6.B).
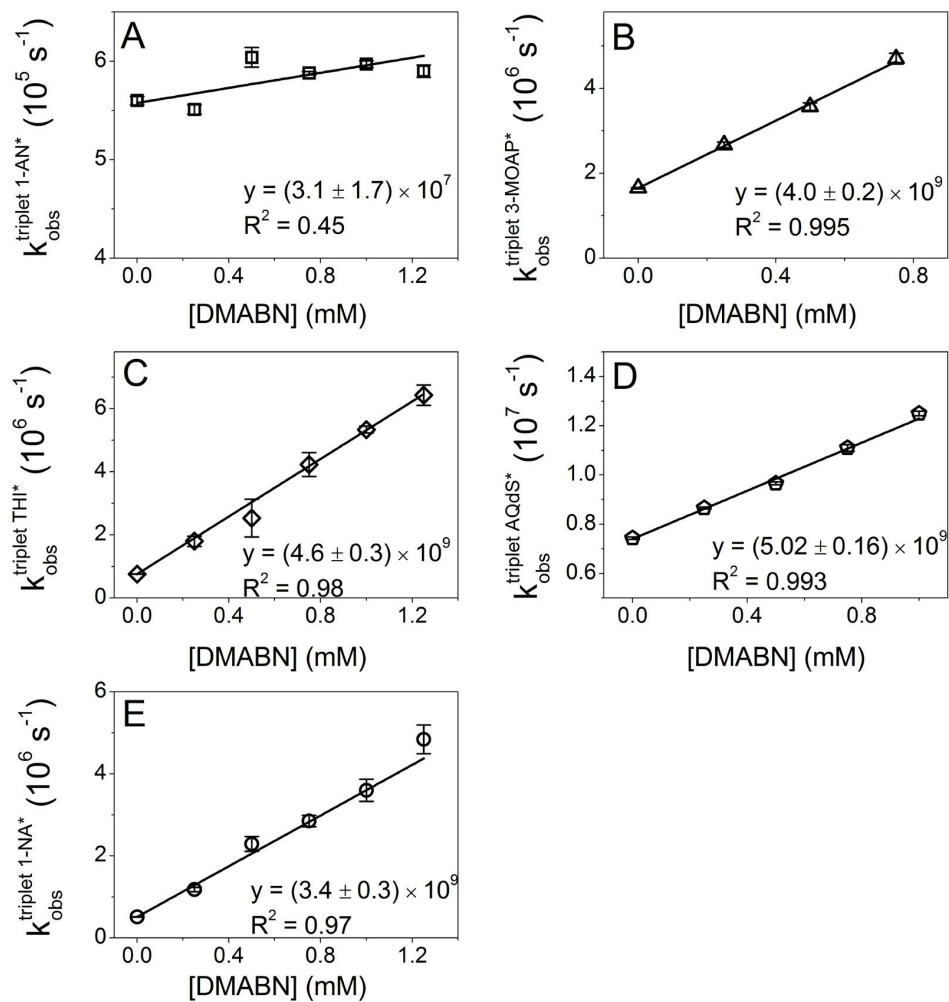
Figure S3.7. Stern-Volmer plots used for the determination of the second-order rate constant for the quenching of excited triplet photosensitizers by DMABN (see Table 3.2 in the main paper). (A) 1-Acetonaphthone (1 mM); (B) 3-Methoxyacetophenone (10 mM, with 10% (v/v) acetonitrile as a co-solvent); (C) Thionine (50 μM); (D) 9,10-Anthraquinone-1,5-disulfonate (1 mM). (E) 1-Naphthaldehyde (300 μM, with 0.6% (v/v) acetonitrile as a co-solvent). All measurements were done in aerated pH 8 phosphate-buffered solutions.

Inside figure text box:
name: 150217 DM133uM N2O 266nm 500nm 20000ns 2
measured: 2015-02-17 03:38
A0 = 8.1371e-03
Ainf = -1.9701e-03
Amax = 1.9084e-02
k(1) = 1.234721e+04 ± 5.764970e+02
A0 - Ainf(1) = 1.0107e-02
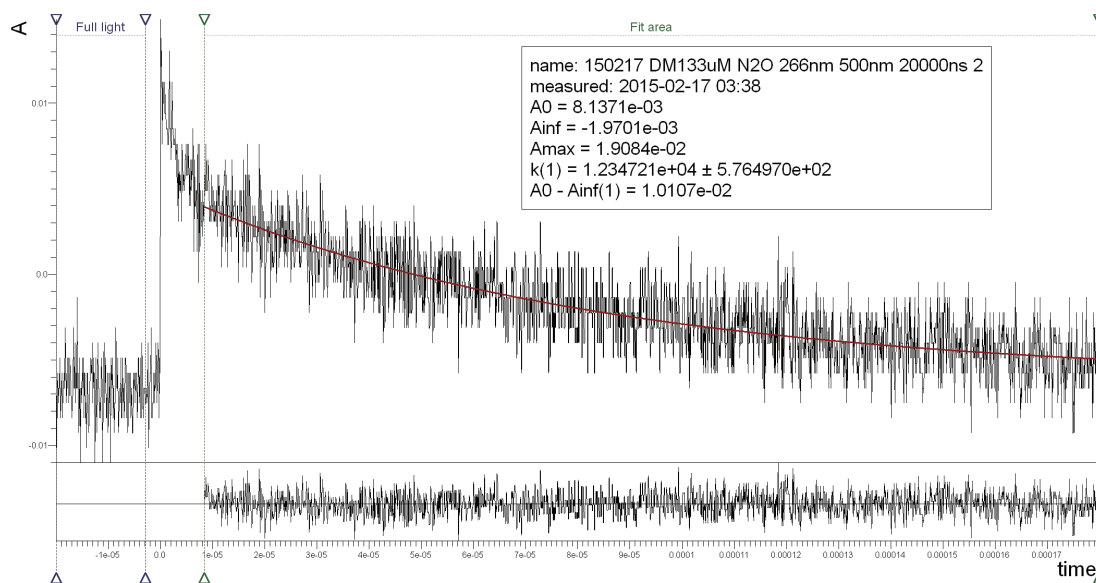
Figure S3.8. Kinetic trace obtained upon 266 nm laser flash excitation (at time t = 0 ms) of DMABN (133 μM) under N_2O-ventilated conditions in pH 8 phosphate-buffered aqueous solution. Wavelength of detection: 500 nm. The fitting was performed neglecting the first 9 μs using the software FlashFit.

Text S3.7. Method to determine the pseudo-first-order decay rate constant of DMABN[•+] formed by photosensitization using 1-naphthaldehyde (1-NA).

The kinetic traces at λ = 500 nm were used for this determination. As the absorption signal at this wavelength consists of a super-position of the absorption signals [3]1-NA* and DMABN[•+], the deconvolution of the two signal was done according to the following method: (A) The [3]1-NA* decay constant was determined separately at λ=600nm where DMABN[•+] signal is absent. For [1-NA] ≥ 50 μM the [3]Sens* decay constants were determined by fitting the kinetic traces at λ = 600 nm; For 1-NA "effective concentration" <50 μM, the [3]Sens* decay was no longer measurable due to a too weak signal and the decay constant was fixed at 1.2×10^6 s^{-1} (the mean value of the measurements at higher 1-NA concentration that does not to vary with 1-NA concentration). (B) The kinetic traces at λ=500 nm were then fitted to extract DMABN[•+] decay constants using a double exponential model function, whereby one of the exponential decay constants was fixed at the value corresponding to the [3]Sens* decay determined under (A).

Text S3.8. Kinetic model used to fit the measured decay curves of ^{3}DMABN*, DMABN$^{\bullet+}$ and e^-_{aq} in degassed solution

Reaction equations (with corresponding rate constants given on the right):

(A) ^{3}DMABN* → DMABN $\hspace{6cm}$ k_0

(B) ^{3}DMABN* + ^{3}DMABN* → DMABN + ^{1}DMABN* $\hspace{2.5cm}$ k_{TT}

(C) e^-_{aq} + DMABN → DMABN$^{\bullet-}$ $\hspace{4.5cm}$ k_{e-}

(D) DMABN$^{\bullet+}$ + DMABN$^{\bullet-}$ → 2 DMABN $\hspace{3.3cm}$ k_{redox}

(E) ^{1}DMABN* → ^{3}DMABN* $\hspace{5cm}$ k_{isc}

(F) ^{1}DMABN* → DMABN $\hspace{5cm}$ $k_f + k_{ic}$

(G) DMABN$^{\bullet+}$ → products $\hspace{5cm}$ k_{RAD}
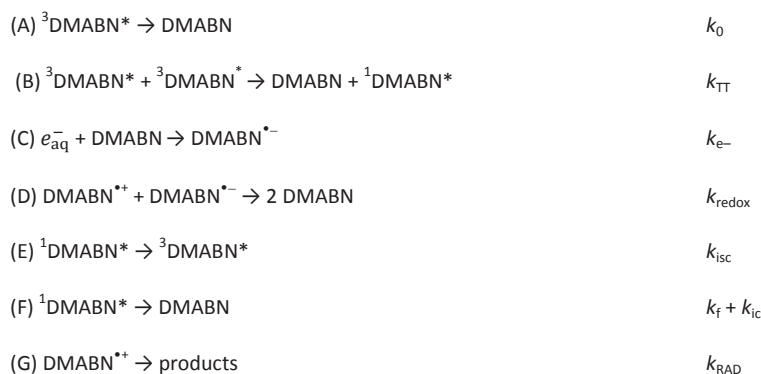
Differential equations for the concentrations of ^{3}DMABN*, e^-_{aq} and DMABN$^{\bullet+}$:

$$dc_T/dt = -k_0 * c_T - (2 - \phi_{isc}) * k_{TT} * c_T^2 \hspace{4cm} \text{(S3.1)}$$

$$dc_{e-}/dt = -k_{e-} * c_{e-} * c_{DMABN} \hspace{4.5cm} \text{(S3.2)}$$

$$dc_{RAD}/dt = -k_{RAD} * c_{RAD} \hspace{5cm} \text{(S3.3)}$$

To describe the fate of the various transient species formed upon LFP of DMABN in degassed solution, we constructed a kinetic model based on processes A to G. Thereby, it is important to note that the excited singlet state of DMABN (^{1}DMABN*) decays much faster than all other transient species. Equation S3.1 represents the differential rate equation for the deactivation of the excited triplet state of DMABN (^{3}DMABN*, concentration defined as c_T), consisting of a unimolecular decay (Process A, with rate constant k_0) and a triplet–triplet annihilation process (Process B, with rate constant k_{TT}). The coefficient of the second-order member, i.e. (2 − ϕ_{isc}), takes the reformation of ^{3}DMABN* through intersystem crossing from ^{1}DMABN* (which is a product of triplet–triplet annihilation) into account, whereby $\phi_{isc} = k_{isc} / (k_f + k_{ic} + k_{isc})$ is the intersystem crossing quantum yield (from ^{1}DMABN*). ϕ_{isc} is not known for aqueous solutions at room temperature, but was determined to be 0.80 and 0.55 in *n*-hexane and ethanol solutions, respectively.[12] The differential rate laws for the hydrated electron (e^-_{aq}) (Process C, with rate constant k_{e-}) and the cation radical of DMABN (DMABN$^{\bullet+}$) (Process D, with rate constant k_{RAD}) are given in Equations S3.2 and S3.3, where c_{e-} and c_{RAD} are the concentrations of e^-_{aq} and DMABN$^{\bullet+}$, respectively. The concentration of DMABN in the electronic ground state was considered to be constant (c_{DMABN} = 90 µM) during the reaction time, as we considered that c_{DMABN} was not significantly changing after excitation. The concentrations of ^{3}DMABN* and DMABN$^{\bullet+}$ obtained from minimization were about two orders of magnitude smaller (c_T= 1.77 µM; c_{RAD}= 0.63 µM) than c_{DMABN}. Therefore, we approximated the quenching of solvated electrons by ground-state DMABN (C, k_{e-}) as a pseudo first order process.

To determine the rate constants of the individual deactivation processes of the transients (k_0, k_{TT}, k_{e-}, k_{RAD}), absorbance kinetic traces of laser flash-excited DMABN (c = 90 µM) in degassed aqueous solutions were measured at 400, 500 and 600 nm, where the absorption of three transients, ^{3}DMABN*, e^-_{aq}, and DMABN$^{\bullet+}$ contributed to the kinetic traces. Note that the ground state of DMABN does not absorb at wavelengths longer than 360 nm.

The most accurate estimates of the rate constants were obtained by the global fit of the differential rate equations (Equations S3.1–3) to three kinetic traces at 400, 500 and 600 nm measured under otherwise identical experimental conditions (see an example in Figure S3.9). For the fit of each kinetic trace, the initial concentrations of ^{3}DMABN*, e^-_{aq} and DMABN$^{\bullet+}$ were set as initial estimates: The concentration of ^{3}DMABN* was calculated from the absorbance at 400 nm, the concentration of DMABN$^{\bullet+}$ was estimated from the absorbance at 500 nm and the concentration of e^-_{aq} was set equal to the concentration of DMABN$^{\bullet+}$. The corresponding molar absorption coefficients of transients were taken from literature (see Table S3.4). The first-order (k_0; k_{RAD}); pseudo-first-order (k_{e-}) and second-order (k_{TT}) rate constants obtained from the minimization of three sets of kinetic traces are summarized in Table S3.5.

Table S3.4. Molar absorption coefficients applied for the estimates of the initial concentrations of the transient species for the global fit.

	extinction coefficient / M^{-1} cm^{-1}			Initial concentration / M
	400nm	500nm	600nm	
e_{aq}^{-} [a]	2000	5200	12500	8.95×10^{-7}
^{3}DMABN* (in EtOH) [b]	9000	3800	4000	1.77×10^{-6}
DMABN$^{\bullet+}$ [b]	1000	7800	0	6.32×10^{-7}

Note: [a]from Ref. 6 , [b]from Ref. 12

Table S3.5. Rate constants of the studied transients obtained from three independent measurements by applying the global fitting procedure described above.

k_0 / s^{-1}	$(2-\Phi_{isc}) \times k_{TT}$ / M^{-1} s^{-1}	k_{e-} / M^{-1} s^{-1}	k_{RAD} / s^{-1}
$(3.57 \pm 0.17) \times 10^4$	$(3.2 \pm 0.6) \times 10^9$	$(9.7 \pm 1.1) \times 10^9$	$(5.33 \pm 0.99) \times 10^3$
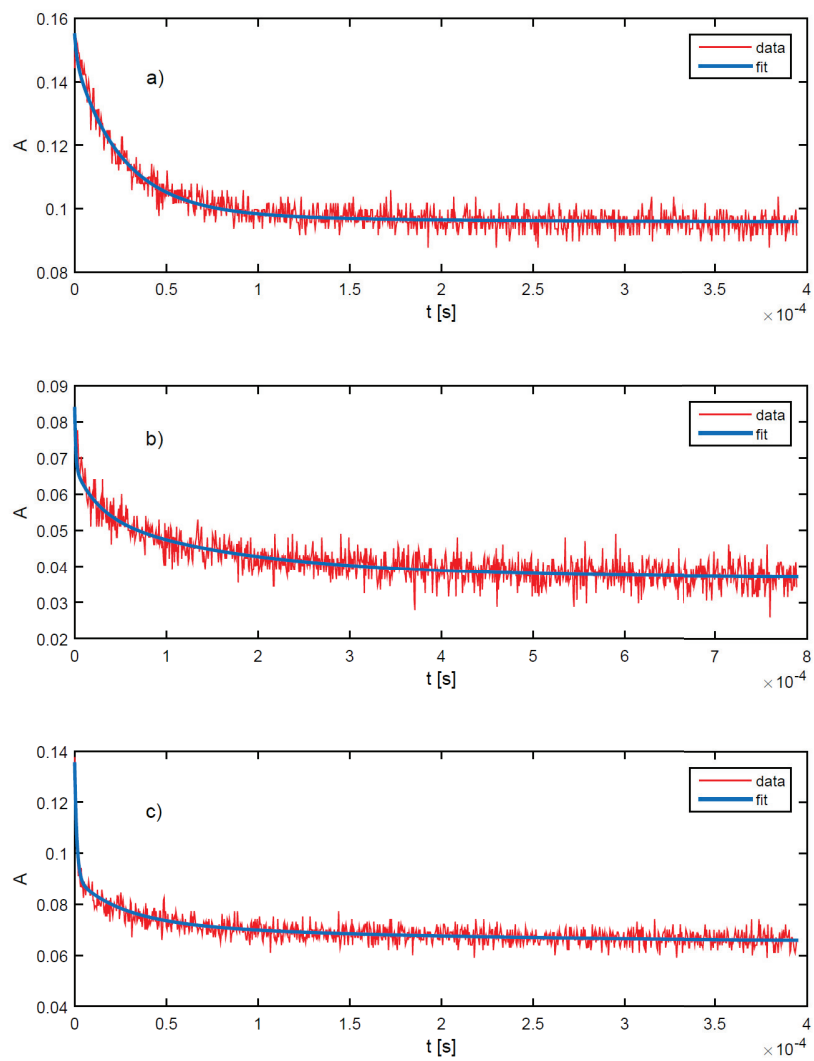
Figure S3.9. Fits of the kinetic traces measured at: (a) 400 nm, (b) 500 nm and (c) 600 nm.

References for the supporting information

1. J. C. Ianni, Kintecus Windows version 5.20, 2014. www.kintecus.com (accessed August 2016)
2. M. Anbar and E. J. Hart, *J. Am. Chem. Soc.*, 1964, **86**, 5633-5637.
3. F. Leresche, U. von Gunten and S. Canonica, *Environ. Sci. Tech.*, 2016, **50**, 10997-11007.
4. B. H. J. Bielski, D. E. Cabelli, R. L. Arudi and A. B. Ross, *J. Phys. Chem. Ref. Data*, 1985, **14**, 1041-1100.
5. E. Janata and R. H. Schuler, *J. Phys. Chem.*, 1982, **86**, 2078-2084.
6. G. V. Buxton, C. L. Greenstock, W. P. Helman and A. B. Ross, *J. Phys. Chem. Ref. Data*, 1988, **17**, 513-886.
7. W. M. Haynes, *CRC handbook of chemistry and physics*, CRC press, 2014.
8. A. Treinin and E. Hayon, *J. Am. Chem. Soc.*, 1976, **98**, 3884-3891.
9. A. Samanta and R. W. Fessenden, *Chem. Phys. Lett.*, 1988, **153**, 406-410.
10. J. N. Moore, D. Phillips, N. Nakashima and K. Yoshihara, *J. Chem. Soc., Faraday Trans. 2*, 1987, **83**, 1487-1508.
11. H. Shizuka and H. Obuchi, *J. Phys. Chem.-Us*, 1982, **86**, 1297-1302.
12. G. Köhler, G. Grabner and K. Rotkiewicz, *Chem. Phys.*, 1993, **173**, 275-290.

Chapter 4

Quenching of an Aniline Radical Cation by Dissolved Organic Matter and Phenols: A Laser Flash Photolysis Study

Frank Leresche, Lucie Ludvíková, Dominik Heger, Petr Klán, Urs von Gunten, Silvio Canonica

Abstract

Aromatic amines are compounds often found in aquatic environments that are susceptible to oxidative phototransformation induced by dissolved organic matter (DOM). This reaction is mainly attributed to electron transfer from the aromatic amine to excited triplet states of DOM (^{3}DOM*) to produce a radical cation of the amine. The resulting radical cation intermediate can undergo reduction to the parent amine, and this is believed to be the reason for the inhibition of excited triplet-induced oxidation caused by DOM or model phenolic antioxidants. To provide new evidence for these reaction steps we present in this paper a laser flash photolysis investigation of the photosensitized oxidation of *N,N*-dimethyl-4-cyanoaniline (DMABN). The produced radical cation (DMABN$^{\bullet+}$) was observed to react with several phenols and different types of DOM on a time scale of up to hundred microseconds. The determined second-order rate constants for the quenching of DMABN$^{\bullet+}$ by phenols increased with increasing electron-donating strength of the aromatic ring substituent, reaching values close to the diffusion-controlled limit for 4-methoxyphenol. For DOM, such rate constants were proportional to the electron donating capacity of the DOM. The oxidation of sulfadiazine brought about by excited triplet state of a series of aromatic ketones was also investigated and found to proceed by electron transfer, yielding a radical cation intermediate. This radical was shown to react with 4-methoxyphenol, suggesting a similar reaction mechanism as for the reduction of DMABN$^{\bullet+}$.

4.1   Introduction

Aromatic amines are a class of compounds often present as contaminants in the aquatic environment. Under sunlight irradiation they can undergo both direct and indirect phototransformation, [1-9] the latter process being sensitized by dissolved organic matter (DOM). [10] Excited triplet states of DOM (^{3}DOM*) are the reactive intermediate formed upon DOM photoirradiation that are believed to be mainly responsible for the DOM-photosensitized transformation of such aromatic amines. The initiation of the transformation is attributed to a one-electron transfer from the aromatic amine to ^{3}DOM*, which generates the corresponding aminyl radical cation. [11-13]

Besides acting as a photosensitizer, DOM can also inhibit the indirect phototransformation of some classes of organic contaminants, in particular aromatic amines. [7] This inhibition, observed as a slowing down of the phototransformation upon increase in DOM concentration, has been the subject of extensive studies in our research group during the last ten years. [14-16] It was postulated that the inhibition originates from the reduction of oxidation intermediates of the target organic contaminant, formed upon reaction of the contaminant with ^{3}DOM*, by electron-donating (also named antioxidant) moieties of the DOM. In the case of aromatic amines, such oxidation intermediates are probably identical with the corresponding aminyl radicals or radical cations.

While extensive work has been done to characterize the inhibitory effect of DOM and model phenolic antioxidants on the photosensitized transformation of contaminants under steady-state irradiation, the direct observation of the transient radical species formed upon oxidation of the contaminant by ^{3}DOM* and their reaction with DOM is still outstanding. To our knowledge, the only case of direct observation of a radical formed by direct photoionization and reacting with DOM is described in a recent study by McNeill and coworkers,[11] who investigated the tryptophanyl radical cation reacting at pH 3 with DOM and a few phenolic antioxidants. The goal of the present study is to show that analogous reactions of DOM and phenols can occur with aniline radical cations at neutral pH after photosensitized oxidation of selected anilines. The radical cation of *N,N*-dimethyl-4-cyanoaniline (DMABN) was selected as the main radical species subject of this study. This radical cation was produced by laser flash excitation through direct photoionization or photosensitized oxidation of DMABN, as detailed in a preceding study. [17] Its decay kinetics in the presence of various concentrations of a few types of DOM and some phenols, was measured. A similar, but limited investigation was also performed using the radical cation of sulfadiazine, a sulfonamide antibiotic.

4.2   Experimental Section

4.2.1   Chemicals and Solutions

All chemicals were commercially available and used as received. A complete list of chemicals is given in the Supporting Information (SI, text S4.1). All experiments were done in phosphate-buffered water (2 mM total phosphate concentration, final pH 8.0 except when otherwise mentioned) using stock solutions prepared in water except for most photosensitizers. Stock solutions of 3-methoxyacetophenone, 1-naphthaldehyde, 2-acetonaphthone and 1-acetonaphthone were made in acetonitrile (MeCN) because of the limited solubility of these compounds in water. The concentration of the cosolvent MeCN in the sample solutions did not exceed 10% (v/v) and do not affect the experiments. The water used in the experiments was obtained from a Aqua Osmotic 02A purification system. Suwannee river fulvic acid (SRFA, catalogue number 1S101F), Suwannee river humic acid (SRHA, 1S101H), Pony lake fulvic acid (PLFA, 1R109F) were purchased from the International Humic Substances Society (IHSS, St. Paul, Minnesota), stock solutions of the fulvic and humic acids were prepared at concentrations of 50–100 mg$_C$/L, the carbon content of the first stock solution was quantified by a total organic carbon (TOC) analyzer, while the concentration of subsequent stock solutions were quantified spectrophotometrically using the first solutions as references. Please refer to the SI for the full characteristics of the fulvic and humic acids.

Natural water was collected on November 14th 2014, near the outlet of Etang de la Gruère (EG) (47.2376N, 7.0494 E), a small pound (area ≈80'000m^2) surrounded by timbers and boggy wetlands. EG water was filtered on pre-washed 0.45μM pore size cellulose nitrate filter and stored at 4° in the dark. It has a high DOM concentration of 22.8 mg$_C$/L and a pH of 7.7 (see Ref. 13 for full characteristics of the water).

4.2.2   Laser Flash Photolysis (LFP) Setup

Nanosecond LFP experiments using pulses of ≤170 ps duration from a Nd:YAG laser were conducted as detailed elsewhere.[17] The observation wavelengths of the different transient species are given in the SI, Table S4.2. Absorbance values of the sample solutions were usually adjusted to 0.5–0.8 (for 1 cm optical path length) at the excitation wavelength. Solutions were sparged using a gentle stream of N$_2$O for 15 minutes prior to measurements or naturally aerated. Electronic absorption spectra of the sample solu-

tions were measured regularly in-between laser flashes to test for possible photodegradation of the solution components using the hereafter mentioned diode-array spectrophotometer. Experiments were conducted in an air-conditioned room at an ambient temperature of 21±1 °C.

4.2.3 Kinetic Analyses

The kinetic traces were mainly fitted to single or multiple exponential decay model functions using the software Flash Fit v. 0.11. The statistical errors of the first-order rate constants given in the tables are expressed as 95% confidence intervals and were calculated using the values of at least triplicate measurements.

4.2.4 Analytical Instrumentation

Electronic absorption spectra in the ultraviolet (UV) and visible (Vis) range were measured on an Agilent Cary 100 UV-Vis or an Agilent 8654 diode-array spectrophotometer. A BNC pHTestr 10 pH meter equipped with a calibrated glass electrode or an equivalent Eutech Instruments pH600 was used to measure pH. The total organic carbon of the humic and fulvic acids solutions and of EG water were measured on a Shimadzu TOC-L CSH total organic carbon analyzer.

4.3 Results and Discussion

4.3.1 Radical Cation of *N,N*-Dimethyl-4-cyanoaniline (DMABN), DMABN$^{\bullet+}$

4.3.1.1 Kinetics of the Reaction between DMABN$^{\bullet+}$ and Phenols as Model Antioxidants

Using the LFP methods developed recently, the radical cation of DMABN (DMABN$^{\bullet+}$) was generated either by direct photoionization (eq. 4.1) or by triplet-photosensitized oxidation (eqs. 4.2–3). [17] Kinetic traces corresponding to the absorption of DMABN$^{\bullet+}$ were recorded for solutions containing various concentrations of one of the selected phenols, and the first-order rate constants for the decay of DMABN$^{\bullet+}$ were determined for the direct photoionization experiments (Fig. 4.1A) and for the triplet photosensitization experiments (Fig. 4.1B). These rate constants are plotted in Figure 4.1 versus the concentration of the various phenols. A linear increase with increasing concentrations of the phenols can be observed for the decay rate constant of DMABN$^{\bullet+}$. Therefore, a Stern-Volmer analysis was used to obtain $k^{q}_{\text{DMABN}\bullet+,\text{PhOH}}$, the second-order rate constant for the quenching reaction between DMABN$^{\bullet+}$ and the phenols (eq. 4.4), using the following equation: $k^{\text{obs}}_{\text{DMABN}\bullet+} = k^{0}_{\text{DMABN}\bullet+} + k^{q}_{\text{DMABN}\bullet+,\text{PhOH}} [\text{PhOH}]$, where $k^{\text{obs}}_{\text{DMABN}\bullet+}$ is the observed first-order decay rate constant of DMABN$^{\bullet+}$ in the presence of phenol and $k^{0}_{\text{DMABN}\bullet+}$ is the analogous rate constant in the absence of phenol.

Fig. 4.1B was constructed neglecting the data with low or no phenol concentration to ensure that the used phenol was the main quencher in the reaction. It can be observed that the accuracy of the obtained results is higher for photosensitization experiments (Fig. 4.1B, coefficient of determination R^2 of 0.96-0.995) than for direct photoionization experiments (Fig. 4.1A, coefficient of determination R^2 of 0.35-0.86), which is probably due to the relatively low efficiency of the photoionization process at the employed excitation wavelength, resulting in the generation of weak transient signals.

$$\text{DMABN} + hv \rightarrow \text{DMABN}^{\bullet+} + e^{-} \tag{4.1}$$

$$\text{Sens} + hv \rightarrow {}^{1}\text{Sens}^{*} \rightarrow {}^{3}\text{Sens}^{*} \tag{4.2}$$

$$ {}^{3}\text{Sens}^{*} + \text{DMABN} \rightarrow \text{DMABN}^{\bullet+} + \text{Sens}^{\bullet-} \tag{4.3}$$

$$\text{DMABN}^{\bullet+} + \text{Phenol} \rightarrow \text{DMABN} + \text{Phenol}^{\bullet+} \tag{4.4}$$

The $k^{q}_{\text{DMABN}\bullet+,\text{PhOH}}$ values obtained in the direct photoionization system show similar trends as the ones obtained in the triplet photosensitization system, with higher rate constants for electron-rich phenols (Table 4.1). However, the values obtained for the direct photoionization system were systematically higher by a factor ≈2 than the others. Following this comparison between the two systems, the direct photoionization system was not used for further experiments but is presented here as a proof of the validity of the photosensitized system.

Figure 4.1C shows a Hammett plot of $k^{q}_{\text{DMABN}\bullet+,\text{PhOH}}$ values from Fig. 4.1B vs the Hammett substituent descriptor σ^{+} (often used in the case of oxidation of a substrate)[18, 19] of the corresponding phenols. The Hammett plot shows a good linearity and a linear regression analysis of these data yields a slope (the so-called "reaction constant") ρ of −2.0±0.6.
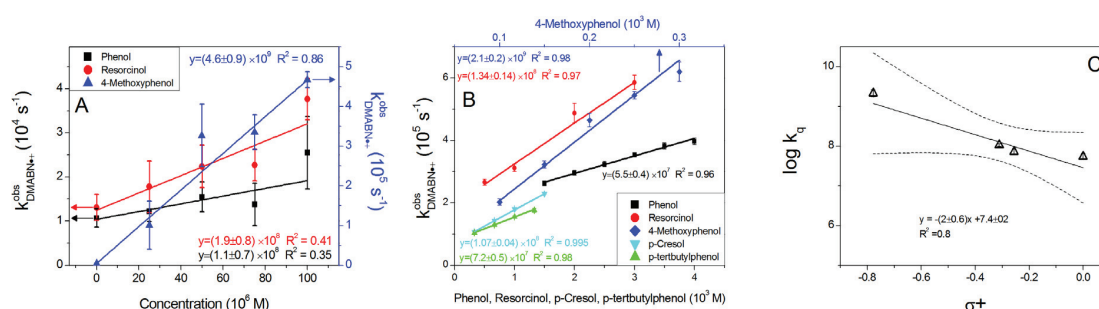
Figure 4.1. (A) Stern-Volmer plot for the reaction between the radical cation of 4-(dimethylamino)benzonitrile (DMABN$^{\bullet+}$), obtained by photoionization (266-nm laser pulse), and several phenols. (B) Stern-Volmer plot for the reaction between DMABN$^{\bullet+}$, obtained by 300μM 1-naphthaldehyde photosensitization of 500μM DMABN (355nm laser pulse) and several phenols. (C) Decadic logarithm of the second-order rate constant for the quenching reaction of DMABN$^{\bullet+}$ by phenols ($k^q_{DMABN\bullet+,PhOH}$) obtained in the photosensitized system vs the electrophilic substituent descriptor σ^+ from Ref. 18. Errors bars represent 95% confidence intervals obtained from the mean of at least triplicate measurments. (A) and (B), errors on the slopes represent 95% confidence intervals from linear regressions, (C) errors on the slope and intercept represent standard error obtained from linear regression.

Table 4.1. Measured second-order rate constant for the quenching reaction of DMABN$^{\bullet+}$ by several phenols ($k^q_{DMABN\bullet+,PhOH}$) or DOM ($k^q_{DMABN\bullet+,DOM}$) obtained in aqueous solutions at pH8 either by direct photoionization of DMABN or by triplet photosensitization using 1-naphthaldehyde.

	σ^+ (para) [a]	$k^q_{DMABN\bullet+,PhOH}$ Direct photoionization (10^8 M^{-1} s^{-1}) [b]	$k^q_{DMABN\bullet+,PhOH}$ Photosensitized experiments (10^8 M^{-1} s^{-1}) [c]
4-Methoxyphenol	-0.778	46 ±9	21.3 ±0.2
Resorcinol		1.9 ±0.8	1.34 ±0.14
p-Cresol	-0.311		1.07 ±0.04
p-Tertbutylphenol	-0.256		0.72 ±0.05
Phenol	0	1.1 ±0.7	0.55 ±0.04
	EDC (μMe$^-$ mgC^{-1}) [d]		$k^q_{DMABN\bullet+,DOM}$ (10^3 L mgC^{-1} s^{-1}) [c]
SRFA (I)	2848 [e]		2.9 ±0.4
PLFA	1203		0.76 ±0.16
SRHA	3684		5.6 ±0.5
Etang de la Gruère			1.1 ±0.4

Notes: [a] Electrophilic substituent constants from Ref. 18; [b] 266 nm laser excitation wavelength, 133 μM DMABN in N$_2$O-purged solution; [c] 355nm laser excitation wavelength, 1-naphthaldehyde 300μM + DMABN 500μM under aerated condition. [d] electron donating capacity (EDC) calculated using data from Ref. 20 and carbon content given on www.humicsubstances.org accessed on 14.03.2016; [e] EDC of SRFA (II), The EDC of SRFA (I) and SRFA (II) are nearly identical.[21]

4.3.1.2 Second-Order Rate Constants for the Reaction of DMABN$^{\bullet+}$ with DOM

Similarly as for phenols, the decay of DMABN$^{\bullet+}$ produced by 1-NA photosensitization (eq.4.3) is accelerated by the presence of DOM (Fig.4.2). The first-order rate constants for the decay of DMABN$^{\bullet+}$ were determined and a linear increase in rate constant with increasing concentration of the DOM can be observed. Therefore, as for the phenols a Stern-Volmer analysis was used to obtain the second-order rate constant for the reaction of DMABN$^{\bullet+}$ with DOM ($k_{DMABN\bullet+,DOM}^{q}$). The various types of investigated DOM included a few commercially available fulvic and humic acid extracts and the DOM of a natural water (used without extraction). For the extracts, $k_{DMABN\bullet+,DOM}^{q}$ values resulted to be proportional to the electron donating capacity (EDC) of these materials (Table 4.1).

Interestingly the quenching rate constant value for the natural water (Étang de la Gruère, EG) falls between the corresponding values for SRFA (of almost pure allochthonous origin) and PLFA (of almost pure autochthonous origin). This probably reflects the provenance of the DOM of EG water, from both autochthonous (algal and bacterial derived) and allochthonous (from the degradation of plants) sources.

The rate constant obtained for SRFA, $(2.9\pm0.4)\times10^{3}$ L mg$_{C}^{-1}$ s^{-1}, is lower by a factor of 4 than the value of the rate constant for the quenching of the radical cation of tryptophan by SRFA obtained at pH3 in a previous study, i.e. $(1.1\pm0.2)\times10^{4}$ mg$_{C}^{-1}$ L s^{-1}. [11] This difference is hard to explain, since one would expect DMABN$^{\bullet+}$ (one-electron oxidation potential of $\approx$1.3 V vs. SHE) [17] to be a stronger oxidant than the tryptophanyl radical cation (oxidation potential of 1.0 V), [11] and SRFA should be a better electron donor at pH 8 than at pH 3. Thus for DMABN$^{\bullet+}$ a higher rate constant for quenching by SRFA would be expected than for the tryptophanyl radical cation.
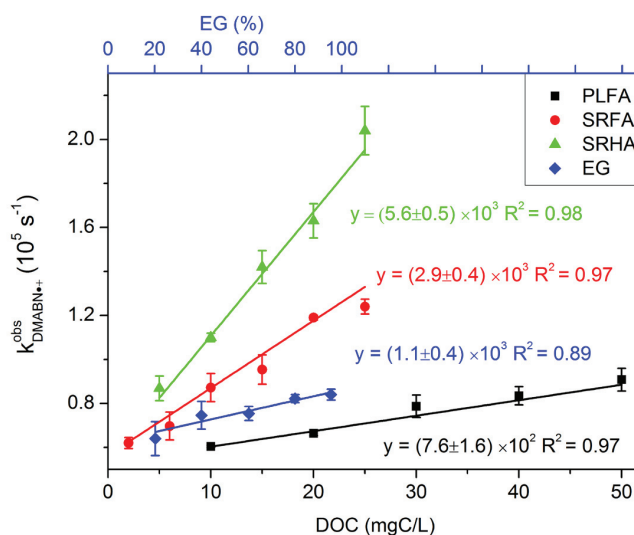

Figure 4.2. Stern-Volmer plot for the reaction between DMABN$^{\bullet+}$ obtained by 1-naphthaldehyde photosensitization (355nm laser pulse) with Suwannee River or Pony Lake fulvic acids (SRFA or PLFA, respectively), Suwannee River humic acid (SRHA), and Étang de la Gruère water (EG).

4.3.1.3 Deuterium Isotope Effect on the Rate Constants for the Quenching of DMABN$^{\bullet+}$ by Phenols

Two alternatives should be considered for the mechanism of the reaction between the phenols and DMABN$^{\bullet+}$: hydrogen atom transfer or electron transfer. To test the two alternatives, the measurement of the deuterium isotope effect was employed. Deuteration of the phenolic hydrogen, which undergoes a rapid proton exchange with water, was implemented by using D$_2$O as the solvent.[22] The second-order rate constants in D$_2$O, $k_{DMABN\bullet+,PhOD}^{q}$, were determined to be $(3.3\pm0.4)\times10^{7}$ M^{-1} s^{-1} for phenol and $(1.36\pm0.19)\times10^{9}$ M^{-1} s^{-1}, resulting in isotope effect ($k_{DMABN\bullet+,PhOH}^{q}/k_{DMABN\bullet+,PhOD}^{q}$) values of 1.66 and 1.57, respectively. These relatively small values tend to exclude a H atom abstraction mechanism, suggesting either a pure electron transfer or a proton-coupled electron transfer mechanism.[22]

4.3.1.4 Phenoxyl Radical Formation

The detection of a phenoxyl radical formed during the reaction of DMABN$^{\bullet+}$ with phenols (eq. 4.4) would be a further evidence for the postulated reaction.

It as to be noted that the radical cation of a given phenol (PhOH$^{\bullet+}$) is the postulated primary product of the reaction of DMABN$^{\bullet+}$ with the phenol (eq. 4.4), but it cannot be observed with the experimental methods of the present study due to its very fast deprotonation (pK$_a$ <0)[23] yielding the corresponding phenoxyl radical (PhO$^{\bullet}$, eq. 4.5). This radical can in turn be observed on the timescale used.

$$PhOH^{\bullet+} \rightarrow PhO^{\bullet} + H^{+} \tag{4.5}$$

A solution containing a photosensitizer, DMABN, and a phenol generates relatively complex transient signals upon LFP, and an unambiguous observation of a phenoxyl radical is not evident. To pursue this goal, 2-acetonaphthone (2-AN) was selected as a photosensitizer and the unsubstituted phenol was chosen as the quencher of DMABN$^{\bullet+}$ (Fig. 4.3). Thereby, the possible side-reaction consisting in the formation of the phenoxyl radical from the oxidation of phenol by excited triplet 2-AN (eq. 4.6) has to be considered.

$$^{3}2\text{-AN*} + PhOH \rightarrow 2\text{-ANH}^{\bullet} + PhO^{\bullet} \tag{4.6}$$

An unambiguous production of PhO$^{\bullet}$ following oxidation of phenol by DMABN$^{\bullet+}$ (eq. 4.4 and 4.5) could be shown by performing four different LFP experiments presented in the following list (letters designing each item correspond to the panels in Fig. 4.3).

(A) The excited triplet state of 2-AN ($^{3}2$-AN*) is generated as the only observable transient from a solution containing 500 µM 2-AN (Fig. 4.3A). $^{3}2$-AN* has an absorption spectrum with a maximum at ≈440 nm, in accordance with previous studies. [24, 25] Its first-order decay rate constant measured in aerated solution, $(7.54\pm0.16)\times10^{5}$ s^{-1}, is similar to a previously determined value $(6.44\pm0.12)\times10^{5}$ s^{-1}. [26] The singlet state of 2-AN is not observed in this system due to its very fast decay to the triplet sate.

(B) Upon addition of 500 µM DMABN to the solution containing 2-AN (Fig. 4.3B), DMABN$^{\bullet+}$ is produced through oxidation of DMABN by $^{3}2$-AN* (eq. 4.7) with a second-order rate constant of $(2.1\pm0.3)\times10^{8}$ M^{-1} s^{-1}. [17] The radical anion of 2-AN (2-AN$^{\bullet-}$) is not clearly visible under these conditions, because its main absorption band in the observation windows (centered at ≈410 nm) is largely hidden by the $^{3}2$-AN* spectrum. [17]

$$^{3}2\text{-AN*} + DMABN \rightarrow 2\text{-AN}^{\bullet-} + DMABN^{\bullet+} \tag{4.7}$$

(C) To quantify the production of the phenoxyl radical formed in the side-reaction of $^{3}2$-AN* with phenol (eq. 4.6), measurements were performed with a solution of 2-AN and phenol alone (Fig. 4.3C). The second-order rate constant for the quenching of $^{3}2$-AN* by phenol was determined to be $(4.2\pm1.7)\times10^{7}$ M^{-1} s^{-1}, in accordance with the value of $(3.3\pm1.3)\times10^{7}$ M^{-1} s^{-1} from a previous study. [26] The phenoxyl radical exhibits a weak absorption band at ≈420 nm. [27]

(D) The transient signal after LFP of a solution containing all three components, namely 2-AN, DMABN and PhOH obviously exhibits the most complex features (Fig. 4.3D). At time t=0 only the signal attributed to $^{3}2$-AN* is present, and upon $^{3}2$-AN* decay one observe the apparition of the signals of DMABN$^{\bullet+}$ and PhO$^{\bullet}$. The DMABN$^{\bullet+}$ signal decays faster than the PhO$^{\bullet}$ signal, leaving only the PhO$^{\bullet}$ signal for longer measuring times. The signal corresponding to PhO$^{\bullet}$ is much more important in this system than observed in system C (fig. 4.3C). Overall, this is an important piece of evidence showing the production of PhO$^{\bullet}$ from the reaction of PhOH with DMABN$^{\bullet+}$ (eq. 4.4).
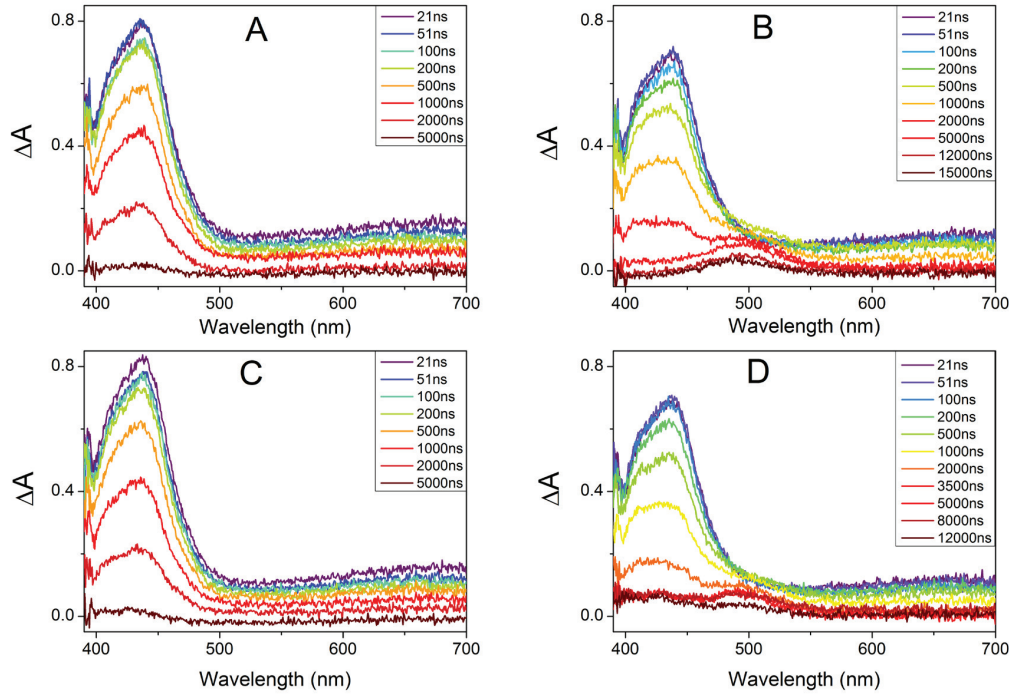
Figure 4.3. Transient absorption spectra following 355nm irradiation of: (A) 2-Acetonaphthone (2-AN) 500µM; (B) 2-AN 500 µM and 4-dimethylaminobenzonitril (DMABN) 500µM; (C) 2-AN 500 µM and Phenol 500µM; (D) 2-AN 500 µM + DMABN 500µM +Phenol 500µM. All measurements in aqueous solutions containing ≈1% (v/v) MeCN at pH 8.

4.3.1.5   Comparison of the Inhibitory Effect of Phenol and Fulvic Acids in Steady-State Irradiation and LFP Experiments

It is possible to compare the measurment of the inhibitory effect obtained in steady-state experiments ($[DOM]_{1/2}$ and $[PhOH]_{1/2}$, see Table 2.1) [7, 13, 14] with the second-order rate constants for the reaction between DMABN$^{\bullet+}$ and PhOH or fulvic acids ($k^q_{DMABN\bullet+,PhOH}$ or $k^q_{DMABN\bullet+,DOM}$) and of the first-order decay rate constant of DMABN$^{\bullet+}$ ($k^d_{DMABN\bullet+}$), both obtained by LFP.

The parameters obtained in steady-state experiments ($[PhOH]_{1/2}$ or $[DOM]_{1/2}$) are the concentrations of phenol or DOM needed to reduce the phototransformation rate by 50%. They can be expressed as: [7]

$$[PhOH]_{1/2} = k^d_{DMABN\bullet+}/k^q_{DMABN\bullet+,PhOH}$$

and $$[DOM]_{1/2} = k^d_{DMABN\bullet+}/k^q_{DMABN\bullet+,DOM}$$

Table 4.2. Comparison between the inhibitory effect observed in steady-state experiments and the LFP measurements. Errors represent 95% confidence interval obtained from non-linear fittings (steady-state experiments) or of Stern-Volmer plots (LFP experiments).

	Steady-state experiments	LFP experiments	
	$[DOM]_{1/2}$ or $[PhOH]_{1/2} = k^d/k^{q\ a}$	$k^q_{DMABN\bullet+,PhOH}$ or $k^q_{DMABN\bullet+,DOM}{}^b$	$k^d/k^{q\ c}$
PLFA	3.2 ±1.2 (mgC L^{-1})	(0.76 ±0.16) ×10^3 (mgC^{-1} s^{-1} L)	6.6 ±1.9 (mgC L^{-1})
SRFA	1.5 ±0.4 (mgC L^{-1})	(2.9 ±0.4) ×10^3 (mgC^{-1} s^{-1} L)	1.7 ±0.4 (mgC L^{-1})
PhOH	3.7 ±1.2 (μM)	(5.5 ±0.4) ×10^7 (M^{-1} s^{-1})	91 ±19 (μM)
PhOD ^{d}	4.4 ±0.6 (μM)	(3.3 ±0.4) ×10^7 (M^{-1} s^{-1})	152 ±35 (μM)

Notes: ^{a}From Table 2.1, see text for the definition of k^d and k^q, ^{b}second-order rate constant for the quenching of DMABN$^{\bullet+}$ by PhOH from Table 4.1, obtained in the ^{3}1-NA* photosensitized system. ^{c}using a value of (5±1)×10^3 s^{-1} for k^d. ^{d} Mono-deuterated phenol, resulting from proton exchange in the solvent D_2O.

The values for $[PLFA]_{1/2}$ and $[SRFA]_{1/2}$ obtained in the steady-state experiments and in the LFP experiments are similar in the two systems. On the contrary, the values for $[PhOH]_{1/2}$ and $[PhOD]_{1/2}$ differ by a factor ≈30 in the two systems. One explanation of this difference would be that phenol has additional effects in steady-state experiments. For example, one could envisage a second inhibitory effect of phenol on the deprotonated form of DMABN$^{\bullet+}$ (DMABNr$^\bullet$, eqs. 4.8-9). This deprotonated form is believed to be the first step in the phototransformation of DMABN$^{\bullet+}$. [13] This explanation does not agree well with the absence of important kinetic isotopic effect that would be expected for a H atom transfer, and one should expect this effect to be of minor importance, if occurring at all.

$$DMABN^{\bullet+} \rightarrow DMABNr^\bullet \tag{4.8}$$

$$DMABNr^\bullet + PhOH \rightarrow DMABN + PhO^\bullet \tag{4.9}$$

Another possible explanation is an overestimation of the parameters $[PhOH]_{1/2}$ and $[PhOD]_{1/2}$ by the fitting procedure in the steady-state experiments, as it was observed that such fitting procedures are prone to relatively important errors. [14]

One of the estimation parameter in the LFP experiments is the disappearance constant k_d of DMABN$^{\bullet+}$. k_d was estimated to be around (5±1)×10^3 s^{-1} but the measurement of the constant were seen to be sensitive to the presence of the superoxide radical anion ($O_2^{\bullet-}$) and to the starting concentration of the photosensitizer. [17] From the FAs measurements, k_d seems to be well estimated, but the FAs screen part of the light at the irradiation wavelength (absorbance = 0.5 for PLFA and 0.2 for SRFA at the maximum used concentrations) and that could have led to an overestimation of k_d.

The last parameter that could lead to the observed discrepancy in the estimation of $[PhOH]_{1/2}$ and $[PhOD]_{1/2}$ in the two systems is the second-order rate constant measurement. It was postulated in the LFP measurements that $O_2^{\bullet-}$ is interfering in the estimation of k_d by recombining with DMABN$^{\bullet+}$ (eq. 4.10) [17] and one could expect also such interference in the measurement of $k^q_{DMABN\bullet+,PhOH}$ if phenol is influencing $O_2^{\bullet-}$ concentration. Such an influence could be a recombination reaction between the phenoxyl radical produced by the reaction of PhOH with DMABN$^{\bullet+}$ (eq. 4.4) or $O_2^{\bullet-}$ (eq.4.11). Such reactions occur with a high rate constants ($k^q_{PhO\bullet,O2\bullet-}$ = 2×10^9 M^{-1} s^{-1}) [28] and could lead to an underestimation of the second-order rate constant $k^q_{DMABN\bullet+,PhOH}$.

$$DMABN^{\bullet+} + O_2^{\bullet-} \rightarrow DMABN + O_2 \tag{4.10}$$

$$PhO^\bullet + O_2^{\bullet-} \rightarrow PhO^- + O_2 \tag{4.11}$$

4.3.2   Sulfadiazine

4.3.2.1   Quenching of Excited Triplet Photosensitizers (^{3}Sens*) by Sulfadiazine (SD)

Contaminants can react with ^{3}Sens* through energy transfer (eq. 4.12), electron transfer (eq. 4.13) or physical quenching (eq. 4.14). The energy transfer reaction can be avoided by choosing photosensitizers with a lower triplet energy than the target contaminants,

in the case of sulfadiazine (SD), the triplet state of SD (^{3}SD*) has an energy of 3.02V, [29] higher than the triplet energy of the photosensitizers used except for 3-Methoxyacetophenone (see Table 4.3), thus excluding the energy transfer reaction from all other photosensitizers to SD.
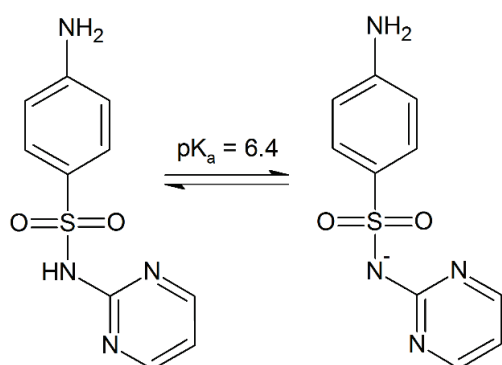
$$^3Sens* + SD \rightarrow Sens + {}^3SD* \tag{4.12}$$

$$^3Sens* + SD \rightarrow Sens^{\bullet-} + SD^{\bullet+} \tag{4.13}$$

$$^3Sens* + SD \rightarrow Sens + SD \tag{4.14}$$

Figure 4.4. Structure of sulfadiazine, pK$_a$ value from Ref. [6]

The pKa of SD is 6.4±0.6, therefore only a small fraction (3%) of the SD will be present as the neutral form (Fig.4.4). Towards oxidation by triplet photosensitizer the deprotonated form is expected to be more reactive than the neutral form of SD (one electron oxidation potential estimated by quantum chemical calculation of 1.1V for the deprotonated form vs 1.3 V for the neutral form [30]), which can therefore be neglected in this work. Using the value of 1.1V for the one electron oxidation potential of SD and the value from Table 4.3 for the reduction potential of the photosensitizers in their triplet state ($E^{°'*}$red), the electron transfer reaction can be calculated to be exergonic for any of the photosensitizers used in this study.

Table 4.3. Second-order rate constants for the quenching of excited triplet photosensitizers (^{3}Sens*) by sulfadiazine (SD) in aerated aqueous solution at pH 8.0.

Photosensitizer (Sens)	$E^{°'*}_{red}$ (V vs SHE) [a]	Triplet energy eV [a]	$k^q_{3Sens*,SD}$ (10^9 M^{-1} s^{-1}) [e]
3-Methoxyacetophenone [b]	1.71 [d]	3.14 [d]	2.22 ±0.13
Thionine	1.45	1.70	2.84 ±0.10
1-Naphthaldehyde [c]	1.34	2.45	0.90 ±0.04
2-Acetonaphthone [c]	1.34	2.59	0.102 ±0.017
1-Acetonaphthone [c]	1.26	2.52	0.029 ± 0.004

Notes: [a] Standard one electron reduction potentials of the photosensitizers in their excited triplet state ($E^{°'*}$red) except if otherwise mentioned from Ref. 31, [b] Solutions containing 10% (v/v) MeCN as co-solvent. [c] Solutions containing ≈1% (v/v) MeCN. [d] from Ref.32, [e] Errors represent 95% confidence intervals obtained from the linear regression lines (Stern-Volmer plots).

4.3.2.2   Electron Transfer Fitting

The second-order rate constants for triplet quenching by SD ($k^q_{3Sens*,SD}$) follow the extent of the reaction exergonicity, with higher reaction rate constants for the photosensitizers with a high one electron reduction potential in their triplet state (table 4.3). The

electron transfer reaction can be modelled through the electron transfer reaction theory using the Rehm-Weller relationship (eq. 4.15): [33-35]

$$k^q = \cfrac{k_d}{1 + \cfrac{k_d}{K_d Z}\left\{\exp\left[\left(\sqrt{\left(\dfrac{\Delta_r G_{et}^0}{2}\right)^2 + \left(\dfrac{\lambda}{4}\right)^2} + \left(\dfrac{\Delta_r G_{et}^0}{2}\right)\right)/RT\right] + \exp\left(\dfrac{\Delta_r G_{et}^0}{RT}\right)\right\}}$$ (4.15)

Where k_d is the diffusion-controlled second-order rate constant, $K_d = k_d/k_{-d}$ is the equilibrium constant for the formation of the encounter complex. Z is the universal collision frequency factor, $\Delta_r G°_{et}$ is the standard molar free energy change of the electron transfer reaction, i.e., the standard molar free energy difference between successor complex and precursor complex, λ is the reorganization energy, R is the universal gas constant and T the absolute temperature.

The fitting procedure was done similarly as in Refs. [17, 26] using a value of 0.1 for the ratio $k_d/(K_d \times Z)$ and setting $\Delta G°_{et} = \Delta G°_{et,calc} + \delta\Delta G°$ to take into account the uncertainties in the calculated one electron oxidation potential of SD. $\Delta G°_{et,calc}$ was calculated using the $E^{o,red}*$ for the photosensitizers (table 4.3) and using the calculated value of 1.1V for the oxidation potential of SD. [30] The fit parameters were $\delta\Delta G°$ and λ, and a fixed value of 5×10^9 M^{-1} s^{-1} was used for k_d. The best fit to the rate-constant data gives for λ 26.6 kJ/mol and for $\delta\Delta G°$ 21.7kJ. This λ value is in the lower end of the value usually observed but similar to the one found in the quenching of the triplet state of methylene blue by aromatic amines [12] and for the triplet state of the same set of photosensitizers used in this study and DMABN. [17] Fits with more typical value for λ of 40 and 50 kJ give values for $\delta\Delta G°$ of 13.7 and 4.3 kJ, respectively and fit the data points reasonably well.
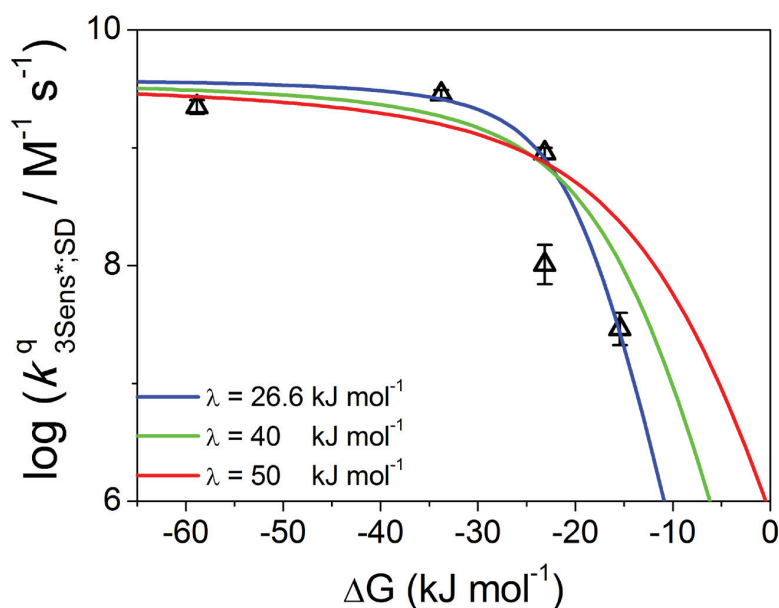

Figure 4.5. Measured second-order rate constant for the quenching of excited triplet photosensitizers by sulfadiazine ($k^q_{3Sens*,SD}$) (black triangles), in a logarithmic representation. The lines represent fits to the Rehm-Weller model with reorganization energy (λ) values as given in the legend. The fitting procedure is explained in the text. Errors bars represent 95% confidence interval obtained from Stern-Volmer plots.

4.3.2.3 The Sulfadiazine Radical Cation (SD•+)

To select an appropriate detection wavelength for the generated radical of sulfadiazine (SD•+) and to assign with certitude the observed spectra, the same procedure as described in Ref.17 was used: (A) generation of the ³Sens* from a solution of the photosensitizer alone. (B) Generation of the ³Sens* and by reaction of the ³Sens* with triethanolamine (TEA) of the Sens•⁻ (the radical formed from the triplet oxidation of TEA do not absorbs in the observation windows). (C) Generation of the ³Sens* and by reaction

with the ^{3}Sens* of Sens$^{\bullet-}$ and of SD$^{\bullet+}$. This procedure was applied with two photosensitizers, 1-Naphthaldehyde (1-NA) and 3-Methoxyacetophenone (3-MOAP), to have an improved reliability in the assignment of the absorption band of SD$^{\bullet+}$.

For the 1-NA system, the transients observed are (Fig. 4.6A-C): (A) Upon irradiation of a 1-NA solution, ^{3}1-NA* is generated, which absorbs in the 520nm area and has a decay rate constant of $(5.11\pm0.04)\times10^5$ s^{-1}. The triplet spectra match those found in previous studies. [24, 36] (B) Upon irradiation of a solution of 1-NA + TEA, in addition to ^{3}1-NA*, a second longer-lived species that can be attributed to 1-NA$^{\bullet-}$ and has an absorbance centered at 420nm. (C) Upon irradiation of a solution of 1-NA + SD, both ^{3}1-NA* and 1-NA$^{\bullet-}$ are produced in this system and a third transient species with a long-lived absorbance in the 420-500 nm range can be attributed to the radical cation of SD (SD$^{\bullet+}$).

The bands in the 3-MOAP system can be attributed similarly, with ^{3}3-MOAP* absorbing in the 380-500nm (Fig. 4.6D) which matches literature data. [32] The spectrum of 3-MOAP$^{\bullet-}$ overlaps with the ^{3}3-MOAP* spectrum but has an absorbance maxima at ≈420nm (Fig. 4.6E) and the spectrum of SD$^{\bullet+}$ is visible in the system with 3-MOAP + SD (Fig. 4.6F) alongside the spectra of ^{3}3-MOAP* and 3-MOAP$^{\bullet-}$ with an absorption spectrum similar as in the 1-NA system.

The decay rate constant of SD$^{\bullet+}$ was seen to be of $(4.5\pm1.3)\times10^3$ s^{-1} in a 300μM 1-NA +300μM SD system and of $(6.1\pm0.3)\times10^3$ s^{-1} in a 10mM 3-MOAP +300μM SD system, using 450nm as detection wavelength.
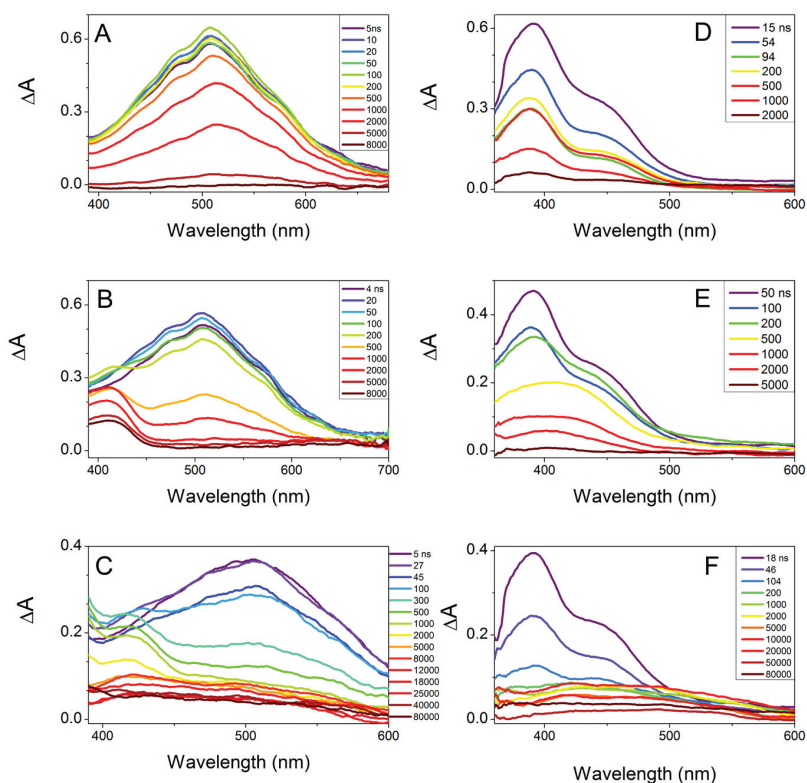
Figure 4.6. Transient spectra obtained upon LFP of sparged aqueous solutions at pH 8 of: (A) 1-Naphthaldehyde (1-NA) 300μM; (B) 1-NA 300μM + triethanolamine (TEA) 10mM; (C) 1-NA 300μM + Sulfadiazine (SD) 3mM; (D) 3-Methoxyacetophenone (3-MOAP) 10mM; (E) 3-MOAP 10mM + TEA 10mM; (F) 3-MOAP + SD 4.4mM. Solutions A, B and C in the presence of ≈0.5% (v/v) MeCN as a co-solvent. Solutions D, E and F in the presence of ≈10% (v/v) MeCN as a co-solvent.

4.3.2.4   Second-Order Rate Constants for the Reaction of SD$^{\bullet+}$ with Phenols in H_2O and D_2O

The measurements of the second-order rate constants for the quenching of SD$^{\bullet+}$ by the same set of phenols and DOM previously used in the DMABN system failed except for 4-methoxyphenol for which the rate constant was determined to be $(1.18\pm0.10)\times10^8$ $M^{-1}\,s^{-1}$ (see the corresponding Stern-Volmer plot in Fig. 4.7).

The failure to measure the rate constants with the other phenols or DOM was probably due to both the low intensity of the signal of SD$^{\bullet+}$ on the one hand, and the expected low second-order rate constants for the other phenols.

Measurement of the second-order quenching rate constant $k^q_{4\text{-methoxyphenol,SD}\bullet+}$ in D_2O where the acidic proton of phenol is exchanged for a deuterium atom, shows a very small kinetic isotopic effect ($k_H/k_D = 1.04$), indicating that the reaction is occurring by electron transfer.
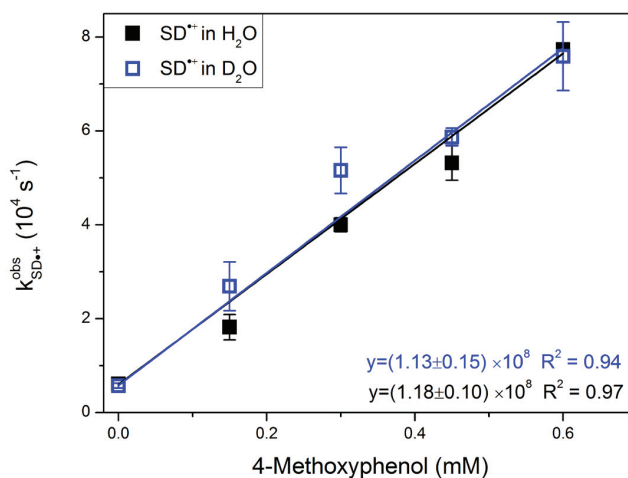

Figure 4.7. Stern-Volmer plot of the first-order decay rate constant of the observed radical of sulfadiazine (obtained by ^{3}1-naphthaldehyde* sensitization and measured at the observation wavelength of 450 nm) vs the 4-methoxyphenol concentration in H_2O (black) and D_2O (blue). Error bars represent 95% confidence intervals from at least triplicate measurements. Composition of the solvent for the D_2O experiments: 85% (v/v) D_2O, 5% H_2O, 10% MeCN.

4.3.2.5   Alternative Reaction Scheme

An explanation for the relatively low rate constant observed between 4-methoxyphenol and SD$^{\bullet+}$ could be that the radical cation is in equilibrium with its deprotonated from, having a calculated pK_a of 6.3 (scheme 4.1). [30] The water based protonation rate would be too low at pH 8 to allow for the equilibrium but the buffer could assists the protonation, making it fast enough to be in equilibrium. If this hypothesis is correct, the measured radical would not be SD$^{\bullet+}$ but its deprotonated form and the measured rate constant should be corrected by the relative fraction of the two radicals, this would lead to a second-order rate constant between SD$^{\bullet+}$ and phenol closer to a diffusion controlled reaction.
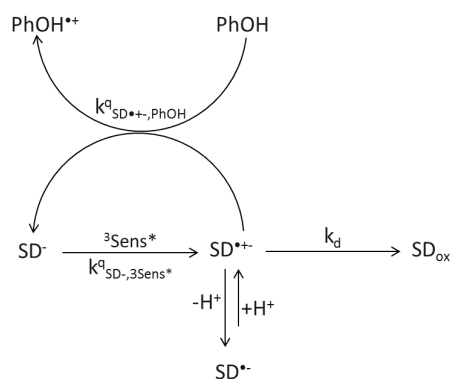
Scheme 4.1. Proposed reaction scheme for the sulfadiazine (SD) system with the radical cation in equilibrium with its deprotonated form.

4.4 Environmental Implications

This study provides further evidence that the inhibitory effects of DOM on the phototransformation of aromatic amines can proceed by reduction of the amines radical cation. This inhibition reaction was seen to proceed with model phenolic antioxidants by electron transfer and to be proportional to their Hammett σ^+ coefficient. This suggests that the inhibitory effect could be more important at higher pH, phenolates being better electron donors than phenols. With DOM isolates, the extend of the inhibition reaction was seen to be proportional to the EDC of the DOM, the DOMs with the higher EDC reacting the faster with the radical cation. The inhibitory effect of a whole water (EG) was seen to be intermediates to the one of two fulvic acid isolate that where chosen as end-members representatives of DOM of autochthonous (PLFA) and allochthonous (SRFA) sources, indicating that this intermediate reactivity was related to the DOM provenance of this whole water.

The comparison of the rate constants measured by LFP and the indicators for the inhibition obtained through steady-state experiements shows that there is a good correspondence between the two set of results in the case of DOMs. This indicates that the LFP measurments allow for a good prediction of the inhibitory effect.

4.5 Acknowledgements

4.6   References for chapter 4

1.   Stone, W. W.; Gilliom, R. J.; Ryberg, K. R., Pesticides in U.S. streams and rivers: occurrence and trends during 1992-2011. *Environ. Sci. Technol.* **2014,** *48*, (19), 11025-11030.

2.   Schafer, R. B.; von der Ohe, P. C.; Kuhne, R.; Schuurmann, G.; Liess, M., Occurrence and Toxicity of 331 Organic Pollutants in Large Rivers of North Germany over a Decade (1994 to 2004). *Environ. Sci. Technol.* **2011,** *45*, (14), 6167-6174.

3.   Moschet, C.; Wittmer, I.; Simovic, J.; Junghans, M.; Piazzoli, A.; Singer, H.; Stamm, C.; Leu, C.; Hollender, J., How a complete pesticide screening changes the assessment of surface water quality. *Environ. Sci. Technol.* **2014,** *48*, (10), 5423-3542.

4.   Miao, X. S.; Bishay, F.; Chen, M.; Metcalfe, C. D., Occurrence of antimicrobials in the final effluents of wastewater treatment plants in Canada. *Environ. Sci. Technol.* **2004,** *38*, (13), 3533-3541.

5.   Guerard, J. J.; Miller, P. L.; Trouts, T. D.; Chin, Y. P., The role of fulvic acid composition in the photosensitized degradation of aquatic contaminants. *Aquat. Sci.* **2009,** *71*, (2), 160-169.

6.   Boreen, A. L.; Arnold, W. A.; McNeill, K., Triplet-sensitized photodegradation of sulfa drugs containing six-membered heterocyclic groups: identification of an SO2 extrusion photoproduct. *Environ. sci. Technol.* **2005,** *39*, (10), 3630-3638.

7.   Canonica, S.; Laubscher, H. U., Inhibitory effect of dissolved organic matter on triplet-induced oxidation of aquatic contaminants. *Photochem. Photobiol. Sci.* **2008,** *7*, (5), 547-551.

8.   Ratti, M.; Canonica, S.; McNeill, K.; Bolotin, J.; Hofstetter, T. B., Isotope Fractionation Associated with the Indirect Photolysis of Substituted Anilines in Aqueous Solution. *Environ. sci. Technol.* **2015,** *49*, (21), 12766-12773.

9.   Othmen, K.; Boule, P., Photochemical behaviour of dichloroanilines in water and formation of aminochlorophenoxazones. *J. Photoch. Photobio. A* **1999,** *121*, (3), 161-167.

10. Richard, C.; Canonica, S., Aquatic phototransformation of organic contaminants induced by coloured dissolved natural organic matter. In *Handbook of Environmental Chemistry*, Hutzinger, O., Ed. Springer-Verlag Berlin, Heidelberger Platz 3, D-14197 Berlin, Germany: 2005; Vol. 2, pp 299-323.

11. Janssen, E. M.; Erickson, P. R.; McNeill, K., Dual roles of dissolved organic matter as sensitizer and quencher in the photooxidation of tryptophan. *Environ. Sci. Technol.* **2014,** *48*, (9), 4916-4924.

12. Erickson, P. R.; Walpen, N.; Guerard, J. J.; Eustis, S. N.; Arey, J. S.; McNeill, K., Controlling factors in the rates of oxidation of anilines and phenols by triplet methylene blue in aqueous solution. *J. Physical Chem. A* **2015,** *119*, (13), 3233-3243.

13. This thesis, chapter 2

14. Wenk, J.; von Gunten, U.; Canonica, S., Effect of dissolved organic matter on the transformation of contaminants induced by excited triplet states and the hydroxyl radical. *Environ. Sci. Technol.***2011,** *45*, (4), 1334-1340.

15. Wenk, J.; Canonica, S., Phenolic antioxidants inhibit the triplet-induced transformation of anilines and sulfonamide antibiotics in aqueous solution. *Environ. Sci. Technol.* **2012,** *46*, (10), 5455-5462.

16. Bahnmuller, S.; von Gunten, U.; Canonica, S., Sunlight-induced transformation of sulfadiazine and sulfamethoxazole in surface waters and wastewater effluents. *Wat. Res.* **2014,** *57*, 183-192.

17. This thesis, chapter 3

18. Leffler, J. E.; Grunwald, E., *Rates and equilibria of organic reactions: as treated by statistical, thermodynamic, and extrathermodynamic methods*. Wiley: New York, 1963; p 458.

19. Brown, H. C.; Okamoto, Y., Directive Effects in Aromatic Substitution .30. Electrophilic Substituent Constants. *J. Amer. Chem. Soc.* **1958,** *80*, (18), 4979-4987.

20. Aeschbacher, M.; Graf, C.; Schwarzenbach, R. P.; Sander, M., Antioxidant properties of humic substances. *Environ. Sci. Technol.* **2012,** *46*, (9), 4916-4925.

21. Walpen, N.; Schroth, M. H.; Sander, M., Quantification of Phenolic Antioxidant Moieties in Dissolved Organic Matter by Flow-Injection Analysis with Electrochemical Detection. *Environ. Sci. Technol.* **2016,** 6423-6432.

22. Canonica, S.; Jans, U.; Stemmler, K.; Hoigne, J., Transformation kinetics of phenols in water: photosensitization by dissolved natural organic material and aromatic ketones. *Environ. Sci. Technol.* **1995,** *29*, (7), 1822-1831.

23. Dixon, W. T.; Murphy, D., Determination of Acidity Constants of Some Phenol Radical Cations by Means of Electron-Spin Resonance. *J. Chem. Soc. Farad. T. 2* **1976,** *72*, 1221-1230.

24. Treinin, A.; Hayon, E., Quenching of Triplet States by Inorganic Ions. Energy Transfer and Charge Transfer Mechanisms. *J. Am. Chem. Soc.* **1976,** *98*, (13), 3884-3891.

25. Wenk, J.; Eustis, S. N.; McNeill, K.; Canonica, S., Quenching of excited triplet states by dissolved natural organic matter. *Environ. Sci. Technol.* **2013,** *47*, (22), 12802-12810.

26. Canonica, S.; Hellrung, B.; Wirz, J., Oxidation of phenols by triplet aromatic ketones in aqueous solution. *J. Phys. Chem. A* **2000,** *104*, (6), 1226-1232.

27. Das, P. K.; Bhattacharyya, S. N., Laser Flash Photolysis Study of Electron Transfer Reactions of Phenolate Ions with aromatic carbonyl triplets. *J. Phys. Chem.* **1981,** *85*, (10), 1391-1395.

28. Jonsson, M.; Lind, J.; Reitberger, T.; Eriksen, T. E.; Merenyi, G., Free-Radical Combination Reactions Involving Phenoxyl Radicals. *J. Phys. Chem.* **1993,** *97*, (31), 8229-8233.

29. Venning, D. R.; Mousa, J. J.; Lukasiewicz, R. J.; Winefordner, J. D., Influence of solvent upon the phosphorecence characteristics of several sulfonamides at 77 K. *Analyt. Chem.* **1972,** *44*, (14), 2387-2389.

30.   Tentscher, P. R.; Eustis, S. N.; McNeill, K.; Arey, J. S., Aqueous oxidation of sulfonamide antibiotics: aromatic nucleophilic substitution of an aniline radical cation. *Chem.* **2013,** *19*, (34), 11216-11223.

31.   Loeff, I.; Rabani, J.; Treinin, A.; Linschitz, H., Charge-Transfer and Reactivity of N-Pi-Asterisk and Pi-Pi-Asterisk Organic Triplets, Including Anthraquinonesulfonates, in Interactions with Inorganic Anions - a Comparative Study Based on Classical Marcus Theory. *J. Am. Chem. Soc.* **1993,** *115*, (20), 8933-8942.

32.   Shizuka, H.; Obuchi, H., Anion-Induced Triplet Quenching of Aromatic Ketones by Nanosecond Laser Photolysis. *J. Phys. Chem.* **1982,** *86*, (8), 1297-1302.

33.   Rehm, D.; Weller, A., Kinetics and Mechanics of Electron Transfer during Fluorescence Quenching in Acetonitrile. *Berich Bunsen Gesell* **1969,** *73*, (8-9), 834-839.

34.   Rehm, D.; Weller, A., Kinetics of Fluorescence Quenching by Electron and H-Atom Transfer. *Isr. J. Chem.* **1970,** *8*, (2), 259-271.

35.   Marcus, R. A., On the Theory of Oxidation-Reduction Reactions Involving Electron Transfer .1. *J. Chem. Phys.* **1956,** *24*, (5), 966-978.

36.   Samanta, A.; Fessenden, R. W., On the Triplet Lifetime and Triplet Triplet Absorption-Spectra of Naphthaldehydes. *Chem. Phys. Lett.* **1988,** *153*, (5), 406-410.

Chapter 4, Supporting information for

Quenching of an Aniline Radical Cation by Dissolved Organic Matter and Phenols: A Laser Flash Photolysis Study

Frank Leresche, Lucie Ludvíková, Dominik Heger, Petr Klán, Urs von Gunten, Silvio Canonica

In preparation for submission

Text S4.1: List of Chemicals:

Dimethylaminobenzonitrile (DMABN, Aldrich, 98%), Sulfadiazine (SD, Sigma, 99%), $NaH_2PO_4 \bullet 2H_2O$ (Lachner, 100%), $Na_2HPO_4 \bullet 12H_2O$ (Lachner, 99.3%), H_3PO_4 (Lachema, 85%), Acetonitrile (Sigma Aldrich, HPLC grade), triethanolamine (TEA, Sigma, 99%), O_2 (Siad, technical 2.5), N_2O (Siad, 99.99%), heavy water (D_2O; Aldrich, minimum 99.9%D).

Photosensitizers: Anthraquinone-1,5-disulfonate (AQdS, ABCR 98%), 2-Acetonaphthone (2-AN, Sigma-Aldrich, 99%), 1-Acetonaphthone (1-AN, Sigma-Aldrich, 97%), 1-Naphthaldehyde (1-NA, Aldrich, 95%), Thionin acetate salt (THI, Sigma, for microscopy), 3-Methoxyacetophenone (3-MA, Fluka 97%)

Phenols: 4-methoxyphenol (Fluka, 99%), Resorcinol (Merck, 99%), p-Cresol (Sigma-Aldrich, 99%), p-Tertbutylphenol (Koch, 99%), Phenol (Sigma-Aldrich, 99%)

Table S4.1. Characteristics of the used fulvic and humic acids from the International Humic Substances Society (IHSS).

	Elemental composition[a] (mass %)					Acidic functional groups[b]		Electron donating capacity (EDC)[c]
	C	H	O	N	S	Carboxyl (meq gC^{-1})	Phenolic (meq gC^{-1})	(μmol$_{e^-}$ g$_{HS}$$^{-1}$)
Pony Lake Fulvic Acid (1R109F)	52.47	5.39	31.38	6.51	3.03	Not available	Not available	1203 ±29
Suwannee River Fulvic Acid (1S101F)	52.44	4.31	42.2	0.72	0.44	11.44	2.91	2848 ±85[d]
Suwannee River Humic Acid (1S101H)	52.55	4.40	42.53	1.19	0.58	9.59	4.24	3684 ±85[e]

[a] From the IHSS website: http://www.humicsubstances.org/elements.html, accessed on the 15 August 2016.
[b] Determined by titration.[1]
[c] From Ref. 2, measured using a potential step of 0.73V at pH 7.
[d] Data for another batch of Suwannee River fulvic acid (catalogue number 2S101F).
[e] Data for another batch of Suwannee River humic acid (catalogue number 2S101H).

Table S4.2. Observation wavelengths used in laser flash photolysis for kinetic measurements of transient species.

Species	Observation wavelength (nm)
Excitation Wavelength 266nm	
^{3}DMABN*	400 & 600
DMABN$^{\bullet+}$	500
Hydrated electron (e$^-$)	600 & 700
PhO$^\bullet$	400
4-MethoxyPhO$^\bullet$	400
Resorcinol$^\bullet$	400
Excitation Wavelength 355 or 532 nm	
DMABN$^{\bullet+}$	500 & 520
SD$^{\bullet+}$	450
2-Acetonaphthone triplet (^{3}2-AN*)	440
2-Acetonaphthone radical anion (2-AN$^{\bullet-}$)	400
1-Naphthaldehyde triplet (^{3}1-NA*)	600
1-Naphthaldehyde radical anion (1-NA$^{\bullet-}$)	400
3-Methoxyacetophenone triplet (^{3}3-MOAP*)	400
Thionine triplet (^{3}THI*)	670
Thionine radical anion (THI$^{\bullet-}$)	400
1-Acetonaphthone triplet (^{3}1-AN*)	500
Phenoxyl radical (PhO$^\bullet$)	400
4-Methoxyphenoxyl radical (4-MeO-PhO$^\bullet$)	400
3-Hydroxyphenoxyl radical (3-OH-PhO$^\bullet$)	400
4-*tert*-Butylphenoxyl radical (4-*t*-Bu-PhO$^\bullet$)	400
4-Methylphenoxyl radical (4-Me-PhO$^\bullet$)	400

References for the supporting information

1.   Ritchie, J. D.; Perdue, E. M., Proton-binding study of standard and reference fulvic acids, humic acids, and natural organic matter. *Geochim Cosmochim Ac* **2003,** *67*, (1), 85-96.
2.   Aeschbacher, M.; Graf, C.; Schwarzenbach, R. P.; Sander, M., Antioxidant properties of humic substances. *Environ. Sci. Technol.* **2012,** *46*, (9), 4916-4925.

Chapter 5

General Conclusions and Outlook

General Conclusions and Outlook

Photoinduced transformations are an important removal pathway for organic contaminants in surface waters, and dissolved organic matter (DOM) often plays a significant role in this context. In addition to acting as a photosensitizer, DOM can also inhibit the indirect phototransformation of specific classes of compounds, in particular of anilines, which were in the focus of this PhD thesis.

The inhibitory effect of DOM on the photosensitized transformation of contaminants was characterized in this thesis using N,N-dimethyl-4-cyanoaniline (DMABN) as the main model compound. Investigations performed using steady-state photoirradiation and laser flash photolysis confirm the reaction scheme postulated in previous studies and consisting of the following reaction steps: A one-electron oxidation of the target compound (in this case DMABN) by triplet DOM (^{3}DOM*) results in the formation of a radical cation of the target compound (DMABN$^{\bullet+}$), which subsequently either transforms to non-radical products or reacts with antioxidant moieties of DOM or a model antioxidant. During the latter reaction, the radical cation is reduced back to its parent compound. In steady-state experiments the inhibitory effect was seen to be proportional to the electron donating capacity (EDC) of the studied DOMs, a relation that was analogous to the one observed by the laser flash photolysis for the second-order rate constant of the reaction between DMABN$^{\bullet+}$ and DOM. DOM standard solutions and natural waters yielded comparable results. DOM from allochthonous sources had a higher inhibitory strength than DOM from autochthonous sources, an observation that can help understanding the phototransformation properties of a given aquatic system. Kinetic equations were developed that allow the prediction of phototransformation rates of anilines (and analogous contaminants undergoing DOM-induced inhibition of transformation) in mixtures of DOMs of various origin.

Up-to-date experimental methods were used to investigate the susceptibility of a compound towards the inhibitory effect. The available experimental results, including the ones produced in this thesis, indicate that at least two factors control the magnitude of the inhibitory effect: (A) the rate constant for the reaction between the formed radical cation and the antioxidant. (B) the lifetime of the formed radical cation. Both rate constants can be obtained experimentally with sophisticated experimental and theoretical approach. It would be desirable to develop quantum chemical computation methods to obtain such rate constants for the formed radical cation and ultimately predict the inhibitory effect on the phototransformation of specific organic contaminants.

While the inhibitory effect of DOM on the phototransformation of anilines is now well described by this thesis, other classes of contaminants, for instance electron-poor phenols, would deserve further investigations. Phenols are known to react with ^{3}DOM* by electron or by hydrogen atom transfer to give a phenoxyl radical. The inhibitory effect on such radicals can be envisaged to occur either through electron transfer or through hydrogen atom transfer reaction. Such a study could also be useful in understanding the role of phenolic moieties in DOM: When oxidized, the electron-poor phenolic moieties will tend to be reduced by the electron-rich phenolic moieties.

A related subject that is up to now far less studied is the inhibitory effect of DOM on the direct phototransformation of organic contaminants. This topic has practical implications in the field of UV treatment of water to remove contaminants. Quantum yields for direct phototransformation, usually measured in buffered pure water, may not be applicable in natural water matrices due to the inhibitory effect of DOM. The current knowledge on the inhibitory effect occurring during indirect phototransformation is expected to be decisive for understanding such effects on direct phototransformation and predicting more realistic phototransformation rates for a great variety of organic contaminants in engineered UV-based water treatment systems.

The knowledge acquired in this study about the effect of DOM on the indirect phototransformation of contaminants could be used, in combination with the aforementioned inhibitory effect of DOM on the direct phototransformation of contaminants, to develop predictive tools for the assessment of the fate of contaminants in sunlit surface waters. This would lead to a better prediction of the influence of DOM on the phototransformation of these contaminants in the aquatic environment.

Curriculum Vitae

Frank Jonathan Leresche

Born the 20th of February 1983 in Lausanne, Switzerland
Citizen of Buchholterberg (BE), Switzerland & Germany

Education

2012-2016	Doctoral thesis Eawag, Department of Water Resources and Drinking Water, Switzerland EPFL, School of Architecture, Civil and Environmental Engineering (ENAC), Switzerland
2008-2010	Master in Chemical and Biochemical Engineering Swiss Federal Institute of Technology, Lausanne (EPFL). Master thesis: "*CO_2 reduction at water	supercritical CO_2 interface*".
2004-2008	Bachelor in Science Swiss Federal Institute of Technology, Lausanne (EPFL)
2002-2004	Swiss Federal Baccalaureate, options mathematics, philosophy-psychology and biology Ecole des Arches de Lausanne, Switzerland

Professional experiences

2013-2015	Laboratory assistant for students Eawag & ETH, Zürich, Switzerland
2010-2011	Civilian service EPFL, Photovoltaics and Thin Film Electronics Laboratory, Neuchâtel, Switzerland
2010	Civilian service EMS le Phare-Elim, Salvation Army, La Tour-de-Peilz, Switzerland
2008	Laboratory assistant for students EPFL, Lausanne, Switzerland
2005-2011	Firefighter City of Lausanne, Switzerland